AN EXPERIMENTAL STUDY OF K^+_{e4} DECAY

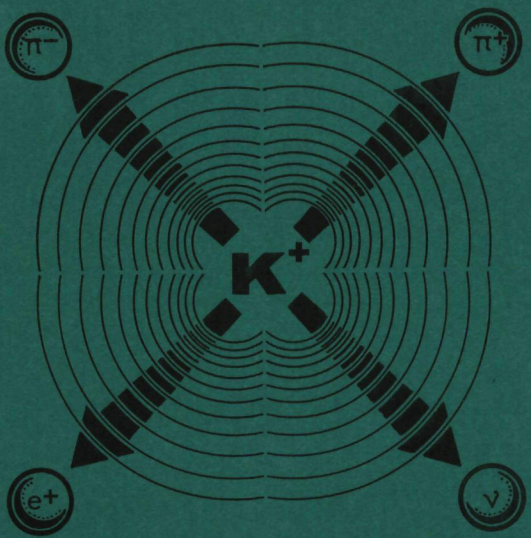

c.d. esveld

AN EXPERIMENTAL STUDY OF K^+_{e4} DECAY

The determination of the branching ratio,
form factors and π-π phase shift

PROMOTOR:

PROF. DR. R.T. VAN DE WALLE

AN EXPERIMENTAL STUDY OF K^+_{e4} DECAY

PROEFSCHRIFT

TER VERKRIJGING VAN DE GRAAD VAN DOCTOR IN DE
WISKUNDE EN NATUURWETENSCHAPPEN
AAN DE KATHOLIEKE UNIVERSITEIT TE NIJMEGEN, OP GEZAG VAN
DE RECTOR MAGNIFICUS PROF.MR. F.J.F.M. DUYNSTEE,
VOLGENS BESLUIT VAN HET COLLEGE VAN DECANEN
IN HET OPENBAAR TE VERDEDIGEN
OP DONDERDAG 4 OKTOBER 1973
TE 14 UUR PRECIES

door

CORNELIS DIRK ESVELD
geboren te Nijmegen

Druk: Offsetdrukkerij Faculteit der Wiskunde en Natuurwetenschappen
Nijmegen

Allen, die hebben bijgedragen aan het tot stand komen van dit proefschrift, wil ik gaarne bedanken. In het bijzonder geldt dit

- de scansters en meetsters van de werkgroep Hoge Energie Fysica
- de medewerkers van het Universitair Rekencentrum
- Mej. drs. W. Buys, drs. J. v. Eyden en drs. A. Reinen voor hun medewerking gedurende hun afstudeerperiode
- Dr. F.A. Berends (Leiden) voor het kritisch lezen van het manuscript
- de afdeling illustratie
- de afdeling fotografie
- de typekamer en de offset afdeling

I thank all colleagues for their clarifying discussions at the collaboration meetings, especially Dr. W.L. Knight (CERN), Dr. D. Bertrand (Brussels) and Dr. F. Bobisut (Padova). I express my gratitude to the leaders of the LRL - UW - UCL collaboration, who allowed me to reanalyze their data. I am grateful to Dr. W. Metzger for his useful suggestions concerning both the contents and the language of this thesis.

O Heer, hoe groot moet dan Uw wijsheid zijn,
Gij hebt het al gemaakt, van groot tot klein.
Vol is de aarde van Uw wonderwerken.

Ps. 104:7

Aan mijn ouders
Aan Iet en
Annet, Petra,
Erik en Marja

CONTENTS

I. INTRODUCTION

The K^+e4 experiment, which is the subject of this thesis, is one of a series of weak interaction [1] experiments in which various decay modes of the K^+ meson were investigated by the so-called X2 collaboration. The K^+ decays were studied with a stopping K^+ beam in the CERN heavy liquid bubble chamber.

The aims of the experiments are:

a) the determination of branching ratios and decay rates
b) the determination of decay parameters, called form factors
c) the determination of the energy dependence of the form factors
d) the test of weak interaction selection rules like CP-conservation and the semileptonic $\Delta S = \Delta Q$ rule.

With respect to the form factors and their energy dependence, a better determination became desirable after the development of new models and calculational techniques based on SU (3) symmetry and current algebra [2]. Those techniques were applied to the hadronic part of the weak interaction Hamiltonian, i.e. essentially for the evaluation of the form factors. These form factors are the quantities which describe the effect of the strong interactions on the weak semileptonic and weak hadronic processes.

The X2 experiment was proposed in 1964 and performed in the second half of 1965. In all 1.35×10^6 photographs were obtained, of which 7.8×10^5 were assigned to the X2 collaboration, while the remaining 5.7×10^5 pictures went to a collaboration of Lawrence Radiation Laboratory (Berkeley), University of Wisconsin (Madison) and University College (London). We will refer to the latter as the LRL-UW-UCL

collaboration.

The X2 collaboration, in which a group of the University of Nijmegen participated from the beginning, started with the form factor analysis, based on the measurement of the polarization of the μ^+ in $K^+\mu 3$ decay [3]. This analysis was followed by a determination of the $K^+\mu 3/K^+e3$ branching ratio, which also led to conclusions about the form factors [4]. A third method to derive the same form factors was the Dalits plot density analysis in $K^+\mu 3$ decay [5]. All three methods were then combined [6] and published in detail in ref. [7]. Finally an analysis of the K^+e3 decay spectra was performed [8].

Around 1968, five laboraties of the X2 collaboration, namely

1. III Physikalisches Institut der Technischen Hochschule - Aachen
2. Service de Physique des Particules Elementaires Université Libre - Bruxelles
3. TCL (former NPA)-division, CERN - Genève
4. Fysisch Laboratorium, Kath. Universiteit - Nijmegen
5. Instituto di Fisica dell' Università - Padova

started with a special scan to collect K^+e4 decays. Apart from its intrinsic interest, this decay mode ($K^+\rightarrow\pi^+\pi^-e^+\nu$) also offers a unique possibility of studying the low-energy π-π interaction in the absence of additional strongly interacting particles. The results, obtained by the collaboration and based on the analysis of 115 K^+e4 events, were first published in ref. [9].

The LRL-UW-UCL collaboration effort was completely devoted to the search for and analysis of K^+e4 decays. They found 269 K^+e4 events and published their results in ref. [10]. Reanalysis of their work is included in this thesis. This reanalysis also includes 69 events, found in 1965 by a collab-

oration of Lawrence Radiation Laboratory and University of Wisconsin (LRL-UW) [11].

The 115 X2 events, the 69 LRL-UW events and the 269 LRL-UW-UCL events added together essentially represent all known Ke4 decays as obtained from bubble chamber pictures.

Especially during recent years much larger samples are obtained with counter techniques [12]. A general problem with these techniques is their limited detection efficiency and acceptance. In spite of the relative small number of events found by the X2 collaboration, it is possible to give reasonable answers to questions like branching ratio, form factors and π-π phase shifts. Methods of analysis were used which avoid as much as possible loss of useful events in the selection procedures necessary to make the sample homogeneous.

With a few exceptions the related literature was closed as of the middle of 1972.

Note: After finishing the manuscript of this thesis, another large statistics counter experiment with K^+e4 and K^-e4 decays was reported by a group of the University of Pennsylvania, Philadelphia; see ref. [13].

References - chapter I

1) see for example
P.K. Kabir (ed.), The development of Weak Interaction Theory (Gordon and Breach, 1963).
R.E. Marshak, Riazuddin and C.P. Ryan, Theory of Weak Interaction in Particle Physics (Wiley-Interscience, vol. XXIV, 1969).
J.D. Jackson in Elementary Particle Physics and Field Theory, 1962 Brandeis Lectures, vol. I (Benjamin, 1963).
T.D. Lee and C.S. Wu, Ann.Rev. Nucl. Science 15, 381 (1965), and 16, 471 (1966).

2) see for example
M. Gell-Mann and Y. Neéman, The eightfold way (Benjamin, 1964).
S.L. Adler and R.F. Dashen, Current Algebras and applications to particle physics (Benjamin, 1968).

3) J. Bettels et al, Nuovo Cimento 56 A, 1106 (1968).

4) T. Eichten et al, Phys. Letters 27 B, 586 (1968).

5) D. Haidt et al, Phys. Letters 29 B, 691 (1969).

6) D. Haidt et al, Phys. Letters 29 B, 696 (1969).

7) D. Haidt et al, Phys. Rev. D 3, 10 (1971).

8) H.J. Steiner et al, Phys. Letters 36 B, 521 (1971).

9) W. Schweinberger et al, Phys. Letters 36 B, 246 (1971).

10) R.P. Ely et al, Phys. Rev. 180, 1319 (1969).
F.A. Berends, A. Donnachie and G.C. Oades, Nucl. Phys. B 3, 569 (1967).
thesis K. Billing, University College London, unpublished.

11) R.W. Birge et al, Phys. Rev. 139, B 1600 (1965).

12) Geneva-Saclay collaboration, Phys. Letters 36 B, 615 (1971), 36 B, 619 (1971), 38 B, 457 (1972).

13) E.W. Beier et al, Phys. Rev. Letters 29, 511 (1972), 30, 399 (1973).

II. THE DECAY OF THE K^+ MESON

II.1 Physical preliminaries

The K^+ decay belongs to the category of weak interactions. Table II.1 gives general information about the K^+ meson and its decay modes [1].

Comparing weak and electromagnetic decays, one notices that the weak interaction is on the average 10^9 times weaker than the electromagnetic interaction. The weak interaction acts between all observed particles, hadrons as well as leptons, except photons. The strong interaction influences the weak processes involving hadrons in an important way.

The present theory of weak interactions, known as V-A theory, was evolved in 1957 [2]. Primarily, it was a theory of leptonic processes. Many developments in the physics of weak interactions are however due to studies of non-leptonic processes. This was the case for the θ-τ puzzle resulting in the discovery of parity non-conservation [3] and for the discovery of CP-violation in $K_2^\circ \to \pi^+\pi^-$ decay [4].

The universal V-A theory interprets the leptonic and semi-leptonic, as well as hadronic weak interactions, as being due to a phenomenological interaction Hamiltonian of the current × current type:

$$H_w = - \frac{G}{\sqrt{2}} J_\lambda \bar{J}_\lambda \qquad (2.1)$$

where G is the universal weak interaction constant with a value $(1.1660 \pm 0.0002).10^{-5}/\mathrm{GeV}^2$ and summation over the Lorentz-index λ is assumed. We use the notation

$$\bar{J}_\lambda = J_\lambda^+ \, (1 - 2\, \delta_{\lambda 4}) \qquad (2.2)$$

Table II.1

mass	$(493{,}715 \pm 0.037)$ MeV/c^2	
mean lifetime	$(1.2371 \pm 0.0026).10^{-8}$ sec	
spin	0	
isospin	$\frac{1}{2}$	
parity	minus	
strangeness	+1	
decay modes	branching ratio	partial decay rate (sec^{-1})
leptonic decays		
$K^+ \to \mu^+ \nu$ (Kμ2)	$(63.52 \pm 0.19).10^{-2}$	$(51.35 \pm 0.15).10^{6}$
$K^+ \to e^+ \nu$ (Ke2)	$(1.38 \pm 0.20).10^{-5}$	$(1.05 \pm 0.16).10^{3}$
hadronic decays		
$K^+ \to \pi^+ \pi^\circ$ (Kπ2)	$(21.06 \pm 0.18).10^{-2}$	$(17.02 \pm 0.15).10^{6}$
$K^+ \to \pi^+ \pi^+ \pi^-$ (τ)	$(5.59 \pm 0.03).10^{-2}$	$(4.52 \pm 0.03).10^{6}$
$K^+ \to \pi^+ \pi^\circ \pi^\circ$ (τ')	$(1.73 \pm 0.05).10^{-2}$	$(1.40 \pm 0.04).10^{6}$
semileptonic decays		
$K^+ \to \pi^\circ \mu^+ \nu$ (Kμ3)	$(3.24 \pm 0.10).10^{-2}$	$(2.62 \pm 0.08).10^{6}$
$K^+ \to \pi^\circ e^+ \nu$ (Ke3)	$(4.85 \pm 0.06).10^{-2}$	$(3.92 \pm 0.05).10^{6}$
$K^+ \to \pi^+ \pi^- e^+ \nu$ (Ke4)	$(3.7 \pm 0.2).10^{-5}$	$(3.0 \pm 0.2).10^{3}$
$K^+ \to \pi^+ \pi^+ e^- \nu$ (Ke4)	$< 5.10^{-7}$ *)	< 40
$K^+ \to \pi^+ \pi^- \mu^+ \nu$ (Kμ4)	$(0.9 \pm 0.4).10^{-5}$	$(0.7 \pm 0.3).10^{3}$
$K^+ \to \pi^+ \pi^+ \mu^- \nu$ (Kμ4)	$< 3.10^{-6}$ *)	$< 3.10^{2}$
$K^+ \to \pi^\circ \pi^\circ e^+ \nu$ (Ke4)	$(1.8^{+2.4}_{-0.6}).10^{-5}$	$(1.5^{+1.9}_{-0.5}).10^{3}$
radiative decays		
$K^+ \to \pi^+ \pi^\circ \gamma$ (Kπ2 rad.)	$(2.66 \pm 0.18).10^{-4}$	$(2.15 \pm 0.15).10^{4}$
$K^+ \to \pi^+ \pi^+ \pi^- \gamma$ (τ rad.)	$(10 \pm 4).10^{-5}$	$(8 \pm 3).10^{3}$
$K^+ \to \pi^\circ e^+ \nu\gamma$ (Ke3 rad.)	$(3.7 \pm 1.4).10^{-4}$	$(3.0 \pm 1.1).10^{4}$

*) forbidden by $\Delta Q = \Delta S$ rule

where + denotes the hermitian conjugate and δ is the Kronecker symbol. J_λ can be written as

$$J_\lambda = L_\lambda^e + L_\lambda^\mu + J_\lambda^o + J_\lambda^1 \qquad (2.3)$$

where the various quantities are defined as

$$L_\lambda^e = i\,\psi_{\nu_e}\,\gamma_\lambda\,(1+\gamma_5)\,\psi_e \quad \text{(electron current)}$$

$$L_\lambda^\mu = i\,\psi_{\nu_\mu}\,\gamma_\lambda\,(1+\gamma_5)\,\psi_\mu \quad \text{(muon current)}$$

$$J_\lambda^o = V_\lambda^o + A_\lambda^o \quad \text{(hypercharge-conserving hadron current)}$$

$$J_\lambda^1 = V_\lambda^1 + A_\lambda^1 \quad \text{(hypercharge-changing hadron current)}$$

The ψ are the particle field operators; the definitions of the 4x4 γ_i matrices (i = 1....5) can be found in appendix A1. As written, both lepton and hadron currents consist of a vector part ($i\,\psi_a\,\gamma_\lambda\,\psi_b$ and V_λ) and an axial-vector part ($i\,\psi_a\,\gamma_\lambda\,\gamma_5\,\psi_b$ and A_λ).

In 1963 Cabibbo [5] proposed to modify the universal current-current interaction by postulating an angle θ_c and replacing the expression $J_\lambda^o + J_\lambda^1$ by

$$\cos\theta_c\,J_\lambda^o + \sin\theta_c\,J_\lambda^1 \qquad (2.4)$$

As a consequence, the $\Delta Y = 0$ (hypercharge-conserving) semileptonic processes involve the additional factor $\cos^2\theta_c$ (compared to the purely leptonic processes); whereas the $|\Delta Y| = 1$ semileptonic processes involve the additional factor $\sin^2\theta_c$. The built-in in hypothesis that θ_c has the same value for vector current and axial-vector current interactions agrees experimentally within $\sim$15% ($\sin\theta_V \approx 0.22$, $\sin\theta_A \approx 0.265$).

Ke4 decay is an example of hypercharge-changing semi-leptonic meson decay; its interaction Hamiltonian takes the following form:

$$H_w = \frac{-G}{\sqrt{2}} \{ \sin\theta_c \, (V_\lambda^1 + A_\lambda^1) \, \bar{L}_\lambda + \text{hermitian conj.} \} \qquad (2.5)$$

where $L_\lambda = i \, \psi_{\nu_e} \, \gamma_\lambda \, (1 + \gamma_5) \, \psi_e$.

This expression contains a number of (experimentally well verified) assumptions:

i) invariance under the proper orthochronous Lorentz group.
ii) a two-component neutrino.
iii) a local lepton current coupled to hadrons by vector and axial-vector currents only.
iv) lepton number conservation.
v) μ-e universality.
vi) a universal Cabibbo angle.

II.2 Mathematical preliminaries

The notation used for the Feynman amplitude and the decay probabilities will be the same as in the work of Jackson [6].

In general, the S-matrix between two different states A and B is in first order given by

$$S_{BA} \equiv \langle B|S|A \rangle \simeq -i \int d^4x \, \langle B|H_{int}(x)|A \rangle \qquad (2.6)$$

where $H_{int}(x)$ is the interaction Hamiltonian density. This Hamiltonian involves products of field operators for bosons and fermions. Operating on the states $|A\rangle$ and $|B\rangle$, one obtains a factor for each particle created or destroyed. For

bosons the particle factor is the product of a normalization factor $\frac{1}{\sqrt{2E}}$ and a plane wave function; for fermions it is the product of a normalization factor $\sqrt{\frac{m}{E}}$, a plane wave function and a spinor. The integration over d^4x in Eq. (2.6) with the plane waves coming from the particle factors yields a four-dimensional delta-function, ensuring energy and momentum conservation.

The so-called Feynman amplitude (matrix element) M involves products of the fermion spinors and is defined by

$$S_{BA} = -i(2\pi)^4 \, \delta^4(p_B - p_A)\left(\prod_i \frac{m_i}{E_i} \prod_j \frac{1}{2E_j}\right)^{\frac{1}{2}} . M \qquad (2.7)$$

It is a Lorentz-invariant quantity still depending on the momenta involved. The A → B transition probability is now given by:

$$dw_{A\to B} = (2\pi)^4 \, |M|^2 \prod_i \frac{m_i}{E_i} \prod_j \frac{1}{2E_j} \, \delta^4(p_B - p_A) \prod_f \frac{d^3p_f}{(2\pi)^3} \qquad (2.8)$$

where the index i runs over all fermions, the index j over all bosons and index f over all particles in the final state B.

II.3 Ke4 decay kinematics

Applying the foregoing to Ke4 decay, we obtain for the decay probability

$$dw(K^+ \to \pi^+\pi^-e^+\nu) = \frac{1}{(2\pi)^8} \frac{1}{8E_K} |M|^2 \, m_e m_\nu \, \delta^4(p_+ + p_- + p_e + p_\nu - p_K) \frac{d^3p_+}{E_+} \frac{d^3p_-}{E_-} \frac{d^3p_e}{E_e} \frac{d^3p_\nu}{E_\nu} \qquad (2.9)$$

The amplitude M can be explicitely written as:

$$M = \frac{G \sin\theta_c}{\sqrt{2}} \langle \pi^+(p_+)\pi^-(p_-)|V_\lambda^1 + A_\lambda^1|K^+(p_k)\rangle$$

$$\{\bar{u}_\nu(p_\nu)\gamma_\lambda(1 + \gamma_5)v_e(p_e)\} \qquad (2.10)$$

where u and v denote spinors. Here and in the following the notations used are

$$p_+ = (\vec{p}_+, iE_+) = \pi^+ \text{ four-vector}$$
$$p_- = (\vec{p}_-, iE_-) = \pi^- \text{ four-vector}$$

To find expressions for the hadronic covariants $\langle \pi^+\pi^-|V_\lambda^1|K^+\rangle$ and $\langle \pi^+\pi^-|A_\lambda^1|K^+\rangle$, invariance principles are used [7,8,9,10]. Because of the opposite relative intrinsic parities of the K^+ and the $\pi^+\pi^-$ states, the matrix element of the vector current V_λ^1 between these states should transform as an axial vector; whereas that of the axial vector should transform as an ordinary vector. Using all available four-vectors (p_K, p_+ and p_-), the most general expressions of these types can be written as

$$\langle \pi^+\pi^-|A_\lambda^1|K^+\rangle = \frac{f}{m_K}(p_+ + p_-)_\lambda + \frac{g}{m_K}(p_+ - p_-)_\lambda$$

$$+ \frac{e}{m_K}(p_K - p_+ - p_-)_\lambda \qquad (2.11)$$

and

$$\langle \pi^+\pi^-|V_\lambda^1|K^+\rangle = \frac{h}{m_K^3}\varepsilon_{\lambda\mu\nu\tau} p_{K_\mu}(p_+ + p_-)_\nu(p_+ - p_-)_\tau \qquad (2.12)$$

where $\varepsilon_{\lambda\mu\nu\tau}$ is the antisymmetric Levi-Civita tensor ($\varepsilon_{1234} = 1$, $\varepsilon_{\lambda\mu\nu\tau} = (-1)^n$ with n = the number of permutations of any two indices, $\varepsilon_{\lambda\mu\nu\tau} = 0$ otherwise).

The quantities f, g, e and h are the so-called form factors; they are, in general, functions of the three independent Lorentz scalars which can be constructed from the available four-vectors. A possible set of these scalars consists of

$$S_\pi = -(p_+ + p_-)^2$$
$$S_l = -(p_K - p_+ - p_-)^2$$
$$\eta = -p_K(p_+ - p_-)$$

Every scalar constructed using p_K, p_+ and p_- can be reduced to an expression containing one or more of the scalars given above (in addition to the kaon and the pion mass). The factors m_K^{-1} in Eq. (2.11) and the factor m_K^{-3} in Eq. (2.12) have been inserted to make f, g, e and h dimensionless. It is shown in appendix A1 that the term involving e in Eq. (2.11) gives rise to a term proportional to the lepton mass in the transition amplitude; in the experimental treatment of Ke4 decay this term can therefore be neglected. Again due to kinematical factors, also the vector part of the interaction (form factor h) has a negligable influence on the Ke4 decay probability and the various spectra of the decay particles.

As we have a system of 4 outgoing particles in Ke4 decay, there are in total 12 unknown quantities. Not all these quantities are independent: there are 4 constraints due to four-momentum conservation. In addition, 3 angles can be integrated out, because there is no dynamical information in the overall spatial orientation of an event. We are therefore left with 5 independent quantities or, equivalently, a 5-dimensional configuration space. A common choice for these quantities is the set $M_{\pi\pi}^2$, $M_{e\nu}^2$, $\cos\theta_\pi$, $\cos\theta_l$ and ϕ with the following

definitions (see also fig. II.1):

(1) $M_{\pi\pi}^2 = S_\pi$, the squared effective mass of the di-pion system.

(2) $M_{e\nu}^2 = S_l$, the squared effective mass of the di-lepton system.

(3) θ_π, the angle of the π^+ in the c.m. system of the pions with respect to the direction of flight of the di-pion in the K^+ rest system.

(4) θ_l, the angle of the e^+ in the c.m. system of the leptons with respect to the directions of flight of the di-lepton in the K^+ rest system.

(5) ϕ, the angle between the plane formed by the pions and the corresponding plane formed by the leptons in the K^+ rest system.

The angles θ_π and θ_l are polar angles ($o \leqslant \theta_\pi(\theta_l) \leqslant \pi$); ϕ is an azimuthal angle ($o \leqslant \phi < 2\pi$).

As will be shown in chapter IV, eventually we will have to eliminate events having a pion momentum of less than 48 MeV/c. To introduce this cut in the theoretical distributions of the above variables is a cumbersome task. When we cut in $M_{\pi\pi}$ or $\cos\theta_\pi$ instead, we lose more than is stricly necessary. It is therefore advantageous to use another independent set of variables in which $|\vec{p}_+|$ and $|\vec{p}_-|$ or E_+ and E_- occur explicitly.

In a publication on this experiment [11], the following set was used: $|\vec{p}_+|$, $|\vec{p}_-|$, $\cos\alpha$, $\cos\theta_l$ and ϕ, where α is the angle between $\vec{p}_+$ and $\vec{p}_-$ in the K^+ rest system (fig. II.2). In this thesis we will use another set: E_+, E_-, k, E_e and ϕ, where k denotes the absolute value of the di-pion momentum $|\vec{p}_+ + \vec{p}_-|$ ($= |\vec{p}_e + \vec{p}_\nu|$) in the K^+ rest system (fig. II.3). The reasons for this choice are the simplicity of the expression, obtained for the decay probability and the avoidance of $\cos\theta_l$ (see chapter V for the objection against this quantity).

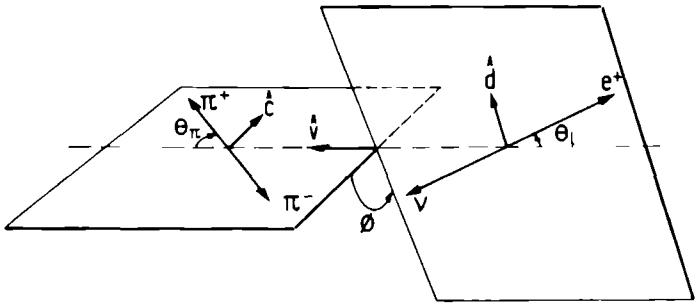

Fig. II.1. Illustration of the variable-set $M^2_{\pi\pi}$, $M^2_{e\nu}$, $\cos\theta_\pi$, $\cos\theta_l$, ϕ.

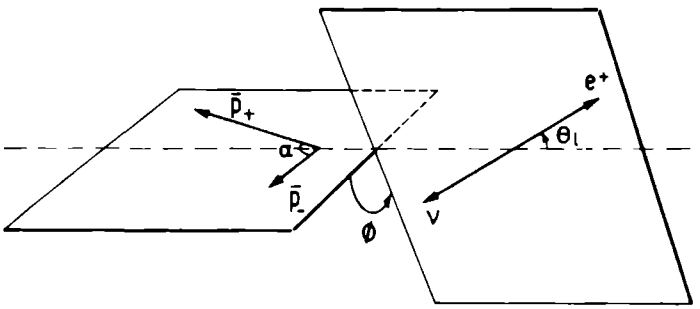

Fig. II.2. Illustration of the variable-set $|\vec{p}_+|$, $|\vec{p}_-|$, $\cos\alpha$, $\cos\theta_l$, ϕ.

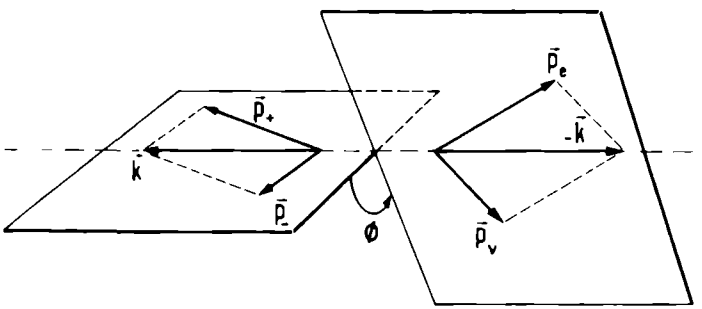

Fig. II.3. Illustration of the variable-set E_+, E_-, $|\vec{k}|$, E_e, ϕ.

The derivation of the decay probability in terms of the last set of variables is given in appendix A1. The result obtained is:

$$d^5w = \frac{G^2 \sin^2\theta_c}{(2\pi)^8 16 m_K} 8\pi^2 V_\mu V'_\nu T_{\mu\nu} \, dE_+ dE_- dk \, dE_e d\phi \qquad (2.13)$$

The same probability expressed in the variable-sets mentioned above, leads to resp.

$$d^5w = \frac{G^2 \sin^2\theta_c}{(2\pi)^8 16 m_K} 4\pi^2 \gamma \frac{|\vec{p}_+|^2 |\vec{p}_-|^2}{E_+ E_-} V_\mu V'_\nu T_{\mu\nu} \, d|\vec{p}_+| \, d|\vec{p}_-|$$

$$d\cos\alpha \, d\cos\theta_1 \, d\phi \qquad (2.14)$$

and

$$d^5w = \frac{G^2 \sin^2\theta_c}{(2\pi)^8 16 m_K} \frac{\pi^2}{2m_K^2} \beta\gamma\chi V_\mu V'_\nu T_{\mu\nu} \, dM^2_{\pi\pi} \, dM^2_{e\nu} \, d\cos\theta_\pi$$

$$d\cos\theta_1 \, d\phi \qquad (2.15)$$

In these formulae, the newly introduced symbols have the following definition °):

$$\gamma = 1 - \frac{m_e^2}{M^2_{e\nu}} \qquad (2.16)$$

$$\beta = \left(1 - \frac{4m_\pi^2}{M^2_{\pi\pi}}\right)^{\frac{1}{2}} \qquad (2.17)$$

°) Note. The factor I, introduced by Pais and Treiman [9], can be expressed as

$$I = \frac{m_K^2}{2\gamma} V_\mu V'_\nu T_{\mu\nu} \qquad (2.22)$$

$$\chi = m_K.k = \tfrac{1}{2}(m_K^4 + M_{\pi\pi}^4 + M_{e\nu}^4 - 2m_K^2M_{\pi\pi}^2 - 2m_K^2M_{e\nu}^2 - 2M_{\pi\pi}^2M_{e\nu}^2)^{\frac{1}{2}} \tag{2.18}$$

$$V_\mu = \frac{f}{m_K} R_\mu + \frac{g}{m_K} Q_\mu + \frac{e}{m_K} R_\mu + \frac{h}{m_K^3} \varepsilon_{\mu\lambda\sigma\rho} K_\lambda R_\sigma Q_\rho \tag{2.19}$$

$$V_\nu' = \frac{f^*}{m_K} R_\nu + \frac{g^*}{m_K} Q_\nu + \frac{e^*}{m_K} R_\mu - \frac{h^*}{m_K^3} \varepsilon_{\nu\lambda\sigma\rho} K_\lambda R_\sigma Q_\rho \tag{2.20}$$

$$T_{\mu\nu} = K_\mu K_\nu - L_\mu L_\nu - \delta_{\mu\nu}(K^2 + m_e^2) + \varepsilon_{\mu\nu\sigma\rho} L_\sigma K_\rho \tag{2.21}$$

where $R = p_+ + p_-$, $Q = p_+ - p_-$, $K = p_e + p_\nu$, $L = p_e - p_\nu$ and * means complex conjugation.

Before integrating this probability function (also called density distribution) over the various variables, we first have a closer look at the form factors.

II.4 Partial wave expansion of the form factors

If we assume the semileptonic $|\Delta I| = \frac{1}{2}$ rule (and hence the $\Delta Y = \Delta S = \Delta Q$ rule) to be valid, I = 2 is excluded from the final di-pion state. The form factors f, g, e and h in Eqs. (2.11) and (2.12) then possess I = 0 and I = 1 parts only. From Bose-Einstein statistics for the two final pions, we know that the I = 0 part must have an even orbital angular momentum; whereas the I = 1 part must have an odd orbital angular momentum. Under the interchange of the two pions we have:

$$p_+ \leftrightarrow p_-,\ S_\pi \leftrightarrow S_\pi,\ S_1 \leftrightarrow S_1,\ \eta \leftrightarrow -\eta,\ \cos\theta_\pi \leftrightarrow -\cos\theta_\pi \quad *)$$

Denoting the isospin by a superscript, we predict the following relations for the various isospin form factors:

$$\begin{aligned}
f^0(S_\pi, S_1, \cos\theta_\pi) &= f^0(S_\pi, S_1, -\cos\theta_\pi) \\
f^1(S_\pi, S_1, \cos\theta_\pi) &= -f^1(S_\pi, S_1, -\cos\theta_\pi) \\
g^0(S_\pi, S_1, \cos\theta_\pi) &= -g^0(S_\pi, S_1, -\cos\theta_\pi) \\
g^1(S_\pi, S_1, \cos\theta_\pi) &= -g^1(S_\pi, S_1, -\cos\theta_\pi) \\
e^0(S_\pi, S_1, \cos\theta_\pi) &= e^0(S_\pi, S_1, -\cos\theta_\pi) \\
e^1(S_\pi, S_1, \cos\theta_\pi) &= -e^1(S_\pi, S_1, -\cos\theta_\pi) \\
h^0(S_\pi, S_1, \cos\theta_\pi) &= -h^0(S_\pi, S_1, -\cos\theta_\pi) \\
h^1(S_\pi, S_1, \cos\theta_\pi) &= h^1(S_\pi, S_1, -\cos\theta_\pi)
\end{aligned} \qquad (2.23)$$

For the angular momentum decomposition we follow the method of Lee and Wu [12] as applied by Berends et al [10]. They define a reference system in the di-pion system with x, y and z-axes along $\hat{c}$, $\hat{v} \times \hat{c}$ and $\hat{v}$ respectively. Vector $\hat{c}$ is the unit vector in the di-pion plane, perpendicular to the direction of flight of the di-pion, characterized by the unit vector $\hat{v}$ (see fig. II.1).

*) Note. The variable η can be written as $\eta = \beta\chi\cos\theta_\pi$; de dependence on η is therefore equivalent with dependence on $\cos\theta_\pi$.

The z-component of the total angular momentum of the di-pion system can only be m = 0 or m = ± 1, because the time component of the current is a scalar operator, while the space component is a vector operator acting on a scalar particle (the K^+ meson).

Denoting the hypercharge-changing hadron current by $J_\lambda^1 = V_\lambda^1 + A_\lambda^1$, we can therefore write:

$$\langle\pi^+\pi^-|J_4^1|K^+\rangle = \sum_{l=0}^{\infty} \langle\pi^+\pi^-|l,m=0\rangle \langle l,m=0|J_4^1|K^+\rangle$$

$$= i \sum_{l=0}^{\infty} P_l(\cos\theta_\pi)\Omega_4^l \qquad (2.24)$$

$$\langle\pi^+\pi^-|J_z^1|K^+\rangle = \sum_{l=0}^{\infty} \langle\pi^+\pi^-|l,m=0\rangle \langle l,m=0|J_z^1|K^+\rangle$$

$$= \sum_{l=0}^{\infty} P_l(\cos\theta_\pi)\Omega_z^l \qquad (2.25)$$

$$\langle\pi^+\pi^-|J_x^1 \pm iJ_y^1|K^+\rangle = \sum_{l=1}^{\infty} \langle\pi^+\pi^-|l,m=\pm1\rangle$$

$$\langle l,m=\pm1|J_x^1 \pm iJ_y^1|K^+\rangle = \sum_{l=1}^{\infty} \sin\theta_\pi \, P_l'(\cos\theta_\pi)\Omega_\pm^l \qquad (2.26)$$

The Ω^l's are the complex amplitudes corresponding with transitions to a state of angular momentum l; whereas the P_l's are the well-known Legendre polynomials.

Comparing Eqs. (2.24), (2.25) and (2.26) with Eqs. (2.11) and (2.12), the latter expressed in the di-pion system, we find

$$\frac{M_{\pi\pi}}{m_K} f + \frac{m_K^2 - M_{\pi\pi}^2 - M_{e\nu}^2}{2m_K M_{\pi\pi}} e = \sum_{l=0}^{\infty} P_l(\cos\theta_\pi)\Omega_4^l \qquad (2.27)$$

$$-\frac{k}{M_{\pi\pi}} e + \frac{M_{\pi\pi}\beta\cos\theta_\pi}{m_K} g = \sum_{l=0}^{\infty} P_l(\cos\theta_\pi)\Omega_z^l \qquad (2.28)$$

$$\frac{2M_{\pi\pi}\beta}{m_K} g = \sum_{l=1}^{\infty} P_l'(\cos\theta_\pi)\ (\Omega_+^l + \Omega_-^l) \tag{2.29}$$

$$\frac{2M_{\pi\pi}\beta k}{m_K^2} h = \sum_{l=1}^{\infty} P_l'(\cos\theta_\pi)\ (\Omega_-^l - \Omega_+^l) \tag{2.30}$$

From these expressions it follows in a straightforward way that

$$f = \sum_{l=0}^{\infty} P_l\left[\ \frac{m_K}{M_{\pi\pi}}\Omega_4^l + \frac{m_K^2 - M_{\pi\pi}^2 - M_{e\nu}^2}{2m_K k}\Omega_z^l\ \right] - \sum_{l=1}^{\infty} P_l'\cos\theta_\pi$$

$$\frac{m_K^2 - M_{\pi\pi}^2 - M_{e\nu}^2}{4m_K k}(\Omega_+^l + \Omega_-^l) \tag{2.31}$$

$$g = \sum_{l=1}^{\infty} P_l'\ \frac{m_K}{2M_{\pi\pi}\beta}\ (\Omega_+^l + \Omega_-^l) \tag{2.32}$$

$$e = -\sum_{l=0}^{\infty} P_l\ \frac{M_{\pi\pi}}{k}\Omega_z^l + \sum_{l=1}^{\infty} P_l'\cos\theta_\pi\ \frac{M_{\pi\pi}}{2k}\ (\Omega_+^l + \Omega_-^l) \tag{2.33}$$

$$h = \sum_{l=1}^{\infty} P_l'\ \frac{m_K^2}{2M_{\pi\pi}\beta k}\ (\Omega_-^l - \Omega_+^l) \tag{2.34}$$

We can rewrite the first equation as

$$f = f_s + f_p\cos\theta_\pi + \ldots\ldots \tag{2.35}$$

where

$$f_s = \frac{m_K}{M_{\pi\pi}}\Omega_4^o + \frac{m_K^2 - M_{\pi\pi}^2 - M_{e\nu}^2}{2m_K k}\Omega_z^o \tag{2.36}$$

$$f_p = \frac{m_K}{M_{\pi\pi}}\Omega_4^1 + \frac{m_K^2 - M_{\pi\pi}^2 - M_{e\nu}^2}{2m_K k}\left(\Omega_z^1 - \frac{\Omega_+^1 + \Omega_-^1}{2}\right) \tag{2.37}$$

With respect to g and h, only the p-wave term is relevant to the experimental treatment; as already shown, the form factor e cannot be determined due to kinematical factors. Note that f, g, e and h satisfy the isospin relations of Eq. (2.23) required by Bose-Einstein statistics.

The formalism developed is still too general for practical applications; we will therefore make the following additional assumptions:

a) We suppose only s- and p-wave π-π final states to be important. This assumptions seems reasonable in view of the dipion energy range involved. The effect of the presence of waves with $l \geqslant 2$ would be e.g. the appearance of $\cos\theta_\pi$ terms of order $\geqslant 2$ in Eq. (2.35) for the form factor f and hence terms of order > 2 in the $\cos\theta_\pi$ distribution.

b) We assume the validity of time-reversal invariance. This assumption is necessary, if one wants to derive π-π phase shifts from $Ke4$ decay.

Time-reversal invariance predicts the following relation between the phases of the amplitudes and the π-π phase shifts to hold (Watson-Fermi theorem [13]):

$$\Omega^l = |\Omega^l| e^{i(\delta_l + n\pi)} \qquad (2.38)$$

If T-invariance and assumption a) are valid, the term with Im gh^* should vanish in the distribution function; the absence of such a term however does not prove time-reversal invariance. Time-reversal violating effects can be studied in a more general way by comparing K_{l4} decay for K^+ and K^- mesons. This has been done in detail by Lee and Wu [12].

Using Eq. (2.38), we can make the decomposition

$$f = \overset{\gamma}{f}_s e^{i\delta_s} + \overset{\gamma}{f}_p e^{i\delta_p} \cos\theta_\pi$$

$$g = \tilde{g}\, e^{i\delta_p}$$
$$h = \tilde{h}\, e^{i\delta_p} \qquad (2.39)$$

where $\tilde{f}_s$, $\tilde{f}_p$, $\tilde{g}$ and $\tilde{h}$ are real.

c) In view of the limited data available we also make the assumption that $\tilde{f}_s$, $\tilde{g}$ and $\tilde{h}$ are constants. We therefore neglect their dependence on S_π, S_1 and $\cos\theta_\pi$ (or η).

Because of the angular momentum barrier we do allow a certain dependence on η for $\tilde{f}_p$; for this dependence we take the somewhat arbitrary substitution used by Ely et al [14]:

$$\tilde{f}_p \cos\theta_\pi = \frac{\eta}{m_K^2}\, \tilde{f}_p' = \frac{E_+ - E_-}{m_K}\, \tilde{f}_p' \qquad (2.40)$$

Assuming now $\tilde{f}_p'$ to be a constant, $\tilde{f}_p$ vanishes if $M_{\pi\pi}$ reaches its threshold value $2m_\pi$.

It is easy to see that the angular momentum barrier with respect to both other p-wave form factors $\tilde{g}$ and $\tilde{h}$ is automatically accounted for by their multiplication with the factor $Q = p_+ - p_-$ (see Eqs. (2.11) and (2.12)).

In our analysis we have also investigated the effect of a dependence of $\tilde{f}_s$ on the s-wave π-π scattering length a_o. We use the relativistic Watson enhancement factor [15]:

$$\tilde{f}_s = \frac{\tilde{f}_s^{\,p} \sin\delta_s}{a_o \beta} \qquad (2.41)$$

In this formula δ_s is the s-wave phase shift and β is the relativistic velocity of each pion in the di-pion rest system (see also Eq. (2.17)). The scattering length a_o is defined as the value of the scattering amplitude at zero kinetic energy.

$$a_o = \lim_{\beta \to 0} \frac{\sin\delta_s}{\beta} \qquad (2.41^a)$$

Extending this equation to non-zero energies, several expansions of $\cot\delta_s$ are used.

Firstly, there is the usual effective range expansion

$$q \cot\delta_s = \frac{1}{a_o} + \tfrac{1}{2} q^2 r_o \qquad (2.42)$$

where q is the π momentum in the di-pion rest frame (in m_π) *)

r_o is the effective range of the π-π potential (in pion wave lengths or m_π^{-1})

a_o is the l=0, I=0 scattering length (in pion wave lengths or m_π^{-1})

This relation is not valid over the whole q-range ($0 < q \lesssim 1.2$) observed in this experiment.

Secondly, one has the Chew-Mandelstam parametrization [16], which is used in the Ke4 analysis of Ely et al [14]:

$$\cot\delta_s = \frac{1}{a_o \beta} + \frac{2}{\pi} \ln \{ \frac{M_{\pi\pi}(1 + \beta)}{2m_\pi} \} \qquad (2.43)$$

It turns out, however, that Eq. (2.43) is in disagreement with recent s-wave π-π interaction results, obtained from single pion production (see section VII.2 and ref. [17]). An alternative expression, used by Zylbersztejn et al [18] and also applied in our analyses, is

$$\tan\delta_s = \beta \{a_o + 2\alpha(M_{\pi\pi}^2 - 4m_\pi^2)\} \qquad (2.44)$$

*) Note that $q = \sqrt{\frac{\beta^2}{1 - \beta^2}} = \sqrt{\frac{M_{\pi\pi}^2 - 4m_\pi^2}{4m_\pi^2}}$.

On the basis of current algebra Weinberg [19] predicted a value $\frac{1}{32f_\pi^2} \simeq \frac{0.025}{m_k^2}$ for the factor α.

Figures II.4^{a,b,c} show δ_s as a function of $M_{\pi\pi}$ for resp. the parametrizations Eqs. (2.44), (2.43) and (2.42) and some typical values of the parameters a_o and r_o.

Substitution of Eqs. (2.39) and (2.40) together with Eqs. (2.19) and (2.20) in Eq. (2.13) shows that it is possible to have $\tilde{f}_s$ as an overall factor in the decay probability. This factor can be evaluated subsequently if we know the partial decay rate (or branching ratio) for Ke4 decay in addition to the quantities determined from the relative spectral shapes now defined as:

$$\begin{aligned} \nu &= \tilde{f}_p' / \tilde{f}_s \\ \eta &= \tilde{g} / \tilde{f}_s \\ \gamma &= \tilde{h} / \tilde{f}_s \\ &<\delta_s - \delta_p> \text{ or } a_o \end{aligned} \qquad (2.45)$$

Note that if we parametrize with the scattering length a_o instead of the mean phase shift difference $<\delta_s - \delta_p>$, we make the additional assumption that in the $M_{\pi\pi}$-region considered the p-wave contribution to the π-π interaction can be neglected.

Pais and Treiman [9] have shown that one can obtain information on $<\delta_s - \delta_p>$ independent of the values of the form factors and of assumptions regarding their energy dependence. Their method is based on the observation that some small correlation coefficients in the combined $\theta_l - \phi$ distribution are equal up to a factor $\tan <\delta_s - \delta_p>$.

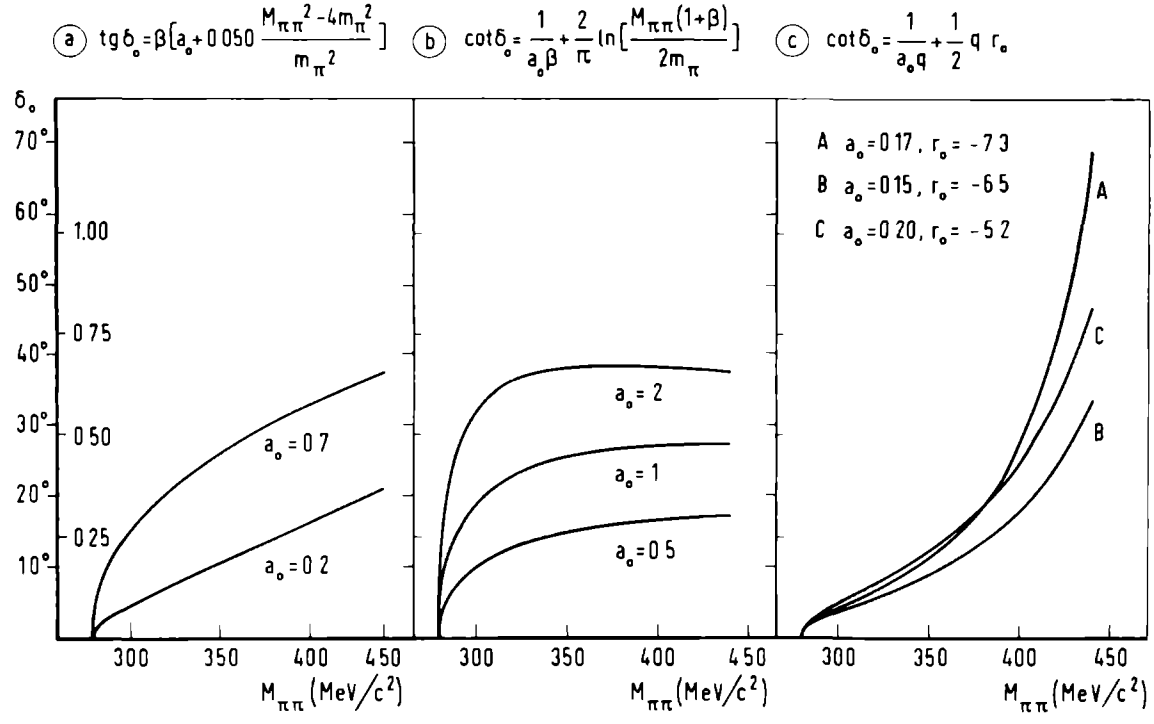

Fig. II.4. Three parametrizations of the π-π s-wave phase shift δ_o as a function of the eff. di-pion mass $M_{\pi\pi}$. Curves are drawn for some typical values of a_o and r_o (both expressed in units m_π^{-1}).

Integration over $\cos\theta_1$ or ϕ cancels all these terms; this method therefore requires distributions which are kept differential in the above variables. For small samples this method becomes of course unpractical.

References - chapter II

1) Particle data group, Rev. Modern Physics 45, S1 (april 1973).
2) R.P. Feynman and M. Gell-Mann, Phys. Rev. 109, 193 (1958) and Proc. Padua-Venice Conf. on Mesons and Recently Discovered Particles (1957).
3) R.H. Dalitz, Phys. Rev. 94, 1046 (1954).
   E. Fabri, Nuovo Cimento 11, 479 (1954).
4) J.H. Christenson et al, Phys. Rev. Letters 13, 138 (1964).
5) N. Cabibbo, Phys. Rev. Letters 10, 531 (1963).
6) J.D. Jackson, "Weak Interactions" in Elementary Particle Physics and Field Theory (Brandeis lectures 1962), W.A. Benjamin (1963).
7) N. Cabibbo and A. Maksymowicz, Phys. Rev. 137, B438 (1965) and Phys. Rev. 168, 1926(E) (1968).
8) C. Kacser, P. Singer and T.N. Truong, Phys. Rev. 137, B1605 (1965) and Phys. Rev. 139, AB5(E) (1965).
9) A. Pais and S.B. Treiman, Phys. Rev. 168, 1858 (1968).
10) F.A. Berends, A. Donnachie and G.C. Oades, Phys. Rev. 171, 1457 (1968).
11) W. Schweinberger et al, Phys. Letters 36 B, 246 (1971).
12) T.D. Lee and C.S. Wu, Ann. Rev. Nucl. Science 15, 381 (1965) and 16, 471 (1966).
13) K.M. Watson, Phys. Rev. 95, 228 (1954).
   E. Fermi, Nuovo Cimento 2, suppl. 1, 17 (1955).
14) R.P. Ely et al, Phys. Rev. 180, 1319 (1969).
15) K.M. Watson, Phys. Rev. 88, 1163 (1952).
16) G.F. Chew and S. Mandelstam, Phys. Rev. 119, 467 (1960).
17) J.L. Peterson, Physics Reports 2C,(1971).
18) A. Zylbersztejn et al, Phys. Letters 38B, 457 (1972).
19) S. Weinberg, Phys. Rev. Letters 17, 616 (1966).

III. EXPERIMENTAL TECHNIQUE AND SET-UP

III.1 The beam

The beam used to obtain and transport K^+ mesons is shown schematically in fig. III.1. The starting point was an internal beryllium target in the 28 GeV proton-synchrotron of CERN, bombarded every 2.3 seconds by about 10% of the circulating proton beam (approx. 7×10^{11} protons per pulse). The beam set-up was built in the so-called North Hall and had a total length of 26 meters. The K^+ beam was electrostatically separated from its π^+ and μ^+ components in two stages. The separated beam had a final momentum of 800 MeV/$_c$.

As both stages of the separation were nearly identical, we describe only the first one in somewhat more detail. The beam, produced at an angle of 15° with respect to the PS ring, was first sent through a special bending magnet (M1) giving a second deviation of 15°. It then met two collimator slits (D1, D2) and two quadrupole magnets (Q1, Q2), focussing the beam horizontally and vertically resp. In a subsequent bending magnet (M2) the beam was again deviated (22°) and sent into the first electrostatic separator (S1). A quadrupole magnet (Q3) focussed the beam vertically and a collimator slit (MS1) stopped the particles of unwanted mass. Beyond the field magnet Q4 the particle and momentum selection set-up described above was repeated (in a second stage: M3 to MS2) in order to improve the selection.

To make the kaons stop approximately in the middle of the bubble chamber in a well-spread manner, a copper degrader was placed in front of the entrance window of the chamber, lowering the average momentum of the kaons to about 550 MeV/$_c$.

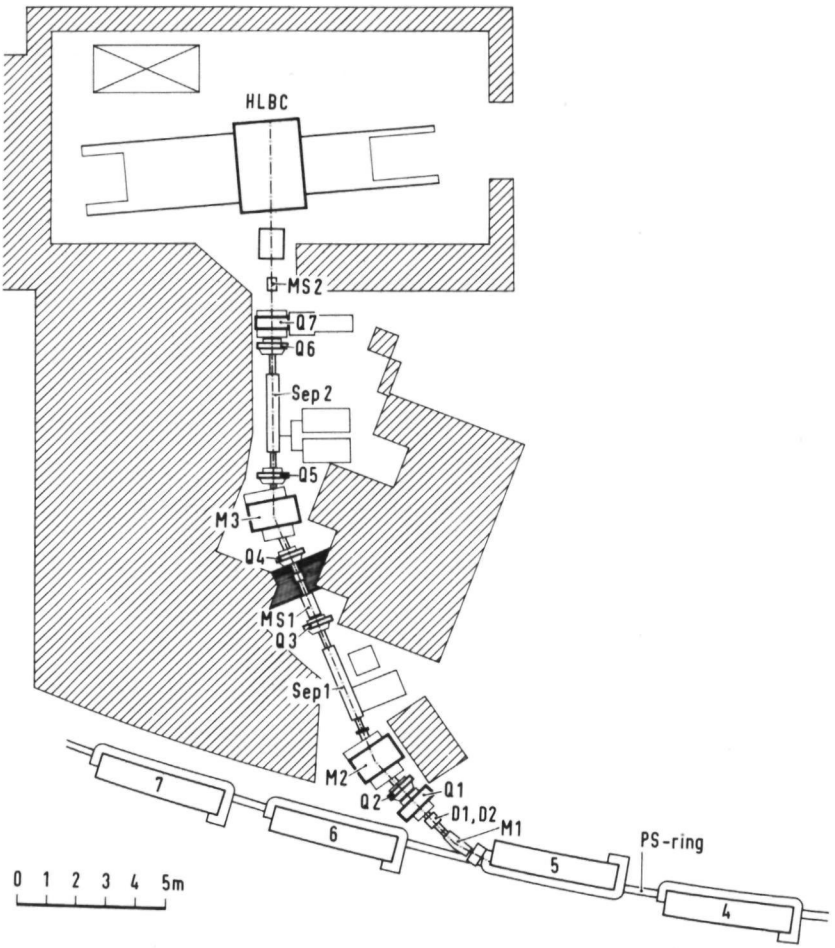

Fig. III.1. The beam set-up.

In this experiment an average of 7 kaons entering the chamber per pulse was maintained.

In the chamber we had about 15% contamination from pions and muons, which mainly orginated from kaons decaying in flight after the second separator stage. They did not cause any significant decay background as most of them crossed the chamber.

III.2 The bubble chamber

The bubble chamber used was the enlarged heavy liquid bubble chamber of CERN, shown schematically in fig. III.2. Its shape is a horizontal cylinder with a diameter of 1.2 meters, a depth of 1.0 meter and a capacity of 1182 liters. The cylinder is illuminated by 8 flash tubes situated along the inner wall parallel to the cylinder axis.

The compression and decompression of the liquid is accomplished by a plastic membrane, masked by a freely suspended plate to improve the hydrodynamic flow of the liquid during expansion and to hide boiling around the membrane after the expansion. At the frontside the chamber is closed by a glass window with a thickness of 268 mm. On the inner surface of this glass five fiducial marks are engraved, forming a reference frame for the measurements. A 1.8 m long security tank is placed between the window and the cameras.

To obtain good stereoscopic reconstruction three cameras are used simultaneously, taking pictures on 70 mm film. The cameras are placed in such a way that they form the angular points of an equilateral triangle with a base length of 84 cm. The distance between cameras and the inner surface of the glass window is 220.3 cm.

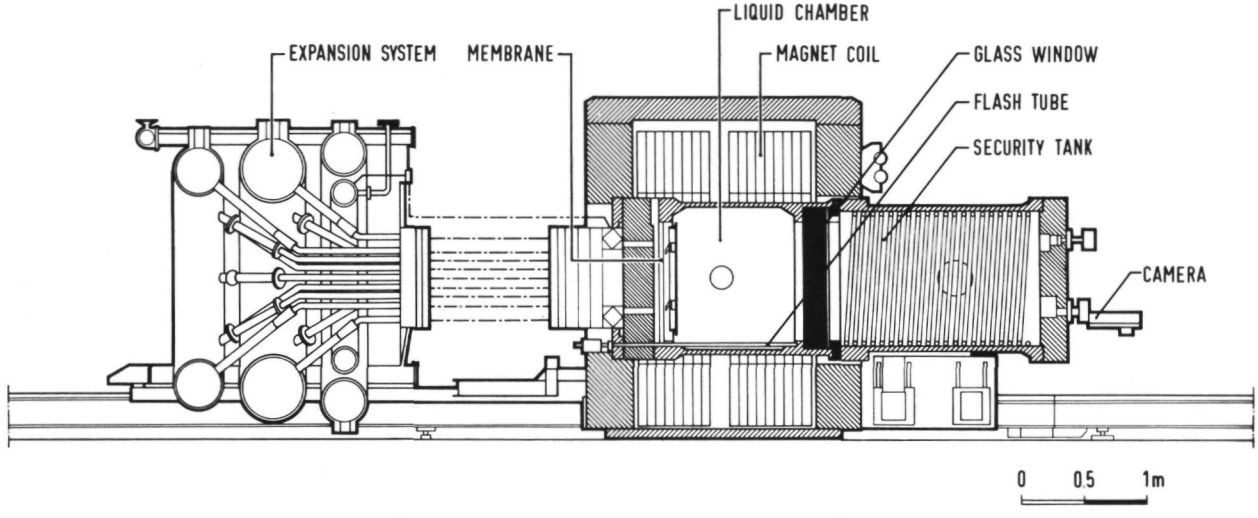

Fig. III.2. Longitudinal section of the CERN heavy liquid bubble chamber.

The chamber body is surrounded by a 100 ton magnet, producing a magnetic field in the middle of the chamber of 1.95 Tesla at a current of 5000 Amperes (power consumption 2 MW). The field axis is along the cylinder axis of the bubble chamber body.

III.3 The liquid

The chamber is designed to work with heavy liquids such as propane or a freon. Table III.1 summarizes some properties of various liquids [1].

In the study of decay processes (including γ-rays), the choice of the liquid is the result of a compromise between γ-conversion probability and stopping power on the one hand, π-μ-e decay *) visibility and measurability on the other hand.

Table III.1

liquid	density ρ ($^{g}/_{cc}$)	min. $\frac{-dE}{dx}$ ($^{MeV}/_{cm}$)	radiation length X_o (cm)	operation temperature	operation pressure (atm)
H_2	0.06	0.248	970	26.5°K	4.5
He	0.12	0.242	683	4.2°K	1.0
C_3H_8	0.41	0.935	109	58°C	19
C_2F_5Cl	1.2	∿2.1	∿25	40°C	14
CF_3Br	1.5	∿2.3	∿11	30°C	18

*) Note. The π^+ meson decays as follows:

$\pi^+ \rightarrow \mu^+ \nu \searrow e^+ \nu\bar{\nu}$; the μ momentum is only 30 $^{MeV}/c$.

As the X2 experiment was primarily intended to study the Kμ3 and Ke3 decay modes, both containing a π^o and hence γ-rays, the γ-conversion efficiency was a primary concern. Therefore C_2F_5Cl was chosen, giving an average probability of ∿70% for one γ-ray to convert into an electron pair within the chamber. In this liquid, the error on the measured γ-ray energy is about 30%.

The longest decay track, namely the μ^+ from Kμ2 decay, has a length of 56 cm in C_2F_5Cl and has therefore a good chance to be seen up to the end, while the probability of seeing the short μ^+, 1.5 mm, from π-μ-e decay is about 60%.

As no γ-rays are produced in Ke4 decay, the chosen liquid is certainly not optimal for the identification and measurement of this particular decay mode. A liquid with less stopping power would have been more desirable.

III.4 Identification of secondary particles

Most secondary products which play a role in K^+ decay can often be recognized by their typical behaviour in the bubble chamber liquid. If the tracks are long enough, distinction between charges is trivial due to the bending of the tracks in the magnetic field of the chamber.

From the point of view of the observed interactions we distinguish between a) decay, b) stopping, c) scattering, d) radiation and e) nuclear absorption. We discuss shortly each phenomenon:

a) Decay occurs for the secondary π^+, μ^+ and π^o particles in the following ways:

i) $\pi^+ \rightarrow \mu^+ \nu$ with a branching ratio of almost 100%

ii) $\mu^+ \rightarrow e^+ \nu \bar{\nu}$ also with a branching ratio of almost 100%

iii) $\pi^o \rightarrow \gamma\gamma$ with a branching ratio of 98.8%

$\pi^o \rightarrow \gamma e^+ e^-$ with a branching ratio of 1.2%

From the sequentially occuring weak decays i) and ii) we get the so-called π-μ-e chain. If the π^+ decays at rest a momentum of only 30 MeV/$_c$ is left for the μ^+, corresponding to a μ^+ range of 1.5 mm in C_2F_5Cl. It is impossible to decide between a μ-e chain and a π-μ-e chain in those cases where the μ of the latter is invisible, for example because of a steep dip of the μ.

The electromagnetic interaction iii) produces 1 or 2 photons or γ-rays. As mentioned in section III.3, a photon becomes observed and measurable through its conversion into an electron pair (often called "gamma" by bubble chamber physisists) or through the Compton-effect, producing only 1 electron. At a photon energy of about 20 MeV both effects are equally probable; at higher energies the probability for pair creation increases, while the probability for the Compton-effect decreases. We define the conversion length as the distance over which the intensity of a photon beam has decreased by a factor e. This length is about 32 cm in C_2F_5Cl. The photon energy is estimated by measuring the energy of the Compton electron or the electron pair.

Because the mean life of the π^o is so short (0.84×10^{-16} sec), one can consider the origin of the decay photons and the origin of the π^o itself as one and the same point(the K^+ decay point). Knowing this point, the directions of the photons and their energies, it is in principle simple to determine the energy and direction of the pion (1 constraint fit).

Because photons play no role in Ke4 decay, we omit a more extensive treatment of this subject.

b) Stopping of the more massive particles is mainly caused by excitation and ionization of atomic electrons. Both are electromagnetic interactions (non-radiative, distant collisions) between the particle and the peripheral electrons of the atoms of the liquid. It is the energy, deposited in the liquid as a consequence of these processes that is responsible for the formation of bubbles.

In a given medium the energy loss per unit length, due to ionization, is a function only of β, the relativistic velocity of the particle [2]. Let E_o and p_o be the initial energy and momentum of a particle with rest mass m. Then it follows from

$$\beta = \frac{p}{E}, \quad \gamma = \frac{1}{\sqrt{1-\beta^2}} = \frac{E}{m}, \quad \beta\gamma = \frac{p}{m} \tag{3.1}$$

that the range R, i.e. the distance travelled by the particle up to its stopping point, is

$$R = \int_m^{E_o} \frac{1}{dE/dx}\, dE = \int_m^{E_o} \frac{1}{f(\beta)}\, dE = m \int_o^{\beta_o} F(\beta)d\beta = mF(\frac{p_o}{m}) \tag{3.2}$$

where f, F and *F* are functions of β. The relation *F* between $\frac{R}{m}$ and $\frac{p}{m}$ is nearly exponential (fig. III.3) and is used to calculate the momentum of pions and muons once their range is known. On the other hand, if we are able to compute the momentum of a particle, this relation enables us to identify the particle from its range.

For electrons $\beta \approx 1$ and therefore $(\frac{\partial E}{\partial x})_{ion.}$ can be considered constant. However, radiative processes make range measurements of electrons useless.

c) Scattering (single or multiple) is the angular deviation due to collisions of a particle with the medium.

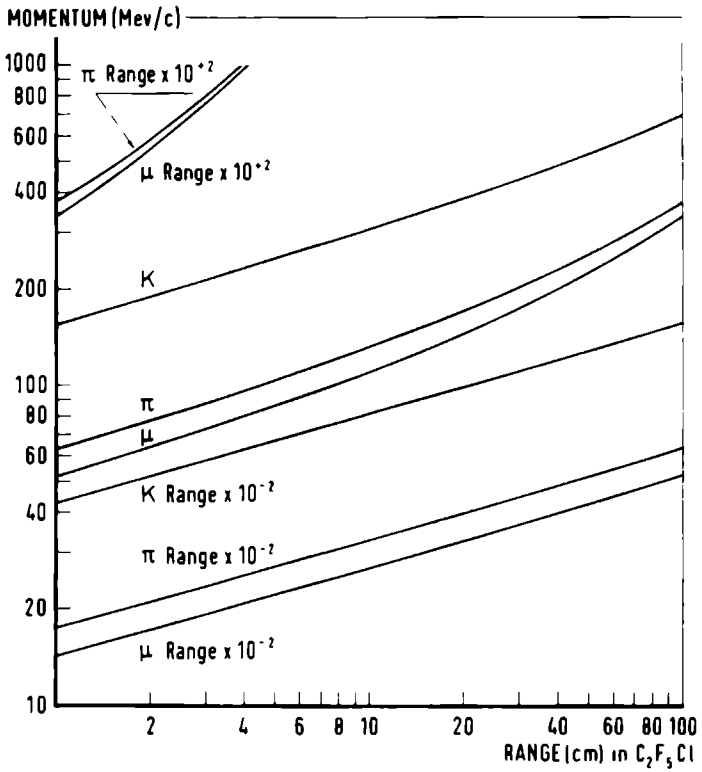

Fig. III.3. Range vs. momentum curves.

All charged particles moving in the bubble chamber suffer more or less from this effect. Sometimes a clearly visible elastic or inelastic scatter occurs, making a measurement of the track curvature useless beyond the scatter point. Much more often however, the scatters are invisible and occur very

frequently along the track. For this reason these tracks will show deviations from a helix, the normal path expected for a charged particle in a magnetic field.

d) Radiative collisions form an important part of the energy loss of electrons traversing matter. For light particles the collisions with nuclei of the medium result in the emission of quanta ("bremsstrahlung"). Quantum theoretically "soft" quanta are more probably emitted than energetic ones. As a consequence of this effect the curvature of an electron track increases rapidly and the track spirals.

The radiation length X_o is defined as the distance over which an electron has on the average its energy reduced by a factor e. This distance is about 25 cm in C_2F_5Cl.
We further define:

$$b = \frac{1}{X_o \ln 2} \quad \text{and} \quad y = \ln \frac{E_o}{E} \tag{3.3}$$

The probability that an electron of initial energy E_o has its energy reduced to a value between E and E + dE as a consequence of bremsstrahlung after traversing a thickness x, is approximately given by the expression [3]:

$$w(x, y)dE = \frac{e^{-y} y^{bx-1}}{\Gamma(bx)} dE \tag{3.4}$$

Γ is the gamma function: $\Gamma(bx) = \int_0^\infty e^{-y} y^{bx-1} dy$ (3.5)

Thus the probability that the electron has an energy $E = E_o e^{-y}$ between x and x + dx is given by

$$U(x, y)dx = - \frac{\partial w(x, y)}{\partial x} dx \tag{3.6}$$

For some y-values we show in fig. III.4 this distribution as a function of the distance x travelled by the electron in the liquid. As can be easily seen, the most probable value for x is $x = \frac{y}{b} = X_o \ln 2 . \ln \frac{E_o}{E}$.

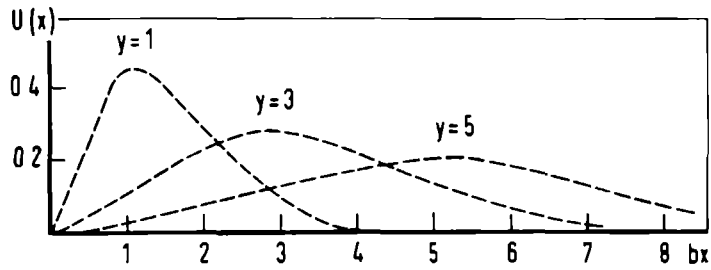

Fig. III.4. Distribution function of the distance travelled by an electron in the liquid for some fixed values of relative energy loss.

In general, one can make the assumption that all quanta of bremsstrahlung are emitted along the targent to the trajectory of the emitting electron. As a consequence, the dip of an electron track is not affected by the radiation process.

e) Nuclear absorption is the process by which most of the negative pions disappear. Instead of the decay $\pi^- \rightarrow \mu^- \bar{\nu}$, almost all negative pions are captured by one of the nuclei of the medium.

III.5 Determination of momenta

The measurement of the momentum of a particle depends on the interaction which this particle undergoes. A standard way is the measurement of the radius of curvature ρ of the track. From this the momentum p (in MeV/c) follows:

$$p = \frac{0.3H\rho}{\cos\lambda} \qquad (3.7)$$

where H is the magnetic field in kilogauss

ρ is the radius in cm

λ is the dip (i.e. angle between the track and a plane perpendicular to the direction of the magnetic field).

Eq. (3.7) is useful as long as Δρ is small and is therefore commonly applied to tracks in hydrogen bubble chambers. However, due to multiple scattering, Δρ is rather big ($\sim$ 30%) in heavy liquids. Therefore the momentum is more accurately ($\lesssim$ 3%) determined by measuring the range of the corresponding track and by applying the range-momentum relation. As the mass of the particle is involved in this relation, the momentum is dependent on the type of particle.

For electrons Eq. (3.7) is equally useless; instead of multiple scattering errors this is now due to the large radiation loss errors. For the same reason a range-momentum relation can not be derived. Moreover, the range of an electron is in general not an easily measurable quantity.

Behr and Mittner [4] have developed a method to determine a more precise estimate for the energy of an electron in heavy liquids. They arrived at a correction to be applied to Eq. (3.7), an expression for the error in the momentum and a method for working out a so-called optimum length. All these

formulae are dependent on the assumption that a single radiation of a quantum with energy greater than a certain fraction of the initial electron energy can be recognized by a sudden change in curvature. Electron tracks can then at most be measured up to such a discontinuity; if it appears at a distance greater than the optimum length or it appears not at all, only measurements up to the optimum length are used in the calculation. Using this method one obtains a momentum error of about 30% at an average optimum length of about 10 cm in C_2F_5Cl.

A theoretically more elaborate method to measure electrons in heavy liquids is the so-called "spiral" method of Morellet [5]. For energies up to 168 MeV (the max. electron energy in $Ke4$ decay), this spiral method has no advantage over the Behr-Mittner method. We therefore used the Behr-Mittner method because it is simpler to program.

As a conclusion of this chapter we show some photographs of the X2 experiment in figs. III.5, 6 and 7.

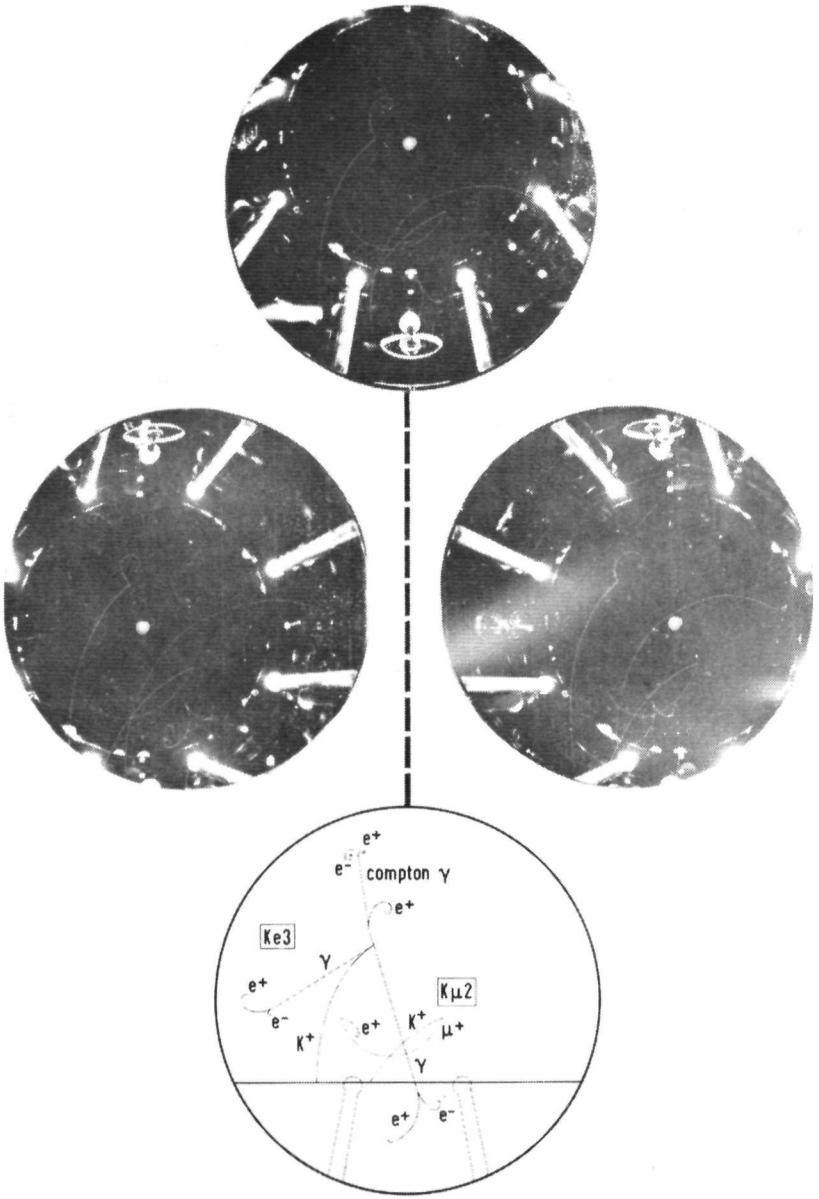

Fig. III.5. A Ke3 and a Kμ2 decay, seen in three views; the horizontal line in the drawing forms the lower boundary of the scanning region.

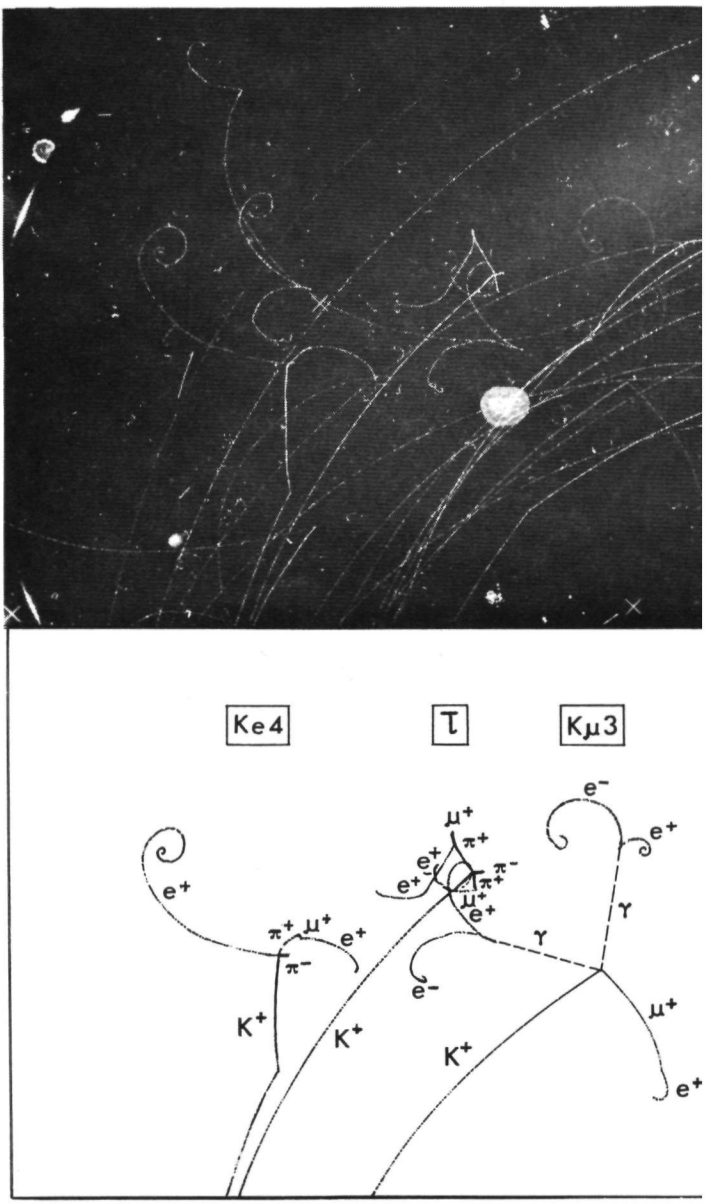

Fig. III.6. A Ke4, a τ and a Kμ3 decay.

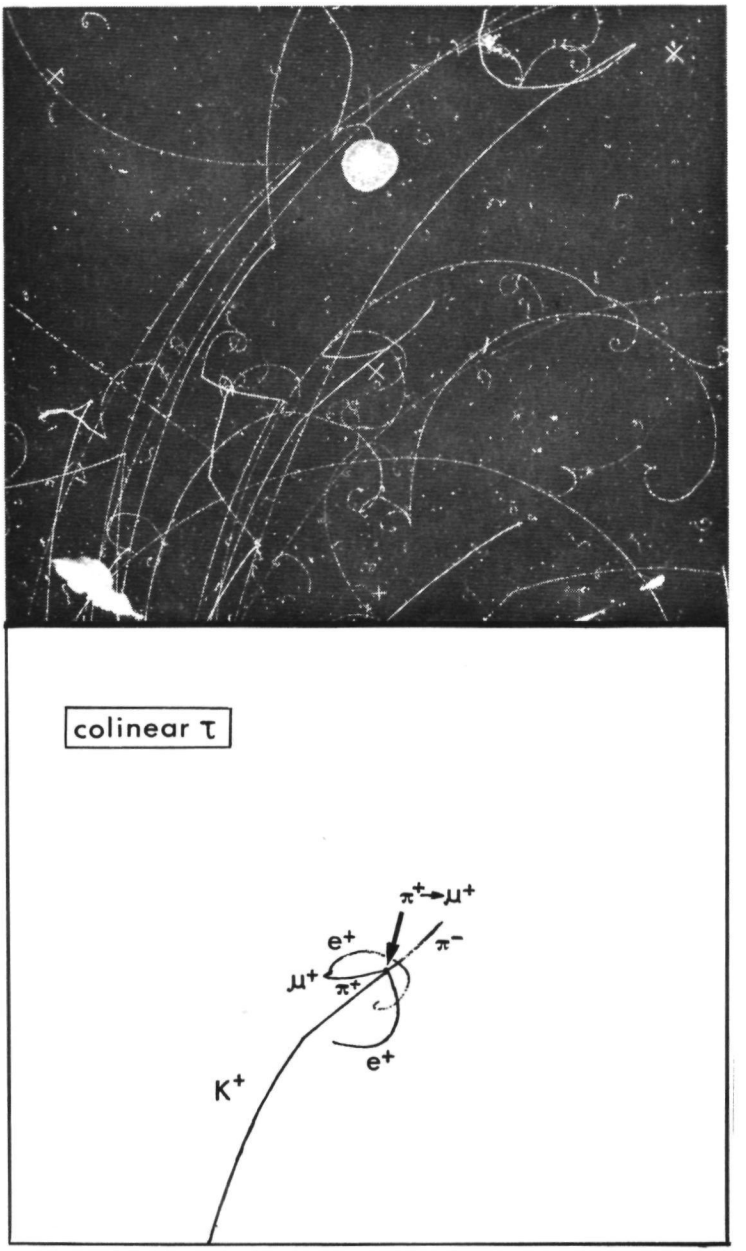

Fig. III.7. Colinear τ decay; decays of this type form the major background for Ke4 scanning.

References - chapter III

1) R.P. Shutt (ed.), Bubble and Spark Chambers, vol. 1 & 2 (Academic Press, 1967).

2) U. Fano, Annual Review of Nuclear Science, 13, 1 (1963).

3) H.A. Bethe and W. Heitler, Proc. Royal Soc., A146, 83 (1934).

4) L. Behr and P. Mittner, Nucl. Instr. and Methods, 20, 446 (1963).

L. Behr and P. Mittner, CERN 63-23, 157 (1963).

5) D. Morellet in Methods in Subnuclear Physics, vol. IV, part 3, 1968 Herceg Novi lectures (Gordon and Breach, 1970).

IV. DATA COLLECTION

IV.1 Scanning

In the fiducial region of each picture, chosen as shown in fig. III.5, a search was made for all topologies compatible with the Ke4 decay. Further, in every tenth picture the number of τ's was recorded. From this counting we decuded the total number of K^+ mesons decaying in the fiducial region, using the known τ branching ratio (5.59 ± 0.03)%.

To be classified as a Ke4 decay candidate a topology must satisfy the following criteria:

a) from ionization the incoming K^+ track must appear to be stopping

b) the secondary tracks must be identified as possibly a π^+, a π^- and an e^+ in the case of Ke^+4 decay; two π^+'s and an e^- in the case of Ke^-4 decay.

Clear τ topologies were eliminated. In principle three charged secondaries were required. To avoid a systematic loss of Ke4's during the scanning, due to bad visibility or wrong identification of secondary tracks, all topologies with only two visible secondaries satisfying criterion b) were also accepted.

For the topologies scanned, the following decay processes are in principle possible:

A. Three charged secondary tracks

1. Ke4 decay, giving two pions and an electron.
2. τ decay, where one of the positive pions has a very short or steeply dipping track and only the electron of the corresponding π-μ-e chain is detected.
3. Kμ4 decay, with two pions and a muon as visible secondaries.

4. Kπ2 decay, accompagnied by a Dalitz pair, i.e. $K^+ \rightarrow \pi^+ \gamma e^+ e^-$.
5. τ' decay, accompagnied by a Dalitz pair, i.e. $K^+ \rightarrow \pi^+ \pi^o \gamma e^+ e^-$.

B. Two charged secondary tracks

1. Ke4 decay, where one of the secondary tracks is undetected because of one of the following reasons:
   undetected π^+: interaction near to the production point or steeply dipping π-μ-e chain.
   undetected π^-: interaction or absorption near to the production point, short or steeply dipping track.
   undetected e^+: short or steeply dipping track.
2. τ decay with one of the pions unseen for one of the same reasons.
3. Kμ4 decay with one of the secondary tracks undetected.
4. Kπ2 or τ' decay with a Dalitz pair of which only the electron or the positron is visible.

The category A2 consists mainly of τ decays with a π^+ and a π^- of approximately the same momentum, flying in opposite directions. This topology is often described as colinear or back-to-back τ. As the τ decay is about 1500 times more probable than Ke^+4 decay and as both the Ke4 and colinear τ topologies are very similar, the latter form the major source of the scanning background (see fig. III.7).

All candidates were noted down for subsequent inspection by a physicist. After the physicists check a sample of about 2000 Ke^+4 candidates was retained for measurement; of this sample approximately 100 were found in Nijmegen.

Not a single candidate for Ke^-4 decay was found.

IV.2 Measurement and reconstruction

In Nijmegen the measurements of the ∿100 Ke4 candidates were done on the so-called NIJDAS tables, equiped with MANGIASPAGO digitizers. With the help of these digitizers the relative lengths of two strings, connected to a viewer, were measured in a bipolar coordinate system with a least count of 50 microns on the projection table. The pulses coming from the digitizers were fed into LABEN counters, connected (via read-out hardware) to an IBM-026 punching device. For each track in each view, a number of coordinates was punched into cards.

These cards were processed on the IBM 360/50 of the University Computing Centre using the geometry program RANGE 4, an adapted version of the Turin RANGE program for heavy liquids [1]. The task of the geometry program is to reconstruct the events in real space and to calculate momenta, azimuth and dip angles for all measured tracks together with the associated external errors. The output from this program was in the form of printed paper and a magnetic tape.

As already mentioned in chapter III the momentum of stopping pions was calculated from range rather than curvature. The electron momenta were calculated using the Behr-Mittner method. Stopping pions having a break point (visible scatter) were measured such, that the total range could be reconstructed from the part before and after this point.

Pions interacting in flight and electrons with a break point were measured up to the interaction point only.

The geometry program also calculated the effective momentum p_m and the effective energy E_m of the assumed di-lepton system these quantities being at the same time resp. the missing

momentum and missing energy with respect to the di-pion system. From p_m and E_m the effective di-lepton mass m_m, which is also the missing mass with respect to the di-pion system, is calculated using

$$m_m^2 = E_m^2 - p_m^2 \qquad (4.1)$$

As E_m and p_m are still unfitted quantities it can happen that m_m^2 is negative; in practice most events with negative m_m^2 appear to be Ke4 or τ decay with the K^+ decaying in flight.

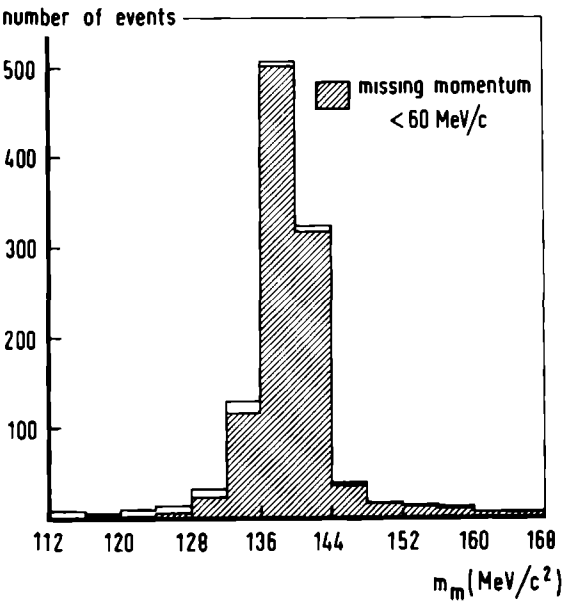

Fig. IV.1. Missing mass distribution of ∿1100 Ke4 candidates.

Fig. IV.1 shows the m_m distribution for ∿1100 events in the region around 140 MeV/c^2. It is clear that there exists a strong peak at the pion mass, indicating that most of the

candidates are τ decays with an undetected π-μ decay chain. This can also be concluded from the shaded area in fig. IV.1, which shows the fraction of the events satisfying the additional criterion $p_m < 60$ MeV/c (pion range < 8.5 mm).

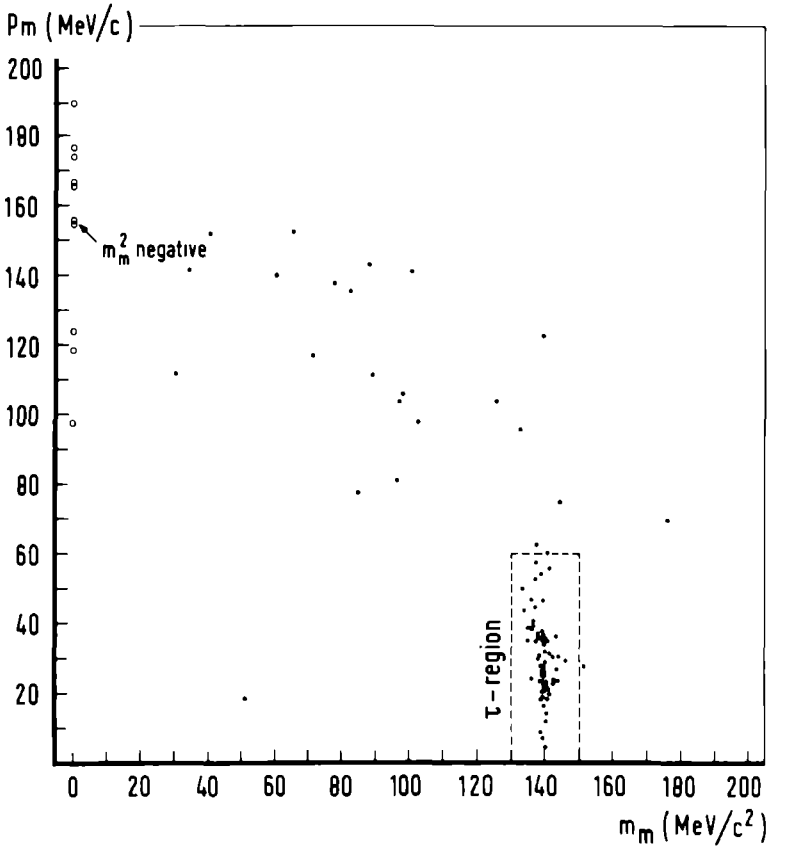

Fig. IV.2. Missing mass vs. missing momentum for 101 Ke4 candidates.

Fig. IV.2 shows the same effect on a m_m versus p_m distribution for the 101 Ke4 candidates, found in Nijmegen.

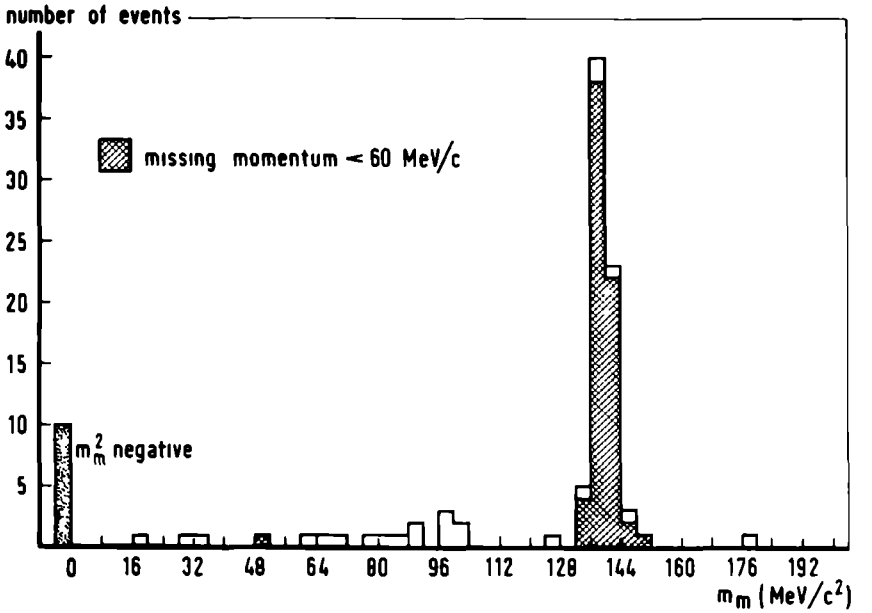

Fig. IV.3. Missing mass distribution of 101 Ke4 candidates.

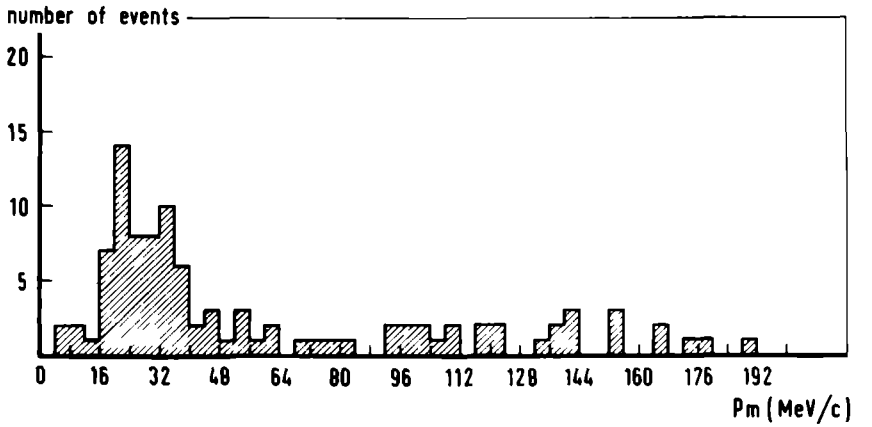

Fig. IV.4. Missing momentum distribution of 101 Ke4 candidates.

Fig. IV.3 and IV.4 are the corresponding projected distributions. To find a method to eliminate the large background of τ decays is not difficult and is in fact suggested by fig. IV.2: we simply rejected all candidates with $p_m < 60$ MeV/c and $130 < m_m < 150$ MeV/c^2. This τ 'box' can also contain good Ke4's, but their number is only about 1% of the total number of Ke4's.

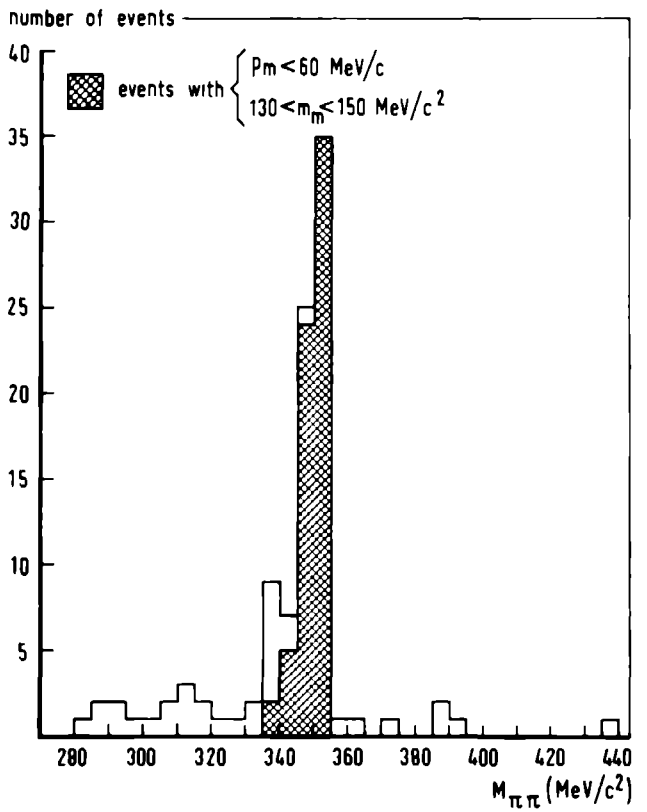

Fig. IV.5. Distribution of the effective di-pion mass.

In fig. IV.5 we show the distribution of $M_{\pi\pi}$, the effective di-pion mass. It can be seen that the τ background peaks

around $M_{\pi\pi} \sim 350$ MeV/c^2. Fig. IV.6 shows the distribution of $\cos\alpha_{\pi\pi}$, the cosine of the di-pion opening angle. From this figure we conclude that the background τ's are indeed colinear.

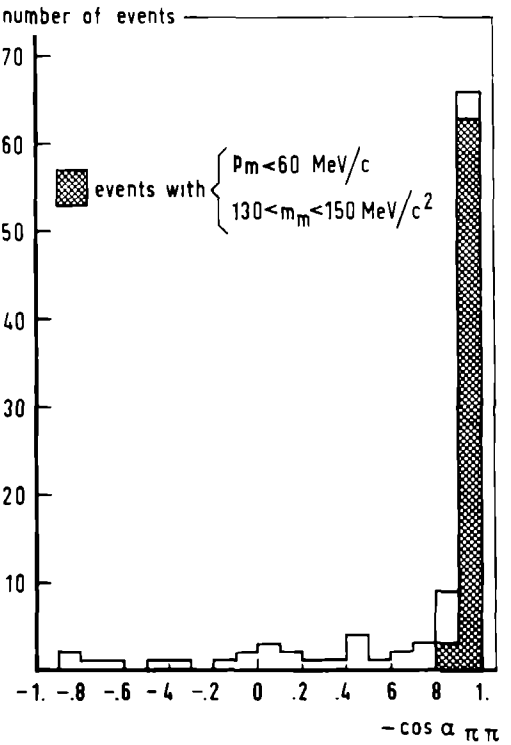

Fig. IV.6. Distribution of the di-pion opening angle.

In fig. IV.7 are given distributions of the sines of the dip angle of e^+, π^+ and π^- resp. For large homogeneous samples one expects flat distributions; fig. IV.7[a] indicates that some events with steeply dipping electrons could have been lost in the scanning. The same effect was observed in the final Ke4 sample of the whole collaboration (fig. IV.8).

After the τ box cut, the Nijmegen sample was reduced to 35 candidates; that of the complete collaboration to $\sim$ 300 events.

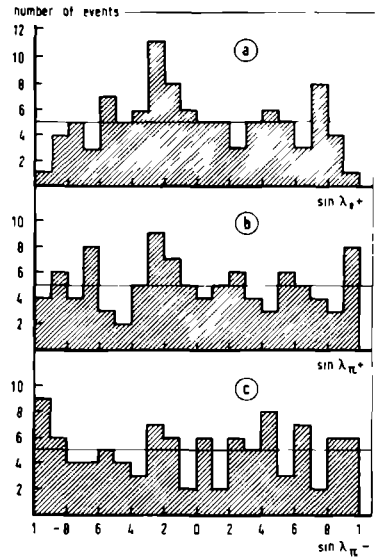

Fig. IV.7. Distributions of the dip angles of 101 Ke4 candidates.

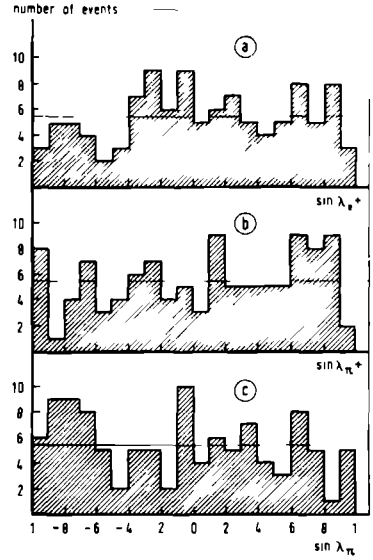

Fig. IV.8. Distributions of the dip angles of 109 Ke4's.

A photographic print was made of each remaining candidate and only this restricted sample was retained for further analysis.

The magnetic output tape of the geometry program served as input for the kinematics program, for which a heavy liquid version of the so-called GRIND program was used [2]. This program can test the candidate against any desired hypothesis; it does so by making mass assignments to all tracks involved and fitting a set of momenta and angles as close as possible to the measured ones. A χ^2 variate is used as a measure for the probability of the fit.

To perform a more homogeneous and compatible analysis, the whole sample was remeasured at CERN with the on-line geometry program DOLL [3]. It was then analyzed in GRIND with the hypotheses of table IV.1.

Table IV.1

	no	hypothesis	number of constraints
Ke4 hypotheses	1	$K_r^+ \to \pi^+\pi^-e^+\nu_u$	1
	2	$K_v^+ \to \pi^+\pi^-e^+\nu_u$	0
	3	$K_r^+ \to \pi_v^+\pi^-e^+\nu_u$	0
	4	$K_r^+ \to \pi^+\pi^-e_v^+\nu_u$	0
	5	$K_r^+ \to \pi^+\pi_v^-e^+\nu_u$	0
τ hypotheses with zero range π^+	6	$K_r^+ \to \pi^+\pi_z^+\pi^-$	4
	7	$K_v^+ \to \pi^+\pi_z^+\pi^-$	3
	8	$K_r^+ \to \pi_v^+\pi_z^+\pi^-$	3
	9	$K_v^+ \to \pi_v^+\pi_z^+\pi^-$	2
	10	$K_r^+ \to \pi^+\pi_z^+\pi_v^-$	3
	11	$K_v^+ \to \pi^+\pi_z^+\pi_v^-$	2
τ hypotheses with unknown π^+	12	$K_r^+ \to \pi^+\pi_u^+\pi^-$	1
	13	$K_v^+ \to \pi^+\pi_u^+\pi^-$	0

The subscripts attached to the particle names have the following meaning:

r = decaying at rest

v = momentum unknown (e.g. decay in flight)

u = momentum and direction unknown

z = "zero range" (see text)

The label "zero range" means that a momentum of (0 ± 15) MeV/c and arbitrary dip and azimuth values (with standard deviations π and 2π resp.) were used as input values in GRIND for one of the secondary π^+'s. The fits with a zero range pion lead to so-called pseudo 2C, 3C and 4C fits.

If a pion track could not be measured up to its stopping point, the GRIND starting values for its momentum p and error Δp were taken in such a manner that $p + \Delta p$ equals the maximum possible pion momentum (204 MeV/c) and $p - \Delta p$ equals the momentum corresponding to the measured range.

A nominal momentum of (100 ± 70) MeV/c was assigned as "measured" value to electrons with unmeasurable momentum, e.g. due to the impossibility of measuring the curvature of the portion of the track, available for measurement ("straight" electron). In the case of hypothesis 1 this leads to a pseudo 1C fit.

IV.3 Selection of Ke4 candidates

The prints of the candidates were compared with the GRIND output and extensively investigated by a group of physicists. The following criteria were adopted to arrive at a final sample of Ke4's:

a) Any accepted candidate was required to have a genuine 1C Ke4 at rest fit with a χ^2-probability larger than 1%.
b) Any candidate fitting the τ hypotheses 6 or 7 (see table IV.1) with a χ^2-probability larger than 10% was rejected.
c) Any candidate fitting one of the other τ hypotheses (8 to 13) was carefully checked to see if the picture of the decay was compatible with the momenta (range) and directions predicted by the τ fit (especially in the case of

hypotheses 12 and 13). If not, the event was kept as a Ke4.

Following these criteria in Nijmegen we finally ended up with a sample of 19 Ke4's; the sum total for the whole collaboration was 115 events. This sample can be divided into the categories of table IV.2.

Table IV.2

	Nijmegen	all labs
"complete" Ke4-decays	18	93
Ke4's with an interacting pion	-*)	11
Ke4's with π^- decay in flight	-	2
Ke4's with a "straight" electron	-	3
Ke4's with a short pion (range < 4 mm)	1	6
	19	115

*) one candidate had an interacting π^+ and an interacting π^-, another had an interacting π^+ and a "straight" electron; for both events no fit to the Ke4 at rest hypothesis was obtained however.

IV.4 Corrections for losses and background

To use the sample of 115 Ke4 events for the calculation of physical quantities we have to make four types of correction:

A. Corrections for random scanning loss.
B. Corrections for loss of Ke4 events by the GRIND fit selection criteria.
C. Correction for τ contamination.
D. Corrections for kinematical cuts.

A distinction can be made between

i) corrections relevant to the determination of the Ke4 branching ratio (A, B, C & D).

ii) corrections which also influence the determination of the form factors and the π-π phase shift (D).

A. Corrections for scanning loss

i) Correction for events lost at random in the scanning

Table IV.3 shows the number of Ke4 decays found in two independent scans.

Table IV.3

	Nijmegen	all labs
events found in scan 1, not in scan 2	4	19
events found in scan 2, not in scan 1	4	22
events found in both scans	11	74
scanning efficiency after 2 scans	.93±.05	.95±.02

If we call $N_1(N_2)$ the number of events found in the first (second) scan and N_{12} the number found in both scans, the overall random scanning efficiency ε is found from:

$$\varepsilon = \frac{N_{12}(N_1 + N_2 - N_{12})}{N_1 . N_2} \qquad (4.2)$$

This formula holds under the assumption that both scans are done independently. The numbers shown in table IV.3 lead to a correction for random scanning loss of (5 ± 2)%.

ii) Correction for loss, due to steeply dipping secondaries

In fig. IV.8 we show the distribution of the sine of the dip angles for electrons, π^+ and π^- resp. Ideally, these distributions should be flat. The distribution of the electron

dip shows possibly some deviation, although not very significant . Nevertheless we have calculated the Ke4 branching ratio with a cut on this electron dip at a value of $|\sin\lambda| = 0.95$ ($|\lambda| \cong 72^{o}$). This cut implies a correction of $(5 \pm 0.5)\%$ and eliminates one event from the experimental sample. As the dip is not one of the kinematical variables and therefore is distributed equally over the phase space, this cut is not necessary for the determination of the form factors.

B. Corrections for loss of Ke4 events by the GRIND fit selection criteria

i) Correction for kinematical fitting losses

Samples of Ke4 events were generated with a Monte-Carlo program using different assumptions for the form factors and s- and p-wave phase shifts. The track parameters of these events were distorted in accordance with the expected experimental errors. The resulting artificial events were then kinematically fitted using the same hypotheses as for the Ke4 candidates. It was found that about $(4 \pm 1)\%$ of the Ke4 decays were lost through the condition that the candidate must satisfy a Ke4 at rest fit with a χ^2-probability > 1%. This percentage includes failures because of a "straight" electron. When determining the branching ratio we must therefore eliminate the three "straight" electron events found before applying this correction (see table IV.2).

ii) Correction for loss of Ke4 events to τ fits

In the same manner as described under i) an estimate was obtained for the loss due to the possibility of real Ke4's fitting τ decay (at rest or in flight) with an undetected π^{+}. The configurations concerned here are of course such that the events do not fall in the excluded τ region

($130 < m_m < 150$ MeV/c^2 and $p_m < 60$ MeV/c, see section IV.2). The estimated loss is about (5 ± 1)%, about one fifth of which comes from Ke4 events with an interacting pion.

iii) Correction for events lost because of an interacting pion

Among the sample of fitted Ke4 a fraction has an interacting pion. In principle a certain number of these events could have been missed, e.g. due to a bad fit. Calculations based on a sample of $K\pi 2$ and τ decays resulting from the same exposure, both with and without interacting pions, show that the expected fraction of Ke4 decays with a strongly interacting pion or a pion decaying in flight is around 10%. This fraction is compatible with the observed number of such events; therefore no extra correction was applied.

iv) Correction for loss of events to K in flight decay

About 50% of all accepted candidates also fit the second Ke4 hypothesis, i.e. the hypothesis where the momentum of the K^+ meson is unknown. Strictly speaking, the solution is not a fit but a straightforward calculation of the four unknown quantities with help of the four momentum-energy conservation constraints. The calculated kaon momentum ranges from 1 to 300 MeV/c. Only a few percent are expected to be real Ke4 in flight decays, but if one assumes that about the same percentage of counted τ decays result from an in flight decaying K^+, there is no reason for correction of the branching ratio.

C. Correction for τ contamination

When a colinear τ decay has a pion track, which scatters very near to its origin, it can be mistaken as a Ke4. The same is possible when the pion decays in flight without notable change in ionization and with the decay muon going in the

same direction. Using Monte-Carlo generated τ samples, the total size of these effects was evaluated to be about (2 ± 2)%.

D. Corrections for kinematical cuts

This group concerns corrections which must be applied because of scanning losses of a non-random character, i.e. losses which are greater in some parts of the kinematical configuration space than in others. In studying the form factors and π-π phase shifts this space has to be integrated over. We must therefore exclude the biased parts of the phase space from the integration.

i) Correction for events, rejected because of the pion range

Events which have a short (almost invisible) pion track have a large chance of being missed in the scanning. The six events found with a pion range shorter than 4 mm (momentum < 48 MeV/c) are poorly determined, due to the large errors on momentum and direction of the short track. From a study of Monte-Carlo generated Ke4 samples, we expect about 20 events with a pion momentum < 48 MeV/c. Compared with the six events found, it is clear that a cut on pion momentum (or energy) is inevitable. At 48 MeV/c such a cut results in a loss of (15 ± 1)%.

ii) Correction for events rejected in the τ region

As already described in section IV.2, events which have a missing mass (with respect to the di-pion system) between 130 and 150 MeV/c^2 together with a missing momentum lower than 60 MeV/c have to be cut away. Again from Monte-Carlo calculations we learned that this cut implies a loss of (1 ± 0.5)%.

Fig. IV.9 shows the $m_m - p_m$ distribution for the sample of 93 events obtained after the cuts described in D.i) and D.ii)

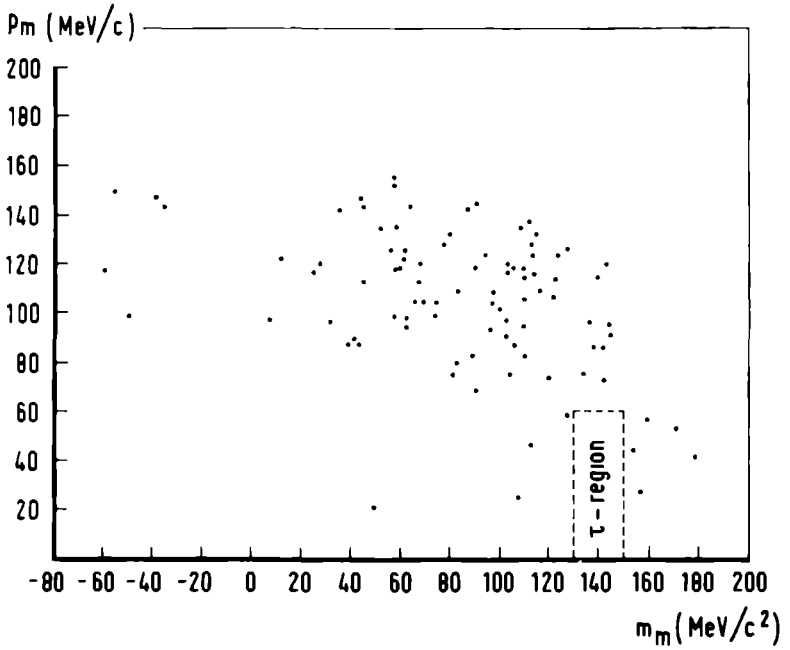

Fig. IV.9. Missing mass vs. missing momentum for 93 Ke4's.

and excluding all events with an incomplete track (see table IV.2).

In table IV.4 we list all applied corrections together with their effect on the calculation of the Ke4 branching ratio. The total percentage correction is found by multiplying all terms (100 + c_i), where c_i is the percentage effect of the i-th correction.

Table IV.4

Type of loss or contamination	effect in %
A.i - random scanning loss	- (5 ± 2)
A.ii - Ke4 decays with steeply dipping electrons	- (5 ± 0.5)
B.i - Ke4 decays failing to fit Ke4	- (4 ± 1)
B.ii - Ke4 decays absorbed by τ fits	- (5 ± 1)
C - τ decays fitting Ke4	+ (2 ± 2)
D.i - Ke4 decays with short pion tracks (p_π < 48 MeV/c)	- (15 ± 1)
D.ii - Ke4 decays in the τ region (cut on m_m and p_m)	- (1 ± 0.5)
total correction	- (30 ± 4)

References - chapter IV

1) G. Rinaudo and A.E. Werbrouck in "Proceedings of the informal meeting on geometry programmes for heavy liquid bubble chambers", CERN report 63-23 (1963).
2) CERN program library, X601 GRIND
3) K. Soop, The DOLL system, CERN report 68-37 (1968).

V. ANALYSIS OF THE KE4 SAMPLE

V.1 Branching ratios

The total number of τ decays counted in every tenth picture during the scanning of the experiment, amounts to 20300 events. Taking the τ branching ratio to be (5.59 ± 0.03)% [1] and knowing the overall τ scanning efficiency to be (0.99 ± 0.01), the total number of examined K^+ decays at rest is estimated as

$$\frac{20300 \times 10}{0.99 \times 0.0559} = (3.67 \pm 0.04) \times 10^6.$$

From the Ke4's listed in table IV.2, we omit the three events with a "straight" electron, the six events with a pion momentum less than 48 MeV/c and the single event with a steeply dipping electron ($|\sin\lambda| > 0.95$). This leaves us with 105 Ke4 events from which we obtain a corrected number of

$\frac{105 \pm 10}{0.70 \pm 0.04}$ = (150 ± 18) events (see table IV.4). This leads to a $Ke4(e^+)$ decay fraction

$$\frac{K^+e4(e^+) \text{ decays}}{\text{all } K^+ \text{ decays}} = (4.1 \pm 0.5) \times 10^{-5}$$

or a partial decay rate of $(3.3 \pm 0.4) \times 10^3$ sec^{-1}.

If we assume the same scanning efficiency and overall correction factor for $K^+e4(e^-)$ decay, the fact that not a single candidate was found implies a decay fraction of this mode of less than 9×10^{-7} with a confidence level of 95%. This is in agreement with the semileptonic $\Delta Q = \Delta S$ rule.

V.2 Methods to determine form factors and π-π phase shifts

To determine the form factors and the π-π phase shifts, two methods were used: 5-dimensional maximum likelihood method and a simultaneous least squares fit to the five 1-dimensional histograms resulting from the projection of the 5-dimensional configuration space

V.2.1 Maximum likelihood method

The maximum likelihood method is based on the principle that the normalized product of the probabilities for each event to decay, taken as a function of its observed variables and some unknown parameters, will show a maximum for the most likely values of these parameters [2]. It can be proven that this method extracts the maximum amount of information from the sample.

Expressed in the kinematical quantities E_+, E_-, k, E_e and ϕ, the probability of an event to decay per unit of time (the so-called density distribution), can be calculated from Eq. (2.13). Also Eq. (2.14) or Eq. (2.15), both using a different set of variables, could be used. The parameters to be determined are the form factors ratios

$$\nu = \tilde{f}'_p/\tilde{f}_s \quad , \quad \eta = \tilde{g}/\tilde{f}_s \quad , \quad \gamma = \tilde{h}/\tilde{f}_s \qquad (5.1)$$

and a parameter related to the π-π phase shifts (see section II.5).

The likelihood expression is normalized with the help of the fivefold integral of the density distribution, obtained by integrating Eq. (2.13) numerically. There exist two areas

in the configuration space, where as a consequence of cuts no events are present: the region for pion momenta below 48 MeV/c and the τ box given by $130 < m_m < 150$ MeV/c^2 and $p_m < 60$ MeV/c, where m_m and p_m are resp. the missing mass and the missing momentum with respect to the di-pion system. Due to the choice of variables these areas are easily subtracted from the integration area. As shown in appendix A2, the integrated decay probability is given by:

$$\Gamma(sec^{-1}) = \frac{1}{\hbar}\int d^5w = |\hat{f}_s \sin\theta_c|^2(1330 + 256\eta^2 + 3.1\gamma^2 + 4.4\nu^2 + 47\,\eta\nu) \qquad (5.2)$$

The likelihood expression can therefore be written as:

$$\mathcal{L}(\nu,\eta,\gamma,\delta) = \prod_{\text{all events}} \frac{d^5w(E_+,E_-,k,E_e,\phi;\ \nu,\eta,\gamma,\delta)}{1330 + 256\eta^2 + 3.1\gamma^2 + 4.4\nu^2 + 47\eta\nu} \qquad (5.3)$$

Instead of maximizing this product it is customary to maximize the natural logarith of this product; this leads to

$$\ln \mathcal{L}(\nu,\eta,\gamma,\delta) = \sum_{\text{all events}} \ln \frac{d^5w(E_+,E_-,k,E_e,\phi;\ \nu,\eta,\gamma,\delta)}{1330 + 256\eta^2 + 3.1\gamma^2 + 4.4\nu^2 + 47\eta\nu} \qquad (5.4)$$

The CERN computer program MINUIT [3] was used to maximize the expression $\ln \mathcal{L}$ in function of ν, η, γ and δ. In general, starting from a given set of parameters, this program finds a maximum by using a stepping procedure. Each of the parameters

is varied consecutively (with decreasing step size) until convergence is obtained. The ultimate value of $\ln \mathcal{L}$ has only relative meaning, i.e. can only be used to compare the results of analyses of the same sample.

The outcome of the stepping procedure is not necessarily a unique solution because $\ln \mathcal{L}$ can have several local maxima. To avoid the loss of solutions, MINUIT has a feature which generates starting values in a random manner and prints a list of the ten best parameter sets out of a preset number of trials. In most cases several of these sets lead to the same maximum, so that one ends up with only a few maxima to be considered.

For each solution the program produces a symmetric covariance matrix (or error matrix) $\mathbf{V}$, based on the assumption that the function depends quadratically on the parameters in the neighbourhood of the maximum. The diagonal elements of this matrix (= variances) form an estimate of the errors on the parameters, the off-diagonal elements (= covariances) of their correlation coefficients. In particular, we have for the standard deviation of parameter i:

$$\sigma_i = \sqrt{\mathbf{V}_{ii}/2} \qquad (5.6)$$

At a distance σ from the maximum the function $\ln \mathcal{L}$ has dropped to 0.5 less than its maximum value. If the behaviour of the logarithmic likelihood function is not parabolic in the neighbourhood of the maximum (i.e. if the likelihood function itself is not Gaussian), the point where the logarithm has dropped by 0.5 can be found by means of another stepping procedure. If this method does not lead to any acceptable likelihood value the program MINUIT proceeds to plot $\ln \mathcal{L}$ in equal steps on both sides of the maximum.

The error in any of the parameters, when estimated independently of all others, is given by its projected distribution, i.e. the distribution obtained by integrating over all other variables. This is equivalent to projecting the -0.5 contour onto the corresponding axis.

The correlation coefficient between parameters i and j is given by:

$$\rho_{ij} = \frac{V_{ij}}{\sqrt{V_{ii}V_{jj}}} \tag{5.7}$$

If $\rho_{ij} \simeq 0$, the parameters i and j are uncorrelated; their correlation is maximum for $\rho_{ij} = \pm 1$. For each set of two correlated parameters, for instance α and β, one can construct a pair of uncorrelated parameters formed by linear combinations of α and β. A possible set is α and

$$\beta - \rho_{\alpha\beta}\frac{\sigma_\beta}{\sigma_\alpha}\alpha = \beta - \frac{V_{\alpha\beta}}{V_{\alpha\alpha}}\alpha \tag{5.8}$$

V.2.2 Least squares method

The second analysis method uses less information than the former. Only the projections of the event distribution onto five independent axes are used. In this way the correlations between the five chosen quantities disappear and are therefore lost.

The fit is performed as follows: Experimental histograms were determined for the quantities E_+, E_-, k, E_e and ϕ. The predicted height for each bin in each histogram can be calculated as a function of the unknown parameters (i.e. of ν, η,

γ and δ). Then a sum over all bins of the square of the difference between experimental and predicted heights, divided by the predicted height, can be found. The fit consists of finding those values of ν, η, γ and δ which give a minimum value for this sum [2]. In other words, we minimized the following expression:

$$\chi^2(\nu,\eta,\gamma,\delta) = \sum_k \sum_{l_k} \frac{[h_{kl}(\text{exp.}) - h_{kl}(\text{pred.})]^2}{h_{kl}(\text{pred.})} \qquad (5.9)$$

where h_{kl} is the number of events in the l^{th} bin of the k^{th} histogram.

This so-called simultaneous least squares (or minimum χ^2) fit leads to values for ν, η, γ and δ which make the predicted distributions fit as good as possible to the experimental histograms.

The minimization of χ^2 was also performed using the program MINUIT. The standard deviation on parameter i is now given by:

$$\sigma_i = \sqrt{\mathbf{V}_{ii}} \qquad (5.10)$$

The difference between this and Eq. (5.6) is only apparent and due to the fact that the probability P for a specific event (in the sense of section V.2.1) is given by:

$$P(\nu,\eta,\gamma,\delta) = \frac{1}{(2\pi)^2} \frac{1}{\sqrt{\det \mathbf{V}}} e^{-\frac{1}{2}\chi^2} \qquad (5.11)$$

Notice the extra factor $\frac{1}{2}$ in the exponent. The one standard deviation points now lay on a contour with χ^2 one unit above the minimum χ^2.

To determine the so-called number of degrees of freedom of the fit we observe the following facts: In general, the number of degrees of freedom is equal to the number of bins

minus the number of parameters, which is four in our case. However, producing k histograms from one and the same sample (with a fixed total number of events) creates (k-1) additional constraints. This reduces the number of degrees of freedom further. We then have

$$n_D = \sum_k l_k - (k-1) - 4$$

where n_D = number of degrees of freedom
k = number of histograms
l_k = number of bins in histogram k

The theoretical χ^2 distribution for n_D degrees of freedom is such that the most likely χ^2 value is equal to (n_D-2), while the mean χ^2 value equals n_D. The so-called confidence level (CL) or χ^2-probability is a quantity which can be approximated for large n_D(> 30) by

$$CL \approx \frac{1}{\sqrt{2\pi}} \int_y^\infty e^{-x^2/2} dx \qquad (5.12)$$

with $y = \sqrt{2\chi^2} - \sqrt{2n_D-1}$.

V.3 Application of analysis methods to Ke4 sample

V.3.1 Maximum likelihood analysis

We have analyzed the total Ke4 sample of 93 events, collected by the X2 collaboration, with the maximum likelihood method described in section V.2.1. Since the effects of unequal measurement errors cannot be built into a likelihood analysis, the 13 events with an interacting pion or a "straight" electron

were discarded. As will be shown later, the effect of these events is negligible (see section V.3.2).

The π-π phase shifts were determined in two different ways. First we used the phase shift difference $\delta = < \delta_s - \delta_p >$ as an average value over the effective mass range considered, i.e. $(280 < M_{\pi\pi} \lesssim 450)$ MeV/c^2. To make a crude investigation of the energy dependence of the phase shifts (and also of the form factors), the analysis was performed three times: once for events with $(280 < M_{\pi\pi} < 330)$ MeV/c^2, once for events with $(330 < M_{\pi\pi} \lesssim 450)$ MeV/c^2 and once for the complete mass region. The results of these three analyses are shown in table V.1.

Table V.1

	$280<M_{\pi\pi}<330$ (46 events)	$M_{\pi\pi}>330$ MeV/c^2 (47 events)	total (93 events)
$\nu = f'_p/f_s$	- 1.8 ± 2.7	- 1.8 ± 2.2	- 2.0 ± 1.8
$\eta = \tilde{g}/f_s$	1.42 ± 0.45	1.18 ± 0.34	1.26 ± 0.30
$\gamma = \tilde{h}/f_s$	2.5 ± 2.0	- 0.8 ± 2.2	1.1 ± 1.4
$\nu + 4.5\eta$	4.6 ± 1.7	3.5 ± 1.4	3.7 ± 1.1
δ(rads)	- 0.01 ± 0.34	0.26 ± 0.28	0.18 ± 0.22

The second way to determine the phase shift is through the use of the so-called s-wave scattering length a_o, neglecting the p-wave phase shift. The details of this parametrization are given in section II.5 (Eq. (2.41) and below). As stated there we used Eq. (2.44) with $\alpha = \frac{0.025}{m_\pi^2}$. The likelihood function

Eq. (5.4) was modified in such a way that instead of a mean δ we used an event dependent δ_i containing a_o as a parameter and given by:

$$\delta_i = \arctan \beta_i \{a_o + 0.05 \frac{(M^2_{\pi\pi})_i - 4m^2_\pi}{m^2_\pi}\} \qquad (5.13)$$

Since the normalization is not dependent on δ, the denominator in Eq. (5.4) is not affected. The results of this second approach are shown in table V.2[a].

Table V.2

solution without f_s enhanced (93 events)		solution with f_s enhanced (93 events)	
$\nu = \tilde{f}'_p/\tilde{f}_s$	-2.0 ± 1.8	$\nu = \tilde{f}'_p/f^o_s$	-2.1 ± 2.2
$\eta = \tilde{g}/f^{\sim}_s$	1.26 ± 0.30	$\eta = \tilde{g}/f^o_s$	1.51 ± 0.38
$\gamma = \tilde{h}/\tilde{f}_s$	1.1 ± 1.4	$\gamma = \tilde{h}/f^o_s$	1.6 ± 1.8
$\nu + 4.5\eta$	3.7 ± 1.1	$\nu + 4.5\eta$	4.6 ± 1.4
$a_o(m_\pi^{-1})$	$0.22 \begin{smallmatrix}+0.42\\-0.38\end{smallmatrix}$	$a_o(m_\pi^{-1})$	$0.30 \begin{smallmatrix}+0.08\\-0.06\end{smallmatrix}$
$\tilde{f}_s \sin\theta_c$	1.24 ± 0.10	$f^o_s \sin\theta_c$	1.00 ± 0.09
$\tilde{f}_p \sin\theta_c$	-0.27 ± 0.24	$\tilde{f}_p \sin\theta_c$	-0.23 ± 0.24
$f'_p \sin\theta_c$	-2.5 ± 2.2	$\tilde{f}'_p \sin\theta_c$	-2.1 ± 2.2
$\tilde{g} \sin\theta_c$	1.56 ± 0.37	$\tilde{g} \sin\theta_c$	1.51 ± 0.39
$\tilde{h} \sin\theta_c$	1.3 ± 1.6	$\tilde{h} \sin\theta_c$	1.6 ± 1.8

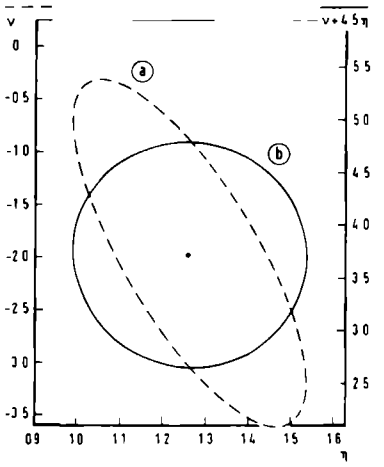

Fig. V.1

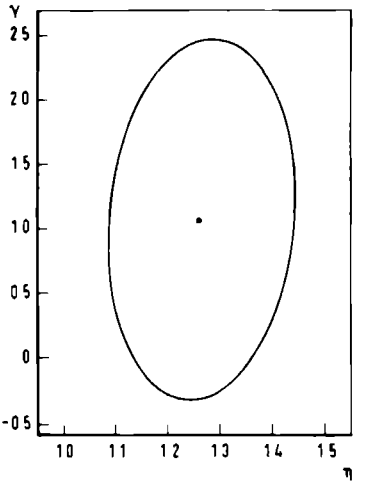

Fig. V.2

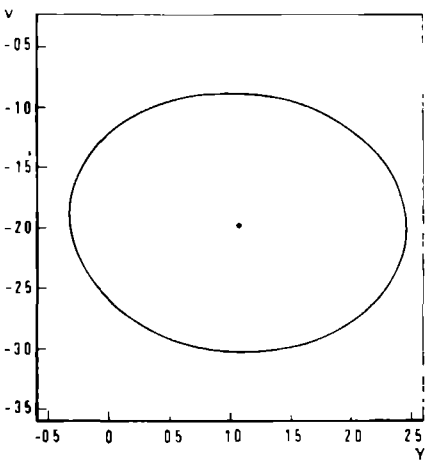

Fig. V.3

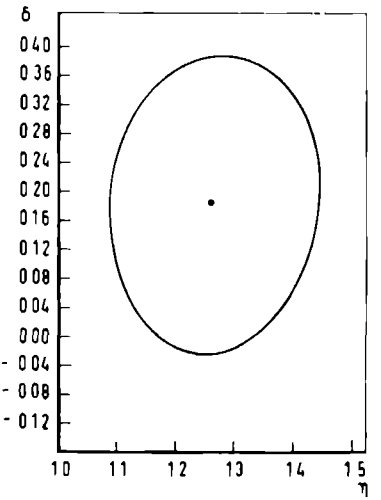

Fig. V.4

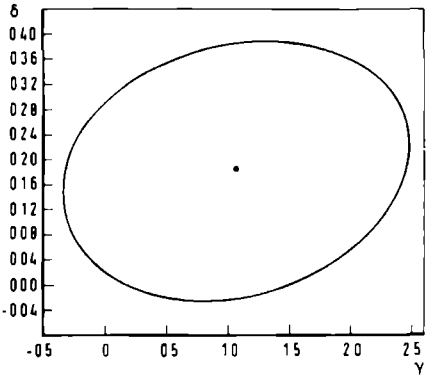

Fig. V.5

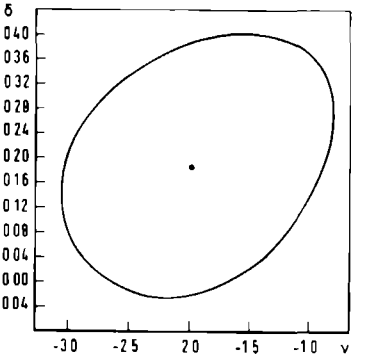

Fig. V.6

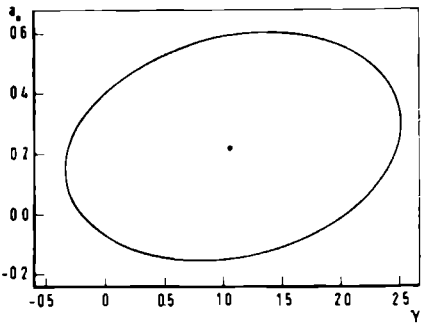

Fig. V.7

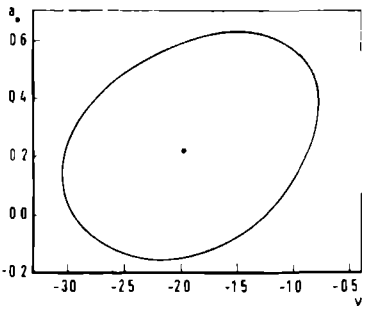

Fig. V.8

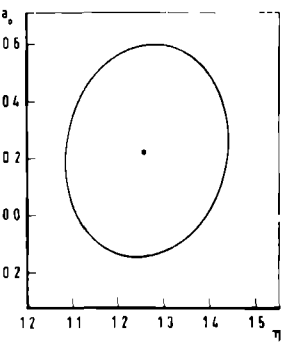

Fig. V.9

In figs. V.1 to V.9 contours, corresponding to a level of 0.5 below the maximum log. likelihood value, are drawn for all two by two combinations of the parameters ν, η, γ, δ and a_o (except δ vs. a_o). From these figures one gets an idea of the correlations between the various parameters. Apparently a strong correlation is present between η and ν (fig. V.1[a]). As already pointed out in section V.2.1, it is possible to construct sets of uncorrelated parameters. A possible choice here is η and $\nu + 4.5\,\eta$ (see also Eq. (5.8)). Using this combination we arrive at the contour drawn in fig. V.1[b] (solid line).

To determine $\tilde{f}_s$ we need, apart from the form factor ratios, also the Ke4 decay probability. This probability Γ is expressed by the following formula:

$$\Gamma(\text{sec}^{-1}) = \frac{1}{\hbar}\int d^5w = |\tilde{f}_s \sin\theta_c|^2(1603 + 313.1\eta^2 + 6.47\nu^2 + 64.9\eta\nu + 3.33\gamma^2) = |\tilde{f}_s \sin\theta_c|^2\{1603 + 150.8\eta^2 + 6.49 \times (\nu + 5\eta)^2 + 3.33\gamma^2\} \qquad (5.14)$$

As in the case of Eq. (5.2) this formula was also evaluated by numerical integration of Eq. (2.13), but now using the whole configuration space as the integration area.

With $\Gamma = (3.0 \pm 0.2).10^3\text{sec}^{-1}$ [1] and the form factor ratios taken from table V.1[c] we find $|\tilde{f}_s \sin\theta_c| = 1.24 \pm 0.10$. It is more meaningful to quote $\tilde{f}_s$ and $\sin\theta_c$ combined. It is impossible to determine the absolute sign of $\tilde{f}_s$; the signs given for the other form factors are therefore relative to $\tilde{f}_s$ only.

Note that the influence of the vector interaction on the decay probability (the term with γ^2) is very small indeed

(see section II.4). Since the coefficient of ν (or $\nu + 5\eta$) is also small, both $\tilde{h}$ and $\tilde{f}'_p$ are only determined with large errors. However, these errors have little influence on the determination of $\tilde{f}_s$ and $\tilde{g}$.

In searching for the maximum likelihood a second maximum was found, but at a much lower likelihood level: $\ln \mathcal{L}$ was approx. seven units lower than the first maximum (see table V.3[b]).

Table V.3

	first maximum	second maximum
ν	- 2.0 ± 1.8	10.9 ± 2.6
η	1.26 ± 0.30	- 0.54 ± 0.23
γ	1.1 ± 1.4	5.4 ± 2.4
$\nu + 4.5\eta$	3.7 ± 1.1	—
$\nu + 8\eta$	—	6.6 ± 1.9
δ(rads)	0.18 ± 0.22	- 0.92 ± 0.16
$\ln \mathcal{L}$	0.0	- 7.04
$\chi^2(n_D = 36)$	34.0	42.2

The reason for the appearance of this local maximum is of analytic origin; the same effect was found during the analysis of Monte-Carlo generated events, even with samples containing many more events than present in the real sample. It is related to the observation (see ref. 4) that many projected distributions, e.g. those of $M_{\pi\pi}$, $M_{e\nu}$, $\cos\theta_\pi$, $\cos\theta_l$, ϕ, E_+, E_-, E_e and k, are rather insensitive to the substitution

given by:

$$\left.\begin{aligned} \nu' &= \nu + 10\eta \\ \eta' &= -\eta \end{aligned}\right\} \nu' + 5\eta' = \nu + 5\eta$$
$$\begin{aligned} \gamma' &= \gamma \\ \delta' &= -\delta \end{aligned} \qquad (5.15)$$

One may therefore expect (especially if the number of events is small) that something of this second solution will subsist, although suppressed and changed by the various correlations.

Note also that the positive δ value of the first solution is in agreement with other phase shift determinations (see section VII).

For all these reasons the second solution is not considered a physical possibility.

The χ^2 values, given in table V.3, were obtained with Eq. (5.9) by comparing the experimental distributions of E_+, E_-, k, E_e and ϕ with the distributions predicted by the parameters in this table (36 degrees of freedom). Minimization of this χ^2 as a function of those parameters is described in the next subsection.

From the form factor $\tilde{f}_p'$, connected with the angular momentum barrier of Eq. (2.40), the original form factor $\tilde{f}_p$ can be found by multiplying $\tilde{f}_p'$ by a factor ~ 0.11.

To find the form factor $\tilde{f}_s^o$, connected with an energy dependence of $\tilde{f}_s$ of the type given by Eq. (2.41), a new calculation of the decay probability and a new normalization of the likelihood function was necessary. The factor with $|\tilde{f}_s^o|^2$ is a function of a_o and can, in the region $(0.15 < a_o < 0.35)m_\pi^{-1}$ approximated by an expression of the type $(x + \frac{y}{a_o} + \frac{z}{a_o^2})$. For

the decay probability we then find instead of Eq. (5.14)

$$\Gamma(\sec^{-1}) = \frac{1}{\hbar}\int_A d^5w = |\overset{\curvearrowright}{f}_s^o \sin\theta_c|^2\{1603 + \frac{186.9}{a_o} + \frac{20.8}{a_o^2} + 150.8\eta^2 + 6.49(\nu + 5\eta)^2 + 3.33\gamma^2\} \qquad (5.16)$$

and for the normalization of the likelihood function instead of the denominator of Eq. (5.4)

$$\frac{1}{\hbar|f_s^o \sin\theta_c|^2}\int_B d^5w = (1330 + \frac{168.6}{a_o} + \frac{19.7}{a_o^2} + 256\eta^2 + 3.1\gamma^2 + 4.4\nu^2 + 47\eta\nu) \qquad (5.17)$$

The integration area A is the total configuration space, while area B is that part of the space which is left after the experimental cuts have been applied.

The results of the maximum likelihood analysis with "enhanced" f_s are shown in table V.2[b]. There is a remarkable decrease in the error on a_o due to the fact that a_o is now appearing in the normalization. Compared with the values in table V.2[a] the values found for $\overset{\curvearrowright}{f}_p$, $\overset{\curvearrowright}{f}_p'$, $\tilde{g}$ and $\tilde{h}$ have practically not changed.

For completeness we give in tables V.4 to V.7 the error matrices belonging resp. to

i) the solution of table V.3[a] with δ (first $\mathcal{L}$ maximum)
ii) the solution of table V.3[b] with δ (second $\mathcal{L}$ maximum)
iii) the solution of table V.2[a] with a_o
iv) the solution of table V.2[b] with a_o (f_s enhanced)

Table V.4

	ν	η	γ	δ
ν	7.147	- 0.928	- 1.120	0.144
η		0.185	0.219	- 0.015
γ			4.223	0.029
δ				0.025

Table V.5

	ν	η	γ	δ
ν	13.68	- 0.818	3.101	0.014
η		0.104	- 0.129	- 0.006
γ			11.93	- 0.134
δ				0.018

Table V.6

	ν	η	γ	a_o
ν	6.684	- 0.857	- 0.991	0.458
η		0.175	0.205	- 0.043
γ			4.278	0.150
a_o				0.330

Table V.7

	ν	η	γ	a_o
ν	9.802	- 1.303	- 2.087	0.017
η		0.283	0.409	- 0.008
γ			6.604	- 0.009
a_o				0.008

V.3.2 Least squares analysis

The minimum χ^2 or least squares method, described in section V.2.2, has been the main method used in analyzing all former Ke4 experiments [4, 5, 6]. Because of this fact and to allow comparison with the results of the maximum likelihood method we have also analyzed our sample with this method.

The usual choice of the histograms has been those in the variables $M_{\pi\pi}$, $M_{e\nu}$, $\cos\theta_\pi$, $\cos\theta_l$ and ϕ or a subset of these five. Because of the experimental cut on short pion tracks ($p_\pi < 48$ MeV/c), the histograms in $M_{\pi\pi}$, $M_{e\nu}$ and $\cos\theta_\pi$ are seriously distorted. Furthermore, the $\cos\theta_l$ distribution shows an asymmetrical distortion due to measurement errors on angles and momenta. This distortion especially affects events for which the laboratory system velocity $\beta_{e\nu}$ of the di-lepton system is close to unity [6]. Corrections can be applied to these histograms:

i) by adding events to some bins, the number of which can be estimated by Monte-Carlo techniques,

ii) by using additional cuts, correcting the shape of the histograms,

iii) by calculating the deformations of the histograms.

The first method is very time consuming as it requires many iterations.

The second method could be applied by cutting events with $|\cos\theta_\pi| > 0.6$ and events with $M_{e\nu} < 50\ \mathrm{MeV}/c^2$. However, these cuts would reduce the sample from 93 to 48 events.

The third method, while in general difficult to apply, is rather simple when variables are chosen which are as closely related as possible to the directly measured quantities. Such a set of quantities is E_+, E_-, E_e and k. Their distributions are affected by the experimental cuts in a simple way and it is relatively easy to account for the changes these distributions undergo as a result of the cuts. They are given in appendix A2.

Table V.8

93 events	solution 1	solution 2
$\nu = \tilde{f}_p'/\tilde{f}_s$	-1.7 ± 1.8	$16.0\ ^{+\ 4.2}_{-\ 3.6}$
$\eta = \tilde{g}/\tilde{f}_s$	1.34 ± 0.35	$-1.86\ ^{+\ 0.47}_{-\ 0.53}$
$\gamma = \tilde{h}/\tilde{f}_s$	-0.7 ± 1.8	2.9 ± 2.1
δ(rads)	0.03 ± 0.32	-0.08 ± 0.25
$\chi^2(n_D = 36)$	32.7	28.0

Table V.8 lists the two solutions found as a result of a simultaneous least squares fit to the E_+, E_-, k, E_e and ϕ distributions. Comparison of solution 1 with the first maximum likelihood solution (see table V.3[a]) shows minor differences, mainly in γ, but still within errors. A larger difference is observed in comparing solution 2 and the second likelihood solution (table V.3[b]).

The difference in χ^2 between solutions 1 and 2 is too small to choose a best solution on the basis of this quantity. However, we prefer solution 1 on the basis of its correspondence with the first likelihood solution.

A set of histograms is drawn in fig. V.10 to fig. V.19 for the distributions of the 93 events as a function of the quantities E_+, E_-, E_e, k, ϕ, $M_{\pi\pi}$, $M_{e\nu}$, $\cos\theta_\pi$, $\cos\theta_l$ and $\cos\alpha_{\pi\pi}$. The curves in these figures refer to the first likelihood solution (table V.3[a]). The predicted distributions of the first five quantities were evaluated numerically (see appendix A2). All other predicted distributions were found by generating 5000 Monte-Carlo Ke4's, using the form factors and π-π phase shift of the corresponding solution.

In least squares procedures events are binned. As our bin size is rather large and surpasses the mean measurement errors on the various quantities even for events with a scattered decay pion or a "straight" electron, it is now no longer necessary to exclude those events. We have therefore also applied the least squares analysis to the original Ke4 sample of 109 events found by the X2 collaboration (without the two cuts mentioned). The outcome of this analysis is listed in table V.9. It hardly differs from the results obtained from the sample with the cuts included (table V.8).

Table V.9

109 events	solution 1	solution 2
$\nu = \tilde{f}_p'/\tilde{f}_s$	- 1.9 ± 1.7	15.9 ± 2.9
$\eta = \tilde{g}/\tilde{f}_s$	1.31 ± 0.35	- 1.88 ± 0.43
$\gamma = \tilde{h}/\tilde{f}_s$	0.3 ± 1.7	3.4 ± 1.9
δ(rads)	- 0.05 ± 0.30	- 0.01 ± 0.22
$X^2(n_D = 36)$	36.1	29.4

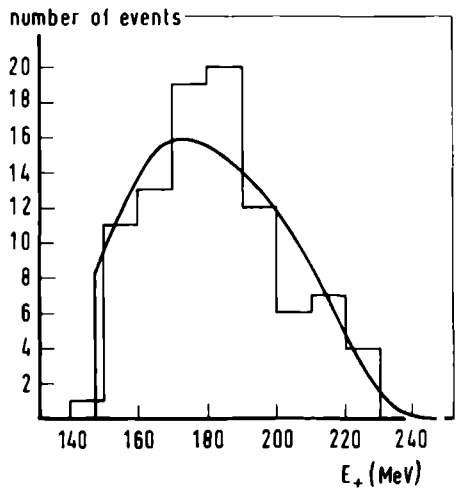

Fig. V.10. Distribution of the π^+ energy (93 Ke4 events).

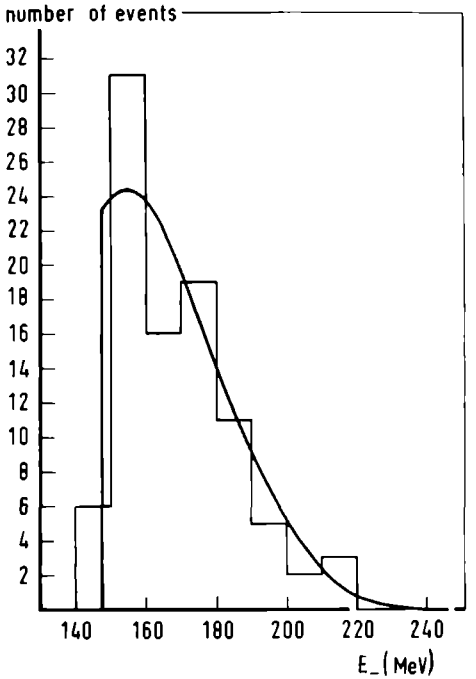

Fig. V.11. Distribution of the π^- energy.

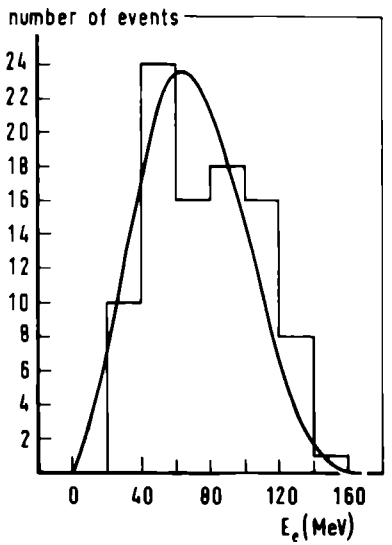

Fig. V.12. Distribution of the positron energy.

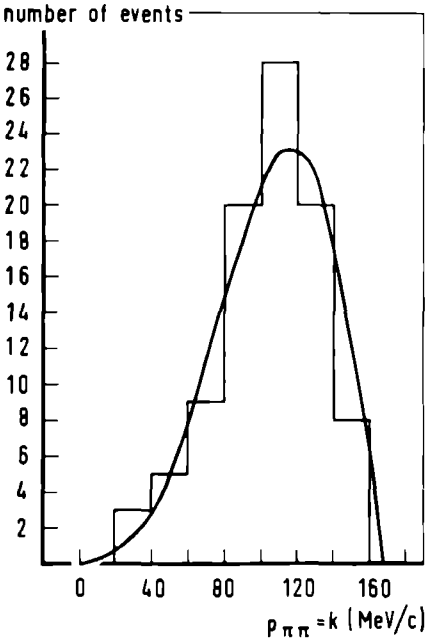

Fig. V.13. Distribution of the di-pion momentum.

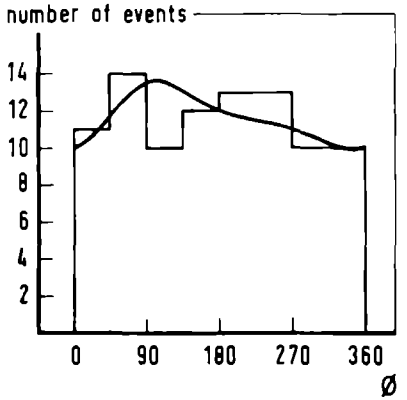

Fig. V.14. Distribution of the angle between the di-pion plane and the di-lepton plane.

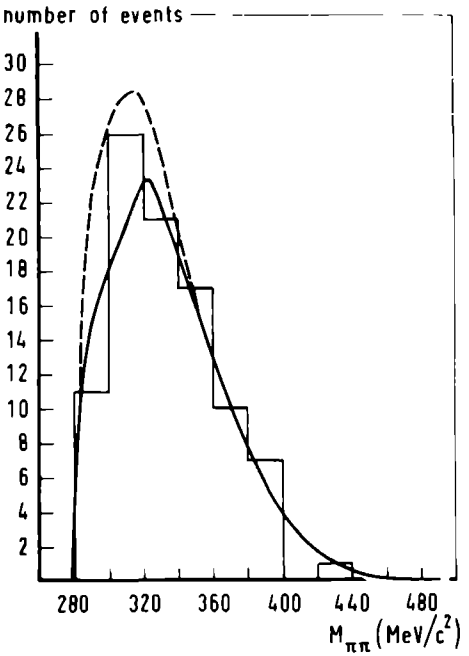

Fig. V.15. Distribution of the effective di-pion mass.

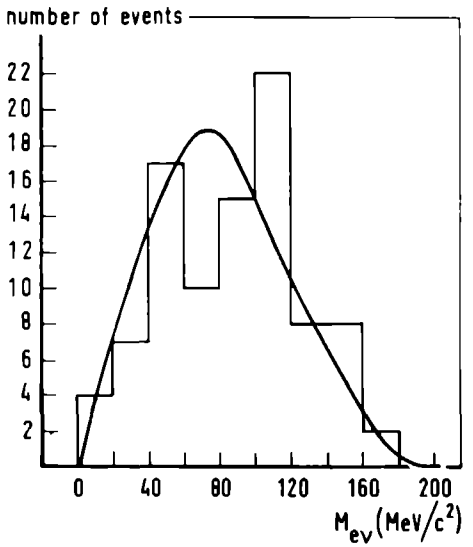

Fig. V.16. Distribution of the effective di-lepton mass.

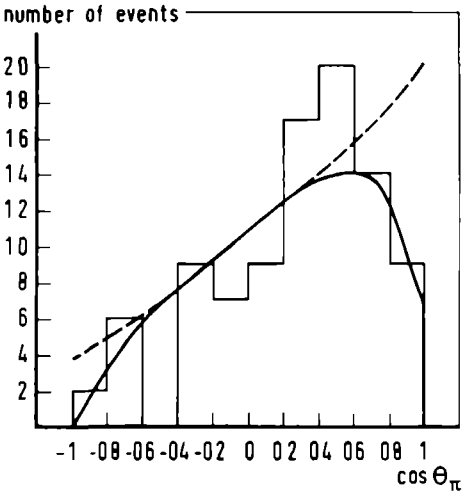

Fig. V.17. Distribution of the cosine of the angle between the π^+ in the di-pion system and the di-pion direction of flight.

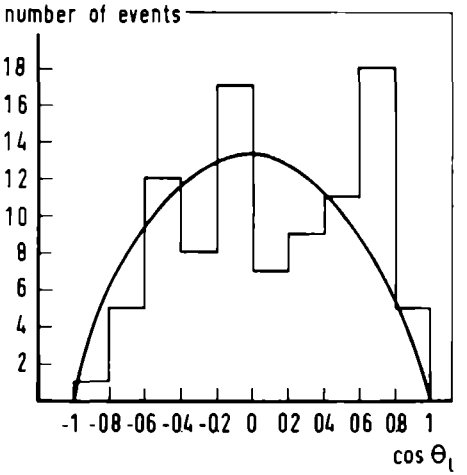

Fig. V.18. Distribution of the cosine of the angle between the e^+ in the di-lepton system and the di-lepton direction of flight.

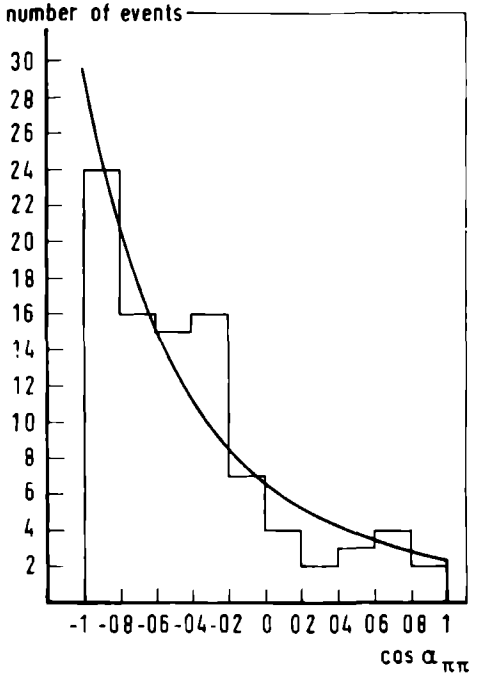

Fig. V.19. Distribution of the cosine of the angle between the two pions in the K^+ rest system.

References - chapter V

1) Particle data group, Rev. Modern Physics 45, S1 (april 1973).
2) L. Jauneau and D. Morellet, CERN report 64-13, volume I, and Methods in Subnuclear Physics, vol. IV, part 3 (Gordon and Breach, 1970).
3) CERN program library, D 506 MINUIT (old version).
4) F.A. Berends, A. Donnachie and G.C. Oades, Phys. Rev. 171, 1457 (1968).
5) R.W. Birge et al, Phys. Rev. 139, B 1600 (1965).
6) R.P. Ely et al, Phys. Rev. 180, 1319 (1969).

VI. COMPARISON WITH OTHER EXPERIMENTS

VI.1 Bubble chamber experiments

In 1965 the first Ke4 experiment was reported by a collaboration from the Lawrence Radiation Laboratory, Berkeley (LRL) and the University of Wisconsin, Madison (UW) [1]. In a heavy liquid bubble chamber a sample of 69 $K^+e4(e^+)$ events was obtained; no $K^+e4(e^-)$ events were observed. The chamber was filled with freon C_3F_8 (density 1.22 $^g/_{cm}3$, radiation length 28 cm).

Some years later a second Ke4 experiment was performed by a collaboration of the same two laboraties with a group from University College, London (UCL). This experiment was already mentioned in chapter I; it was exposed around the same time as the X2 experiment using the same equipment.

The two experiments differ only in track density: an average of 24 stopping K^+ per picture for the LRL - UW - UCL collaboration compared with an average of 7 stopping K^+ per picture in our experiment.

The 269 $K^+e4(e^+)$ events found by the LRL - UW - UCL collaboration were later analysed together with the 69 events of the LRL - UW experiment [2]. A preliminary analysis on a subset of 310 of these 338 events was published in ref. [3] and [4]. A third analysis of this sample was performed by K. Billing (UCL) in his Ph. D. thesis [5]. In all three analyses only the least squares method was used. Further, the set of kinematical variables used was $M_{\pi\pi}$, $M_{e\nu}$, $\cos\theta_\pi$, $\cos\theta_l$ and ϕ. Since this differs from our analysis, and since there are some discrepancies between their results and ours, we have reanalyzed the sample of the joint LRL - UW - UCL

collaboration using the two methods (maximum likelihood and least squares) with variables E_+, E_-, k, E_e and ϕ described in chapter V.

The results are collected in tables VI.1 and VI.2 (solutions with positive and negative phase shift difference resp.). As can be seen from these tables there is good agreement between the various analyses with respect to the mean π-π phase shift difference δ and to a lesser extent also with respect to γ ($\tilde{h}$). However, the other form factor ratios do not agree. There is even a discrepancy in the sign of $\nu(\tilde{f}_p')$. In view of the excellent agreement between our maximum likelihood solutions and least squares fits, we feel confident that our analyses give a more reliable solution for the form factors and π-π phase shift of the combined LRL - UW - UCL sample than the original analyses.

Histograms of the distributions in E_+, E_-, $k(= p_{\pi\pi})$, E_e and ϕ, together with the curves predicted by the max. likelihood solution of table VI.1, are shown in fig. VI.1.

The $K^+e4(e^+)$ decay rates reported by the LRL - UW and the LRL - UW - UCL collaborations were $(2.9 \pm 0.6).10^3 sec^{-1}$ and $(2.7 \pm 0.3).10^3 sec^{-1}$ resp. For $K^+e4(e^-)$ decay the LRL - UW - UCL collaboration found a maximum rate of 56 sec^{-1}.

For a comparison with our results we refer to section VI.3.

VI.2 Counter experiment

A K^+e4 experiment using counters, wire chambers and a spark chamber, was performed at the CERN proton synchrotron in 1969 by groups from the University of Geneva and CEN, Saclay [6, 7, 8]. Their published results are based on a

Table VI.1

solutions with positive δ	max. likelihood method	min. χ^2 method E_+, E_-, k, E_e, ϕ distributions	Berends et al [4] $\cos\theta_\pi$ and ϕ distributions	Ely et al [2] $M_{\pi\pi}$, $\cos\theta_\pi$, $\cos\theta_l$, ϕ distributions	Billing [5] $M_{\pi\pi}$, $M_{e\nu}$, $\cos\theta_\pi$, ϕ distributions
$\nu = \hat{f}_p'/\hat{f}_s$	2.2 ± 1.0	1.6 ± 1.3	-3.1 ± 3.4 *)	-3.1 ± 1.1	1.54 ± 0.91
$\eta = \tilde{g}/\hat{f}_s$	0.41 ± 0.12	0.53 ± 0.21	2.00 ± 0.90	1.33 ± 0.17	0.81 ± 0.16
$\gamma = \tilde{h}/\hat{f}_s$	$-1.8 \,^{+0.8}_{-1.1}$	-1.9 ± 1.1	-4.7 ± 2.0	-1.09 ± 0.81	-3.6 ± 1.3
δ(rads)	0.55 ± 0.18	0.55 ± 0.21	—	0.44 ± 0.15	0.70 ± 0.14
$a_o(m_\pi^{-1})$	0.71 ± 0.45 **)	—	0.71 ± 0.45 °)	$1.26 \,^{+0.68}_{-0.52}$ °)	$2.66 \,^{+1.42}_{-0.88}$ °)
$\chi^2(n_D)$ or $\ln \mathcal{L}$	0.0	55.8(36)	7.83(16)	38.6(29)	25.5(30)
number of events	335	335	310	338	338

*) from $\hat{f}_p/0.11\hat{f}_s$

**) a_o defined in Eq. (2.44)

°) a_o defined in Eq. (2.43)

Table VI.2

solutions with negative δ	max. likelihood method	min. χ^2 method E_+, E_-, k, E_e, ϕ distributions	Berends et al [4] $\cos\theta_\pi$ and ϕ distributions	Ely et al [2] $M_{\pi\pi}$, $\cos\theta_\pi$, $\cos\theta_l$, ϕ distributions	Billing [5] $M_{\pi\pi}$, $M_{e\nu}$, $\cos\theta_\pi$, ϕ distributions
$\nu = \tilde{f}_p'/\tilde{f}_s$	6.6 ± 1.2	8.7 ± 1.6	17.7 ± 2.7 *)	12.5 ± 1.2	11.0 ± 1.0
$\eta = \tilde{g}/\tilde{f}_s$	- 0.39 ± 0.15	- 0.71 ± 0.20	- 2.09 ± 0.42	- 1.61 ± 0.15	- 0.99 ± 0.14
$\gamma = \tilde{h}/\tilde{f}_s$	- 2.1 ± 0.8	- 4.0 $^{+1.5}_{-2.1}$	- 4.8 ± 1.7	- 2.41 ± 0.86	- 3.8 ± 1.4
δ(rads)	- 0.59 ± 0.18	- 0.74 ± 0.22	—	- 0.44 ± 0.14	- 0.70 ± 0.14
$a_o(m_\pi^{-1})$	- 1.1 $^{+0.6}_{-0.4}$ **)	—	- 0.57 ± 0.22 °)	- 0.89 ± 0.28 °)	- 1.42 ± 0.32 °)
$\chi^2(n_D)$ or $\ln \mathcal{L}$	- 2.6	51.0(36)	7.27(16)	26.6(29)	23.3(30)
number of events	335	335	310	338	338

*) from $\tilde{f}_p/0.11\tilde{f}_s$

**) a_o defined in Eq. (2.44)

°) a_o defined in Eq. (2.43)

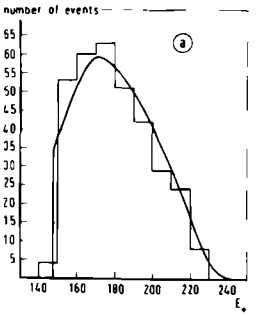

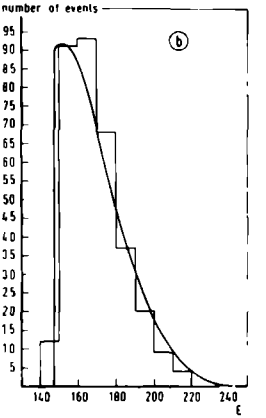

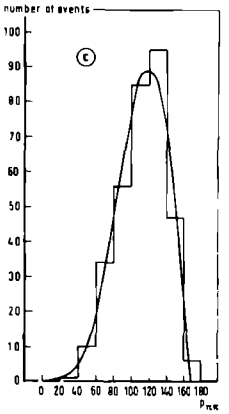

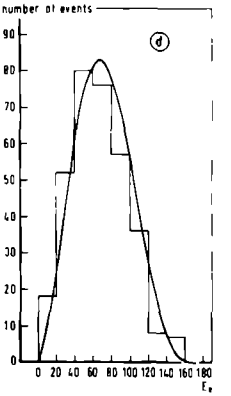

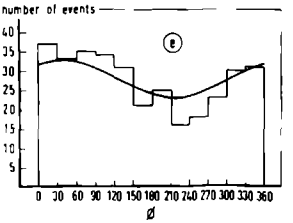

Fig. VI.1.
Distributions of E_+, E_-, $p_{\pi\pi}$, E_e and ϕ for 335 Ke4 events found by the LRL - UW - UCL collaboration.

sample of 1609 $K^+e4(e^+)$ events. This sample was selected from a number of about 450.000 spectrometer triggers.

In evaluating the significance of a sample of such a considerable larger size than that usually obtained in bubble chambers, it is important to stress the fact that counter experiments in general (and the one discussed here in particular) have serious biases in their "raw" (i.e. uncorrected) detection efficiencies. Although one tries to (and usually succeeds in) correcting these biases, the final results obtained are in a very essential way not only dependent on the statistics, but also on the success and the precision of the detection efficiency calculations.

To arrive at the form factors and the π-π phase shift both the maximum likelihood method and the least squares method were used. Using the first method a unique solution for the form factors and the phase shift difference was found. A χ^2 method, applied simultaneously to the $M_{\pi\pi}$, $M_{e\nu}$, $\cos\theta_\pi$, $\cos\theta_l$ and ϕ distributions, yielded two solutions with equal χ^2, one of them being very similar to the likelihood solution.

The size of their sample also allowed the authors to make an analysis without explicit assumptions about the energy dependence of the form factors, following the so-called Pais-Treiman method (see section II.4). This yielded a phase shift result very close to the value obtained with the other methods.

The $K^+e4(e^+)$ decay rate, found by the Geneva-Saclay collaboration , was $(3.32 \pm 0.31).10^3 sec^{-1}$; for the rate of $K^+e4(e^-)$ decay an upper limit of 43 sec^{-1} was given.

VI.3 Conclusions

In table VI.3 we have listed together the results of the LRL - UW - UCL collaboration (as reanalyzed with our maximum likelihood method), the X2 collaboration and the Geneva-Saclay collaboration. The form factor ratios ν, η and γ, the phase shift difference $<\delta_s - \delta_p>$ and the s-wave scattering length a_o all appear to be roughly compatible, with a tendency for the counter results to lie in between the results of the two bubble chamber experiments. It is remarkable to see the excellent agreement between the three values of $\nu + 5\eta$, a variable which, in contrast with ν, is not (or only slightly) correlated with η, γ and δ (see section V.2.1, Eq. (5.14) and Eq. (5.15)).

With respect to the $K^+e4(e^+)$ decay rates there is a very good agreement between X2 and Geneva-Saclay, both being higher than the values $2.9 \times 10^3 sec^{-1}$ and $2.6 \times 10^3 sec^{-1}$ given by the LRL - UW and the LRL - UW - UCL collaborations respectively.

Table VI.3

	LRL-UW-UCL bubble chamber exp.	Geneva-Saclay [2] counter exp.	X2 bubble chamber exp.
$\nu = \tilde{f}_p'/\tilde{f}_s$	2.2 ± 1.0	-0.5 ± 0.5	-2.0 ± 1.8
$\eta = \tilde{g}/\tilde{f}_s$	0.41 ± 0.12	0.87 ± 0.07	1.26 ± 0.30
$\gamma = \tilde{h}/\tilde{f}_s$	$-1.8 \,^{+0.8}_{-1.1}$	-0.85 ± 0.37	1.1 ± 1.4
$\nu + 5\eta$	4.2 ± 0.6	4.0 ± 0.3	4.3 ± 1.1
$\delta = \langle \delta_s - \delta_p \rangle$ (rads)	0.55 ± 0.18	0.39 ± 0.08	0.18 ± 0.22
$a_o (m_\pi^{-1})$	0.71 ± 0.45	0.66 ± 0.17	$0.22 \,^{+0.42}_{-0.38}$
$\Gamma_{Ke4(e^+)} (10^3 sec^{-1})$	2.6 ± 0.3 [1]	3.3 ± 0.3	3.3 ± 0.4
$\Gamma_{Ke4(e^-)} (sec^{-1})$ [3]	< 56 [1]	< 43	< 73

[1] rates calculated from 269 events

[2] errors statistical only

[3] confidence level 95%

References - chapter VI

1) R.W. Birge et al, Phys. Rev. 139, B1600 (1965).
2) R.P. Ely et al, Phys. Rev. 180, 1319 (1969).
3) F.A. Berends, A. Donnachie, G.C. Oades, Nucl. Phys. B3, 569 (1967).
4) F.A. Berends, A. Donnachie, G.C. Oades, Phys. Rev. 171, 1457 (1968).
5) K. Billing, thesis University College, London, unpublished.
6) M. Bourquin et al, Phys. Letters 36B, 615 (1971).
7) P. Basile et al, Phys. Letters 36B, 619 (1971).
8) A. Zylbersztjen et al, Phys. Letters 38B, 457 (1972).

VII. COMPARISON WITH THEORETICAL PREDICTIONS

VII.1 Predictions of the Ke4 form factors

One of the first attempts to calculate Ke4 form factors was made by C.G. Callan and S.B. Treiman [1] using equal-time commutators from current algebra, the PCAC hypothesis and soft pion techniques. They found a relation between the K_{14} axial current form factors f and g and the K_{13} form factors f_+ and f_-, the K_{12} decay constant f_K and the $\pi_{12}(\pi \to \mu\nu)$ decay constant f_π. The relation is valid at the unphysical point where the four-momentum of <u>one</u> of the pions is zero and therefore this pion is "off the mass shell". In particular they predicted f = g. Making the assumption that these off mass shell form factors vary slowly when extrapolated to the mass shell, Callan and Treiman found excellent agreement between the Ke4 form factors of the LRL - UW collaboration and the K_{13} form factors.

A subsequent calculation with <u>both</u> pion four-momenta equal to zero (instead of one) was performed by S. Weinberg [2]. His resulting numerical prediction was $|f \sin\theta_c| = |g \sin\theta_c| = 0.97 \pm 0.03$. Lately, an increasing number of authors have attempted to refine the computations of Callan, Treiman and Weinberg [3]. Still others have made estimations about the vector form factor h [4].

Almost all theories and techniques used are based on current algebra combined with different approaches for treating the strong-interaction current (e.g. the $SU_3 \times SU_3$ model and the Veneziano model). A wide variety of computations, with the pions off as well as on the mass shell, predict values for $|f \sin\theta_c|$ and $|g \sin\theta_c|$ ranging from 0.8 to 2.8 and for $\frac{g}{f}(\eta)$

from 0.5 to 2. The values predicted for the vector form factor $|h \sin\theta_c|$ show even stronger fluctuations (from 0.7 to 6.9).

Most authors neglect the π-π p-wave contribution to the form factor f and also assume the remaining s-wave π-π phase shift to be rather small.

Authors who use or predict the $Ke4$ decay rate in general apply a simplified version of Eq. (5.14), i.e. the expression

$$\Gamma(\text{sec}^{-1}) \cong \sin^2\theta_c \; (1.60\, f^2 + 0.31\, g^2).10^3 \qquad (7.1)$$

Within the wide range of predicted values for f, g and h, there is agreement with all known experiments. Clearly, the theoretical approaches have not yet reached the level of refinement required to make a comparison with the experimental results meaningful.

VII.2 Predictions of the π-π phase shift

In this section we first review the arguments for the choice of the scattering length parametrization used in the analysis of our $Ke4$ sample.

Current algebra calculations concerning π-π interactions were performed by S. Weinberg [5]. Applying the effective range approximation of Eq. (2.42), i.e.

$$q \cot\delta_o = \frac{1}{a_o} + \frac{1}{2} r_o q^2 \qquad (7.2)$$

where q is the pion momentum in the di-pion system, he obtains [6]:

$$a_o = (0.17 \pm 0.02)m_\pi^{-1} \quad , \quad r_o = (-7.3 \pm 0.7)m_\pi^{-1} \qquad (7.3)$$

Botke [7] has done a phenomenological study of the reaction $\pi^- p \to \pi^o \pi^o n$ within the framework of the isobar model. Using both total and differential cross section data he finds

$$r_o = (-6.5 \pm 0.5)m_\pi^{-1} \text{ for } a_o = 0.15 m_\pi^{-1}$$
$$\text{or } r_o = (-5.2 \,{}^{+\,0.2}_{-\,0.5})m_\pi^{-1} \text{ for } a_o = 0.20 m_\pi^{-1} \qquad (7.4)$$

The predictions (7.3) and (7.4), substituted in Eq. (7.2), give dependencies of the π-π s-wave phase shift δ_o on the effective di-pion mass $M_{\pi\pi}$ which are shown in fig. II.4^c. As can be seen, δ_o rises rapidly for $M_{\pi\pi}$ values beyond 450 MeV/c^2. This phenomenon can of course be traced back to the limited validity of Eq. (7.2) but this point is in so far irrelevant so long as we use this formula only in the region below 450 MeV/c^2.

Fig. II.4^b shows three curves which correspond to the substitution of some typical a_o values in the Chew-Mandelstam parametrization of the scattering length (Eq. (2.43)). Note that these curves have a tendency to remain constant or even to decrease for $M_{\pi\pi}$ values beyond 450 MeV/c^2. In comparison with fig. II.4^c a much higher a_o value has to be used to arrive at the same mean δ_o in the region $280 < M_{\pi\pi} < 450$ MeV/c^2.

Le Guillou et al [10] derived a set of curves from very general principles (such as analyticity, unitarity and crossing symmetry) and from the mass and width of the ρ-meson. These curves can be approximated by substituting $a_o = 0.2$ and $a_o = 0.7$ resp. in the parametrization of Eq. (2.44). It can be seen from fig. II.4^a that for higher $M_{\pi\pi}$ values these curves behave quite differently from the curves of fig. II.4^b

and fig. II.4^{c}. It turns out that these curves are reliable bounderies to the experimental data points from forward-backward asymmetry for the reactions $\pi^- p \to \pi^- \pi^o p$ and $\pi^- p \to \pi^+ \pi^- n$ [8, 9] in the region of $M_{\pi\pi}$ values beyond 450 MeV/c^2. For this reason the parametrization of Eq. (2.44) is used in the analysis of the Ke4 sample. Our result $a_o = 0.22 \pm 0.40$ is, within the large errors, in agreement with the rather precise predictions of Weinberg and Botke and also with the predicted a_o values for the above-mentioned data points in $\pi^- p$ interactions.

When introducing the scattering length a_o in section II.4, we made the assumption that the p-wave phase shift δ_1 would be small compared to the s-wave phase shift δ_o. This assumption is justified by predictions about δ_1 [10].

References - chapter VII

1) C.G. Callan and S.B. Treiman, Phys. Rev. Letters 16, 153 (1966).

2) S. Weinberg, Phys. Rev. Letters 17, 336 (1966) and erratum, Phys. Rev. Letters 18, 1178 (1967).

3) R.G. Roberts and F. Wagner, Proceeding of Topical Conference on Weak Interactions, CERN report 69-7.

C.H. Llewellyn Smith, R. Pascual and F.J. Yndurain, Nuovo Cimento 63A, 442 (1969).

S.C. Chhajlany, L.K. Pandit and G. Rajasekaran, Phys. Rev. D2, 1934 (1970).

L.J. Clavelli, Phys. Rev. 154, 1509 (1967).

D.F. Greenberg, Phys. Rev. 174, 1821 (1968) and Phys. Rev. 179, 1623 (1969).

A.Q. Sarker, Phys. Rev. 176, 1971 (1968).

S.N. Biswas, R. Dutt, K.C. Gupta, Annals of Physics (N.Y.) 52, 366 (1969).

R. Dutt, K.C. Gupta and J.S. Vaishya, Phys. Rev. 175, 1884 (1968).

S.N. Biswas, R. Dutt, P. Nanda and L.K. Pandit, Phys. Rev. D1, 1445 (1970).

S. Matsuda and S. Oneda, Phys. Rev. 165, 1749 (1968).

S.M. Berman and P. Roy, Phys. Letters 27B, 88 (1968).

S.P. de Alwis, Phys. Rev. D1, 2131 (1970).

Y. Hara, Phys. Rev. D1, 874 (1970).

M.K. Gaillard, Nuovo Cimento 65A, 135 (1970).

H.P.W. Gottlieb, Nucl. Phys. B36, 278 (1972).

B.R. Wienke and N.G. Deshpande, Phys. Rev. D5, 725 (1972).

N.F. Nasrallah and K. Schilcher, Phys. Rev. D2, 2698 (1970).

N. Tokuda and Y. Oyanagi, Phys. Rev. D1, 2626 (1970).

4) A.K. Mohanti and R.E. Marshak, Nuovo Cimento 52A, 967 (1967) and erratum Nuovo Cimento 54A, 213 (1968).
F.A. Berends, A. Donnachie and G.C. Oades, Nucl. Phys. B3, 569 (1967).
D.F. Greenberg, Phys. Rev. 174, 1821 (1968).
A.Q. Sarker, Phys. Rev. 176, 1971 (1968).
L.E. Wood, Phys. Rev. 181, 1890 (1969) and erratum Phys. Rev. D1, 3203 (1970).
R. Dutt and R. Majumdar, Phys. Rev. 184, 1950 (1969).
N.J. Carron and R.L. Schult, Phys. Rev. D1, 3171 (1970).
5) S. Weinberg, Phys. Rev. Letters 17, 616 (1966).
6) G. Ebel et al, Nucl. Phys. B33, 356 (1971).
7) J.C. Botke, Nucl. Phys. B23, 253 (1970).
8) J.H. Scharenguigel et al, Phys. Rev. 186, 1387 (1969).
9) J.H. Scharenguifel et al, Nucl. Phys. B22, 16 (1970).
10) J.C. le Guillou, A. Morel and H. Navelet, Nuovo Cimento 5A, 659 (1971).
see also J.L. Petersen, Phys. Reports 2C (1971).
C. Schmid, Proceedings of the Amsterdam Int. Conf. on Elementary Particles (North-Holland) (1972).

APPENDIX 1

Starting from the general expressions given in section II.3 we derive in this appendix the Ke4 decay probability expressed in terms of the variables E_+, E_-, $k(= |\vec{p}_{\pi\pi}|)$, E_e and ϕ and the various form factors.

The symbols used here were previously defined in chapter II. For the 4 x 4 γ_i-matrices we use the convention:

$$\gamma_k = \begin{pmatrix} 0 & -i\sigma_k \\ i\sigma_k & 0 \end{pmatrix} \text{ with } \sigma_1 = \begin{pmatrix} 0 & 1 \\ 1 & 0 \end{pmatrix}, \sigma_2 = \begin{pmatrix} 0 & -i \\ i & 0 \end{pmatrix}$$

$$\sigma_3 = \begin{pmatrix} 1 & 0 \\ 0 & -1 \end{pmatrix}$$

$$\gamma_4 = \begin{pmatrix} 1 & 0 \\ 0 & -1 \end{pmatrix} \text{ and } \gamma_5 = \gamma_1\gamma_2\gamma_3\gamma_4 = \begin{pmatrix} 0 & -1 \\ -1 & 0 \end{pmatrix} \quad \text{(A1.1)}$$

Products of these γ-matrices have the following properties:

$$\gamma_k\gamma_l + \gamma_l\gamma_k = 2\delta_{kl} \quad \text{for} \quad k,l = 1,2,3,4,5 \quad \text{(A1.2)}$$

The γ-matrices are self-conjugate or Hermitian, i.e.

$$\gamma_k^+ = \tilde{\gamma}_k^* = \gamma_k \quad (k = 1,2,3,4,5) \quad \text{(A1.3)}$$

With the above convention the Dirac equation is written as

$$\left(\gamma_\mu \frac{\partial}{\partial x_\mu} + m\right) \psi(x_\nu) = 0 \quad \text{(A1.4)}$$

or in the momentum representation

$$(i\gamma_\nu p_\nu + m)\, u^r(p_\nu) = 0 \qquad (A1.4^a)$$

We start evaluating the product of the matrix element M with its complex conjugate M*. Substitution of Eqs. (2.11) and (2.12) into Eq. (2.10) gives

$$M = \frac{G \sin\theta_c}{m_K\sqrt{2}} (fR_\lambda + gQ_\lambda + eK_\lambda + \frac{h}{m_K^2}\, \varepsilon_{\lambda\mu\nu\sigma}\, K_\mu R_\nu Q_\sigma)$$

$$\bar{u}(p_\nu)\gamma_\lambda(1 + \gamma_5)v(p_e) \qquad (A1.5)$$

Summation over the index λ (1.....4) is always implied.

Eq. (A1.5) can be rewritten as

$$M = \frac{G \sin\theta_c}{m_K\sqrt{2}}\, \bar{u}(p_\nu)(1 - \gamma_5)\gamma_\lambda(fR_\lambda + gQ_\lambda + eK_\lambda$$

$$+ \frac{h}{m_K^2}\, \varepsilon_{\lambda\mu\nu\sigma}\, K_\mu R_\nu Q_\sigma)v(p_e) \qquad (A1.6)$$

Taking the complex conjugate of this expression we get

$$M^* = \frac{G \sin\theta_c}{m_K\sqrt{2}}\, \bar{v}(p_e)\gamma_4(f^*R_\lambda^* + g^*Q_\lambda^* + e^*K_\lambda^*$$

$$+ \frac{h^*}{m_K^2}\, \varepsilon_{\lambda\mu\nu\sigma}\, K_\mu^* R_\nu^* Q_\sigma^*)\gamma_\lambda \underbrace{(1 - \gamma_5)\gamma_4}_{\gamma_4(1 + \gamma_5)} u(p_\nu) \qquad (A1.7)$$

Substituting $\gamma_4\gamma_\lambda\gamma_4 A_\lambda^* = -\gamma_\lambda A_\lambda$ (A1.8)

and $\varepsilon_{\lambda\mu\nu\sigma}\, \gamma_4\gamma_\lambda\gamma_4 K_\mu^* R_\nu^* Q_\sigma^* = \varepsilon_{\lambda\mu\nu\sigma}\, \gamma_\lambda K_\mu R_\nu Q_\sigma$ (A1.9)

we rewrite

$$M^* = \frac{-G \sin\theta_c}{m_K\sqrt{2}} \bar{v}(p_e)\gamma_\lambda(f^*R_\lambda + g^*Q_\lambda + e^*K_\lambda$$

$$- \frac{h^*}{m_K^2} \varepsilon_{\lambda\mu\nu\sigma} K_\mu R_\nu Q_\sigma)(1 + \gamma_5)u(p_\nu) \qquad \text{(A1.10)}$$

With the definitions of Eqs. (2.19) and (2.20) we now have for the product $MM^* = |M|^2$ the expression

$$|M|^2 = \frac{-G^2 \sin^2\theta_c}{2} \bar{v}(p_e)\gamma_\lambda V'_\lambda(1 + \gamma_5)u(p_\nu)\bar{u}(p_\nu)(1 - \gamma_5)$$

$$\gamma_\mu V_\mu v(p_e) \qquad \text{(A1.11)}$$

As we are not interested in any particular spin state, we must sum Eq. (A1.11) over the possible spin states both of the neutrino and of the electron. From

$$\sum_{\text{spins}} u(p_\nu)\bar{u}(p_\nu) = \frac{-i\gamma\cdot p_\nu + m_\nu}{2m_\nu} \qquad \text{(A1.12)}$$

we derive

$$\Sigma|M|^2 = \frac{G^2 \sin^2\theta_c}{4m_\nu} \bar{v}(p_e)(\gamma\cdot V')(1 + \gamma_5)i(\gamma\cdot p_\nu)$$

$$(1 - \gamma_5)(\gamma\cdot V)v(p_e) \qquad \text{(A1.13)}$$

In our convention the spinor products are

$$\begin{aligned} \bar{u}_i(p)u_j(p) &= \delta_{ij} \quad \text{(particle)} \\ \bar{v}_i(p)v_j(p) &= -\delta_{ij} \quad \text{(anti-particle)} \end{aligned} \qquad \text{(A1.14)}$$

Note that $v(p) = u(-p)$.

The sum over the two anti-particle spin states can be replaced by the sum over the four orthonormal spinors if we select the two anti-particle states with the help of a special projection operator $\Lambda_-(p)$, defined such that

$$\Lambda_-(p)v(p) = - v(p)$$
$$\Lambda_-(p)u(p) = 0 \qquad \text{(A1.15)}$$

From the Dirac equation one derives

$$\Lambda_-(p) = \frac{- i\gamma\cdot p - m}{2m}$$

Eq. (A1.13) can therefore be rewritten as

$$\Sigma|M|^2 = \frac{G^2 \sin^2\theta_c}{8m_\nu m_1} \bar{u}(p_e)(\gamma\cdot V')i(\gamma\cdot p_\nu)2(1 - \gamma_5)(\gamma\cdot V)$$
$$(- i\gamma\cdot p_e - m_e)u(p_e) \qquad \text{(A1.16)}$$

where all inner products imply summation over four indices. Thus $\bar{u}(p_e).....u(p_e)$ means

$$\sum_{i,\alpha,\beta,\gamma,\delta,\varepsilon = 1....4} \bar{u}^i_\alpha(\gamma\cdot V')_{\alpha\beta}(\gamma\cdot p_\nu)_{\beta\gamma}(1 - \gamma_5)_{\gamma\delta}$$
$$(\gamma\cdot V)_{\delta\varepsilon}(i\gamma\cdot p_1 + m_1)_{\varepsilon\alpha}u^i_\alpha \qquad \text{(A1.17)}$$

This summation is performed by taking the trace as follows:

$$\Sigma|M|^2 = - i \frac{G^2 \sin^2\theta_c}{4m_\nu m_e} \mathrm{Tr}\left[(\gamma\cdot V')(\gamma\cdot p_\nu)(1 - \gamma_5)(\gamma\cdot V)\right.$$
$$\left.(i\gamma\cdot p_e + m_e)\right] \qquad \text{(A1.18)}$$

The only non-zero traces are those of the types

$$\mathrm{Tr}\ (\gamma\cdot A)(\gamma\cdot B)(\gamma\cdot C)(\gamma\cdot D) = 4\ \{(AB)(CD) - (AC)(BD) + (AD)(BC)\} \quad \text{(A1.19)}$$

$$\mathrm{Tr}\ \gamma_5(\gamma\cdot A)(\gamma\cdot B)(\gamma\cdot C)(\gamma\cdot D) = 4\ \varepsilon_{\lambda\mu\nu\sigma} A_\lambda B_\mu C_\nu D_\sigma \quad \text{(A1.20)}$$

Using these relations Eq. (A1.18) becomes

$$\Sigma|M|^2 = \frac{G^2 \sin^2\theta_c}{m_\nu m_e} \left[(V'\cdot p_\nu)(V\cdot p_e) + (V'\cdot p_e)(V\cdot p_\nu) - (V'\cdot V)(p_\nu\cdot p_e) + \varepsilon_{\lambda\mu\sigma\rho} V_\lambda V'_\mu (p_e)_\sigma (p_\nu)_\rho\right] \quad \text{(A1.21)}$$

Using $K = p_e + p_\nu$ and $L = p_e - p_\nu$ we rewrite this as

$$\Sigma|M|^2 = \frac{G^2 \sin^2\theta_c}{2m_\nu m_e} V_\mu V'_\nu \left[K_\mu K_\nu - L_\mu L_\nu - (K^2 + m_e^2)\delta_{\mu\nu} + \varepsilon_{\mu\nu\sigma\rho} L_\sigma K_\rho\right] = \frac{G^2 \sin^2\theta_c}{2m_\nu m_e} V_\mu V'_\nu T_{\mu\nu} \quad \text{(A1.22)}$$

When Eq. (A1.22) is substituted in Eq. (2.19) we obtain

$$dw = \frac{G^2 \sin^2\theta_c}{(2\pi)^8 16 m_K} V_\mu V'_\nu T_{\mu\nu}\ \delta^4(p_+ + p_- + p_e + p_\nu - p_K)\ \frac{d^3p_+}{E_+}\ \frac{d^3p_-}{E_-}\ \frac{d^3p_e}{E_e}\ \frac{d^3p_\nu}{E_\nu} \quad \text{(A1.23)}$$

Let us write

$$dw = F \frac{d^3p_+}{E_+} \frac{d^3p_-}{E_-} \frac{d^3p_e}{E_e} \frac{d^3p_\nu}{E_\nu}$$

$$\delta^4(p_+ + p_- + p_e + p_\nu - p_K) \qquad (A1.24)$$

We want to carry out the integration of dw, keeping E_+, E_-, k, E_e and ϕ differential. It is practical to distinguish between the di-pion system and the di-lepton system in the following way:

$$dw = F\, dK_o \frac{dp_+^3}{E_+} \frac{dp_-^3}{E_-} \delta^4(p_+ + p_- + K - p_K)$$

$$d^3K \frac{d^3p_e}{E_e} \frac{d^3p_\nu}{E_\nu} \delta^4(p_e + p_\nu - K) \qquad (A1.25)$$

Integrating firstly the di-lepton part we get

$$d^3K \frac{d^3p_e}{E_e} \frac{d^3p_\nu}{E_\nu} \delta^4(p_e + p_\nu - K) = d^3K \frac{d^3p_e}{E_e} \frac{1}{E_\nu}$$

$$\delta(E_e + E_\nu - K_o)$$

with $\vec{p}_\nu = \vec{K} - \vec{p}_e$ and $|\vec{p}_\nu|^2 = E_\nu^2 = |\vec{K}|^2 + |\vec{p}_e|^2 - 2|\vec{K}||\vec{p}_e| \cos\alpha$,

where α is the angle between $\vec{p}_e$ and $\vec{K}$.
We now take

$$d^3K = 4\pi|\vec{K}|^2\, d|\vec{K}| = 4\pi k^2 dk \text{ and } d^3p_e = p_e^2\, dp_e\, d\phi\, d(\cos\alpha),$$

where ϕ is the angle between the di-pion plane and the

di-lepton plane. Hence, we have

$$4\pi k^2 \frac{p_e^2}{E_e} \frac{1}{E_\nu(\alpha)} \, dk \, dp_e \, d\phi \, d(\cos\alpha) \, \delta[E_e - K_0 + E_\nu(\alpha)]$$

Making use of the δ-function we integrate with respect to $\cos\alpha$. We recall that if $g(x) = 0$ for $x = x_o$, then

$$\int f(x) \, \delta[g(x)] \, dx = \frac{f(x_o)}{|g'(x_o)|} \tag{A1.26}$$

Here $g(\cos\alpha) = E_e - K_o + (k^2 + p_e^2 - 2kp_e\cos\alpha)^{\frac{1}{2}}$

$$g'(\cos\alpha) = - \frac{kp_e}{E_\nu}$$

Hence $\frac{1}{|g'(x_o)|} = \frac{E_\nu}{kp_e}$ with $E_\nu = K_o - E_e$.

Consequently we obtain

$$4\pi k \, dk \, \frac{p_e dp_e}{E_e} \, d\phi = 4\pi k \, dk \, dE_e \, d\phi \tag{A1.27}$$

where we have used $p_e dp_e = E_e \, dE_e$.
We still have to integrate

$$dK_o \frac{d^3p_+}{E_+} \frac{d^3p_-}{E_-} \delta^3(p_+ + p_- + k) \, \delta(E_+ + E_- + K_o - m_K)$$

$$= \frac{d^3p_+}{E_+} \frac{d^3p_-}{E_-} \delta^3(p_+ + p_- + k) \text{ with } E_+ + E_- + K_o = m_K$$

$$= \frac{d^3p_+}{E_+E_-} \text{ with } \vec{p}_- = - (\vec{k} + \vec{p}_+)$$

$$= \frac{2\pi p_+^2 dp_+ d\cos\beta}{E_+E_-} \text{ where } \beta \text{ is the angle between } \vec{p}_+ \text{ and } \vec{k}.$$

From $\vec{p}_- = -(\vec{k} + \vec{p}_+)$ we derive

$$p_-^2 = k^2 + p_+^2 + 2kp_+ \cos\beta$$

$$d\cos\beta = \frac{p_-}{kp_+}\, dp_-$$

Substitution of this last expression gives

$$\frac{2\pi p_+ dp_+ p_- dp_-}{kE_+E_-} = \frac{2\pi dE_+ dE_-}{k} \qquad \text{(A1.28)}$$

Substituting Eqs. (A1.27 and (A1.28) in Eq. (A1.25) we obtain the result

$$dw = 8\pi^2 F\, dE_+\, dE_-\, dk\, dE_e\, d\phi \qquad \text{(A1.29)}$$

$$= \frac{G^2 \sin^2\theta_c}{(2\pi)^6 8m_K} V_\mu V'_\nu T_{\mu\nu}\, dE_+\, dE_-\, dk\, dE_e\, d\phi \qquad \text{(2.13)}$$

Working out the product $V_\mu V'_\nu T_{\mu\nu}$ we obtain

$$V_\mu V'_\nu T_{\mu\nu} = \frac{|f|^2}{m_K^2}\{(RK)^2 - (RL)^2 - R^2(K^2 + m_e^2\} + \frac{|g|^2}{m_K^2} x$$

$$\{(KQ)^2 - (QL)^2 - Q^2(K^2 + m_e^2)\} + \frac{|e|^2}{m_K^2}\{-(KL)^2 - m_e^2K^2\}$$

$$+ \frac{|h|^2}{m_K^6}[(QRLK)^2 + (K^2 + m_e^2)\{K^2R^2Q^2 + 2(RK)(KQ)(RQ)$$

$$- K^2(RQ)^2 - R^2(KQ)^2 - Q^2(RK)^2\}] + \frac{2Re\ fg^*}{m_K^2}\{(RK)(KQ)$$

$$- (RL)(QL) - (RQ)(K^2 + m_e^2)\} + \frac{2Im\ fg^*}{m_K^2}|QRLK| + \frac{2Re\ fe^*}{m_K^2} x$$

$$\{-(KL)(RL) - m_e^2(RK)\} + \frac{2\mathrm{Re}\ fh^*}{m_K^4}[(RK)\{(RL)(KQ) - (QL)(RK)\}$$

$$- R^2\{(KL)(KQ) - (QL)K^2\} + (RQ)\{(KL)(RK) - (RL)K^2\}]$$

$$+\frac{2\mathrm{Im}\ fh^*}{m_K^4}(RL)\ |QRLK| + \frac{2\mathrm{Re}\ ge^*}{m_K^2}\{-(KL)(QL) - m_e^2(KQ)\}$$

$$+\frac{2\mathrm{Re}\ gh^*}{m_K^4}[(KQ)\{(RL)(KQ) - (QL)(RK)\} - (RQ)\{(KL)(KQ)$$

$$- (QL)K^2\} + Q^2\{(KL)(RL) - (RL)K^2\}] + \frac{2\mathrm{Im}\ gh^*}{m_K^4}(QL)\ |QRLK|$$

$$+\frac{2\mathrm{Im}\ eh^*}{m_K^4}(KL)\ |QRLK|.$$

where QRLK means $\varepsilon_{\mu\nu\rho\sigma} Q_\mu R_\nu L_\rho K_\sigma$ (A1.30)

In deriving this equation we have used the sum rule

$$\sum_\mu \varepsilon_{\mu\alpha\beta\gamma}\,\varepsilon_{\mu\alpha'\beta'\gamma'} = \begin{vmatrix} \delta_{\alpha\alpha'} & \delta_{\alpha\beta'} & \delta_{\alpha\gamma'} \\ \delta_{\beta\alpha'} & \delta_{\beta\beta'} & \delta_{\beta\gamma'} \\ \delta_{\gamma\alpha'} & \delta_{\gamma\beta'} & \delta_{\gamma\gamma'} \end{vmatrix} \qquad \text{(A1.31)}$$

Expressed in the variables E_+, E_-, k, E_e and ϕ (and for convenience also in $E_\nu = m_K - E_+ - E_- - E_e$, $p_\nu^2 = E_\nu^2$ and $p_e^2 = E_e^2 - m_e^2$) we have

$$R^2 = k^2 - (E_+ + E_-)^2$$

$$K^2 = k^2 - (E_e + E_\nu)^2$$

$$Q^2 = (E_+ + E_-)^2 - k^2 - 4m_\pi^2$$

$$RK = -k^2 - (E_+ + E_-)(E_e + E_\nu)$$

$$RQ = 0 \qquad \text{(A1.32)}$$

$$RL = m_K (E_\nu - E_e) + m_e^2$$

$$KQ = m_K (E_- - E_+)$$

$$KL = -m_e^2$$

$$QL = \frac{1}{k^2} \{\lambda(P_+^2, p_-^2, k^2).\lambda(p_e^2, p_\nu^2, k^2)\}^{\frac{1}{2}} \cos\phi -$$

$$\frac{1}{k^2} (E_+^2 - E_-^2)(E_e^2 - E_\nu^2 - m_e^2) - (E_+ - E_-)(E_e - E_\nu)$$

$$QRLK = i \frac{m_K}{k} \{\lambda(p_+^2, p_-^2, k^2).\lambda(p_e^2, p_\nu^2, k^2)\}^{\frac{1}{2}} \sin\phi$$

where $\lambda(x, y, z) = x^2 + y^2 + z^2 - 2xy - 2xz - 2yz$.

As can be easily seen the coefficients of $|e^2|$, Re fe^*, Re ge^* and Im eh^* all contain a factor m_e^2 so that in practice we may omit these terms.

From our definitions

$$f = f_s^{\chi} \left(e^{i\delta_s} + \frac{E_+ - E_-}{m_K} \nu\, e^{i\delta_p}\right)$$

$$g = f_s^{\chi} \eta\, e^{i\delta_p} \qquad \text{(A1.33)}$$

$$h = f_s^{\chi} \gamma\, e^{i\delta_p}$$

it follows that

$$|f|^2 = \overset{\gamma}{f}_s^2 \{1 + \frac{2(E_+ - E_-)}{m_K} \nu \cos(\delta_s - \delta_p) + \frac{(E_+ - E_-)^2}{m_K^2} \nu^2\}$$

$$|g|^2 = \overset{\gamma}{f}_s^2 \eta^2$$

$$|h|^2 = \overset{\gamma}{f}_s^2 \gamma^2$$

$$\text{Re } fg^* = \overset{\gamma}{f}_s^2 \{\frac{E_+ - E_-}{m_K} \nu\eta + \eta \cos(\delta_s - \delta_p)\} \qquad \text{(A1.34)}$$

$$\text{Im } fg^* = \overset{\gamma}{f}_s^2 \eta \sin(\delta_s - \delta_p)$$

$$\text{Re } fh^* = \overset{\gamma}{f}_s^2 \{\frac{E_+ - E_-}{m_K} \nu\gamma + \gamma \cos(\delta_s - \delta_p)\}$$

$$\text{Im } fh^* = \overset{\gamma}{f}_s^2 \gamma \sin(\delta_s - \delta_p)$$

$$\text{Re } gh^* = \overset{\gamma}{f}_s^2 \gamma\eta$$

$$\text{Im } gh^* = 0$$

Eqs. (A1.32) and (A1.34) can be substituted in Eq. (A1.30), so that $V_\mu V'_\nu T_{\mu\nu}$ is then expressed in the variables E_+, E_-, k, E_e and ϕ, the form factor $\overset{\gamma}{f}_s$, the form factor ratios ν, η and γ and the mean phase shift difference $\langle\delta_s - \delta_p\rangle$.

APPENDIX 2

To obtain the integrated Ke4 decay probabilities as given in Eqs. (5.2) and (5.14) we integrated the coefficients of each form factor (or product of a form factor and phase shift) in Eq. (A1.30) after the substitution of Eqs. (A1.32) and (A1.34). A computer program was used to do most of the integrations numerically, applying IBM Gaussian integration routines in double precision.

The following integration order appeared to be convenient

1) integration over ϕ between the boundaries 0 and 2π (analytically)
2) integration over E_e; for given $(E_+ + E_-)$ and k the integration boundaries are

$$(E_e)_{max} = \frac{\{m_K - (E_+ + E_-) + k\}^2 + m_e^2}{2\{m_K - (E_+ + E_-) + k\}} \qquad (A2.1)$$

and

$$(E_e)_{min} = \frac{\{m_K - (E_+ + E_-) - k\}^2 + m_e^2}{2\{m_K - (E_+ + E_-) - k\}} \qquad (A2.2)$$

3) integration over $(E_+ - E_-)$; for given $(E_+ + E_-)$ and k the range of integration is from

$$-k\sqrt{1 - \frac{4m_\pi^2}{(E_+ + E_-)^2 - k^2}} \qquad (A2.3)$$

to

$$+k\sqrt{1 - \frac{4m_\pi^2}{(E_+ + E_-)^2 - k^2}} \qquad (A2.4)$$

4) integration over $(E_+ + E_-)$; this quantity is only dependent on k, its minimum value being $\sqrt{k^2 + 4m_\pi^2}$ (A2.5)

and its maximum value being $m_K - \sqrt{k^2 + m_e^2}$ (A2.6)

5) finally integration over k, ranging from 0 to

$$k_{max} \cong \frac{1}{2m_K}(m_K^2 - 4m_\pi^2) = 168.0 \text{ MeV}/c \quad \text{(A2.7)}$$

To account for the kinematical cuts in the configuration space the following modifications were necessary:

i) The cut on pion momenta lower than 48 MeV/c is accounted for by a change of integration boundaries. Eq. (A2.3) is replaced by the maximum of $(295.2 - E_+ - E_-)$ and Eq. (A2.3); Eq. (A2.4) is replaced by the minimum of $(E_+ + E_- - 295.2)$ and Eq. (A2.4). Further Eq. (A2.5) is replaced by the maximum of 295.2 MeV and Eq. (A2.5).

ii) The probability for an event to lie in the τ 'box' (missing mass between 130 and 150 MeV/c^2, missing momentum lower than 60 MeV/c) is calculated separately and subtracted afterwards from the total probability. The integration boundaries then become

$$m_K - \sqrt{k^2 + 150^2} \leqslant (E_+ + E_-) \leqslant m_K - \sqrt{k^2 + 130^2}$$

and $0 \leqslant k \leqslant 60 \text{ MeV}/c$

There is no overlap with the cut on pion momenta.

The results of the integrations, with and without cuts, are given in Eqs. (5.14) and (5.2) respectively. As can be seen the coefficients of many combinations of form factors and the π-π phase shift difference cancel or are negligible. The one-dimensional distributions in E_+, E_-, k, E_e and ϕ are also found by numerical integrations, keeping the expressions differential in the wanted variable.

As each of these fourfold integrations has its own set of integration limits, we only give the numerical results. Note that the k and the E_e distributions are independent of the π-π phase shift, while the phase shift terms of the E_+ and the E_- distributions have opposite signs.

A) ϕ distribution (with cuts)

$$\partial\Gamma/\partial\phi = (\alpha + \beta \cos\phi + \lambda \sin\phi + \kappa \cos^2\phi)\, A$$

with $\alpha = 498 + 1.65\nu^2 + 116\eta^2 + 0.58\gamma^2 + 17.5\eta\nu$

$\beta = -\,49.9\gamma \cos\delta$

$\lambda = 258\eta \sin\delta$

$\kappa = 1.16\gamma^2 - 40.8\eta^2$

$A = N/(498 + 1.65\nu^2 + 95.9\eta^2 + 1.16\gamma^2 + 17.5\eta\nu)$

B) $E_{\pm}$ distribution (with cuts)

bin(MeV)	
147.6 - 150	$(11.0 + 0.064\nu^2 \mp 1.51\nu\cos\delta + 1.82\eta^2 + 0.014\gamma^2 \mp 7.0\eta\cos\delta + 0.57\eta\nu)$ B
150 - 160	$(50.4 + 0.190\nu^2 \mp 5.10\nu\cos\delta + 7.80\eta^2 + 0.094\gamma^2 \mp 24.7\eta\cos\delta + 1.84\eta\nu)$ B
160 - 170	$(51.3 + 0.107\nu^2 \mp 2.32\nu\cos\delta + 7.60\eta^2 + 0.127\gamma^2 \mp 12.8\eta\cos\delta + 1.17\eta\nu)$ B
170 - 180	$(44.5 + 0.071\nu^2 \pm 0.21\nu\cos\delta + 6.85\eta^2 + 0.125\gamma^2 \mp 1.1\eta\cos\delta + 0.82\eta\nu)$ B
180 - 190	$(34.7 + 0.077\nu^2 \pm 1.69\nu\cos\delta + 6.69\eta^2 + 0.102\gamma^2 \pm 6.8\eta\cos\delta + 0.84\eta\nu)$ B
190 - 200	$(25.3 + 0.093\nu^2 \pm 2.28\nu\cos\delta + 6.30\eta^2 + 0.067\gamma^2 \pm 11.5\eta\cos\delta + 1.00\eta\nu)$ B
200 - 210	$(17.1 + 0.100\nu^2 \pm 2.24\nu\cos\delta + 5.14\eta^2 + 0.035\gamma^2 \pm 12.2\eta\cos\delta + 1.07\eta\nu)$ B
210 - 220	$(10.0 + 0.084\nu^2 \pm 1.67\nu\cos\delta + 3.64\eta^2 + 0.013\gamma^2 \pm 9.6\eta\cos\delta + 0.92\eta\nu)$ B
220 - 230	$(4.0 + 0.038\nu^2 \pm 0.73\nu\cos\delta + 1.74\eta^2 + 0.003\gamma^2 \pm 4.6\eta\cos\delta + 0.45\eta\nu)$ B
230 - 240	$(0.7 + 0.005\nu^2 \pm 0.11\nu\cos\delta + 0.35\eta^2 \pm 0.9\eta\cos\delta + 0.08\eta\nu)$ B

where B = 2A and $\delta = \langle \delta_s - \delta_p \rangle$

C) k distribution (with cuts)

bin($MeV_{/c}$)	
0 - 20	$(0.12 + 0.92\eta^2 + 0.0007\gamma^2 + 0.005\eta\nu)\ A$
20 - 40	$(2.6 + 0.002\nu^2 + 5.3\ \eta^2 + 0.015\ \gamma^2 + 0.11\ \eta\nu)\ A$
40 - 60	$(13.8 + 0.023\nu^2 + 11.9\ \eta^2 + 0.073\ \gamma^2 + 0.66\ \eta\nu)\ A$
60 - 80	$(45.4 + 0.12\ \nu^2 + 21.4\ \eta^2 + 0.218\ \gamma^2 + 2.26\ \eta\nu)\ A$
80 - 100	$(89.5 + 0.34\ \nu^2 + 24.1\ \eta^2 + 0.328\ \gamma^2 + 4.34\ \eta\nu)\ A$
100 - 120	$(129 + 0.55\ \nu^2 + 20.0\ \eta^2 + 0.316\ \gamma^2 + 5.41\ \eta\nu)\ A$
120 - 140	$(130 + 0.44\ \nu^2 + 9.9\ \eta^2 + 0.174\ \gamma^2 + 3.56\ \eta\nu)\ A$
140 - 160	$(79.9 + 0.16\ \nu^2 + 2.4\ \eta^2 + 0.037\ \gamma^2 + 1.15\ \eta\nu)\ A$
160 - 168	$(7.8 + 0.011\nu^2 + 0.11\eta^2 + 0.0005\gamma^2 + 0.06\ \eta\nu)\ A$

D) E_e distribution (with cuts)

bin(MeV)	
0.5 - 20	$(13.5 + 0.059\nu^2 + 3.5\ \eta^2 + 0.060\gamma^2 + 0.60\eta\nu + 0.59\eta\gamma)\ A$
20 - 40	$(62.8 + 0.249\nu^2 + 15.4\ \eta^2 + 0.193\gamma^2 + 2.70\eta\nu + 1.92\eta\gamma)\ A$
40 - 60	$(109.5 + 0.397\nu^2 + 24.1\ \eta^2 + 0.223\gamma^2 + 4.47\eta\nu + 1.46\eta\gamma)\ A$
60 - 80	$(122.6 + 0.414\nu^2 + 23.9\ \eta^2 + 0.210\gamma^2 + 4.58\eta\nu - 0.15\eta\gamma)\ A$
80 - 100	$(101.7 + 0.315\nu^2 + 17.2\ \eta^2 + 0.200\gamma^2 + 3.28\eta\nu - 1.38\eta\gamma)\ A$
100 - 120	$(60.4 + 0.158\nu^2 + 8.8\ \eta^2 + 0.173\gamma^2 + 1.47\eta\nu - 1.60\eta\gamma)\ A$
120 - 140	$(23.2 + 0.045\nu^2 + 2.5\ \eta^2 + 0.086\gamma^2 + 0.36\eta\nu - 0.74\eta\gamma)\ A$
140 - 160	$(4.2 + 0.006\nu^2 + 0.29\ \eta^2 + 0.015\gamma^2 + 0.04\eta\nu - 0.10\eta\gamma)\ A$

SUMMARY

This thesis describes an experiment on K^+ mesons decaying in a bubble chamber. The emphasis lies on the decay mode in which the K^+ meson desintegrates into a π^+, a π^-, an e^+ and a neutrino, usually called the K^+e4 decay. As this decay mode is rather rare (1 in ca 25000) approximately half a million pictures were needed, with an average of seven K^+ decays per picture, to obtain a hundred K^+e4 events. During the analysis of the pictures we also looked for the possible $K^+ \rightarrow \pi^+\pi^+e^-\bar{\nu}$ decay, i.e. K^+e4 decay with a negative electron. In agreement with the semileptonic $\Delta S = \Delta Q$ rule none was found.

Within the framework of the so-called X2 collaboration the K^+e4 candidates were measured and analyzed in five European laboratories, namely in Aachen, Brussels, Cern, Nijmegen and Padova.

After an introduction and a description of the problem in the first chapter, theoretical preliminaries are presented in chapter II. This results in various relations existing between the distribution of measurable and/or calculable quantities on the one hand and the values of the so-called form factors and the π-π phase shift on the other hand.

The next two chapters describe the experimental set-up and the collection of the data. The methods used to separate as many good events as possible from the background and to correct for missed events are also described in chapter IV.

Chapter V treats the analysis of the selected events using both the maximum likelihood method and the least squares method.

The results of these analyses are experimental values for the K^+e4 branching ratio [$(4.1 \pm 0.5) \times 10^{-5}$], the π-π phase shift $<\delta_s - \delta_p>$, the form factors $\hat{f}_s$, $\hat{f}_p$, $\hat{f}_p'$, g and h and their ratios ν, η and γ (see table V.2 on page 70).

In chapter VI these values are compared with the results of similar experiments carried out with bubble chambers as well as with counters and spark chambers. Nearly all K^+e4 events, previously detected in bubble chambers, are reanalyzed. It appears that the various results are roughly in agreement. Good correspondence exists between the values for the branching ratio and between the values for a 'privileged' combination of form factors $\nu + 5\eta$ (see table VI.3 on page 95).

Finally, some theoretical predictions are reviewed in chapter VII and compared with the experimental results. As the predictions of the form factors differ rather strong among themselves a meaningful conclusion is not possible. However, for the π-π phase shift and the scattering length a_o the predicted and experimental values agree well.

SAMENVATTING

Dit proefschrift beschrijft een experiment met in een bellenvat vervallende K^+ mesonen. De nadruk ligt op die vervalswijze, waarbij het K^+ meson desintegreert in een π^+, een π^-, een e^+ en een neutrino, kortweg aangeduid met K^+e4 verval. Daar deze vervalswijze tamelijk zeldzaam is (1 op ca 25.000) waren ongeveer een half miljoen foto's nodig met een gemiddelde van zeven K^+ vervallen per foto, om een honderdtal K^+e4 verschijnselen te verzamelen. Bij het analyseren van deze foto's hebben we ook gezocht naar mogelijk $K^+ \to \pi^+\pi^+e^-\bar{\nu}$ verval, dat is K^+e4 verval met een negatief elektron. Er is geen enkel verschijnsel van dit type gevonden, hetgeen in overeenstemming is met de semi-leptonische $\Delta S = \Delta Q$ regel.

De K^+e4 kandidaten zijn, in het kader van de zogenoemde X2 collaboratie, gemeten en geanalyseerd in vijf Europese laboratoria, nl. in Aken, Brussel, Cern, Nijmegen en Padua.

Na een introduktie en probleemstelling in het eerste hoofdstuk wordt in hoofdstuk II een theoretische inleiding gegeven. Deze resulteert in diverse verbanden, bestaande tussen de distributies van meetbare en/of berekenbare grootheden enerzijds en de zogenaamde vormfaktoren en de π-π faseverschuiving anderzijds.

De beide volgende hoofdstukken beschrijven de experimentele opstelling en de verzameling van de meetgegevens. Tevens zijn in hoofdstuk IV de methoden aangegeven om zoveel mogelijk de juiste verschijnselen te selekteren en te korrigeren.

Hoofdstuk V behandelt de analyse van de geselekteerde verschijnselen, zowel met behulp van de methode van de meest aannemelijke aanpassing als met de kleinste kwadraten methode. Als resultaat van deze analyses zijn experimentele waarden gevonden voor de K^+e4 vertakkingsverhouding [$(4{,}1 \pm 0{,}5) \times 10^{-5}$], de π-π faseverschuiving $<\delta_s - \delta_p>$, de vormfaktoren $\tilde{f}_s$, $\tilde{f}_p$, $\tilde{f}'_p$, g en h en hun verhoudingen ν, η en γ (zie tabel V.2 op pag. 70).

In hoofdstuk VI zijn deze waarden vergeleken met de resultaten van gelijksoortige experimenten, uitgevoerd zowel met bellenvatten als met tellers en vonkenvaten. Vrijwel alle eerder in bellenvaten gedetekteerde K^+e4 verschijnselen zijn opnieuw geanalyseerd. Het blijkt dat de diverse uitkomsten ruwweg met elkaar in overeenstemming zijn. Goede overeenkomst bestaat tussen de waarden voor de vertakkingsverhouding en tussen de waarden voor een 'bevoorrechte' kombinatie van vormfaktoren $\nu + 5\eta$ (zie tabel VI.3 op pag. 95).

Tenslotte zijn in hoofdstuk VII enige theoretische voorspellingen besproken en getoetst aan het experiment. Daar de voorspellingen van de vormfaktoren onderling vrij sterk verschillen, is een zinvolle konklusie niet mogelijk. Wat betreft de π-π faseverschuiving en de verstrooiingslengte a_o komen de voorspelde en de experimentele waarden echter goed met elkaar overeen.

CURRICULUM VITAE

Na het behalen van het diploma H.B.S.-B in 1952 aan het Chr. Lyceum te Arnhem en het diploma H.T.S.-elektrotechniek in 1955 te 's Hertogenbosch werd eerst de militaire dienstplicht vervuld. Vervolgens was ik tot eind 1961 als elektronikus werkzaam bij industrie en universiteit. In genoemd jaar werd begonnen met de studie in de natuurkunde aan de Nijmeegse Universiteit. In juni 1966 werd cum laude het doctoraal examen afgelegd met als hoofdvak experimentele natuurkunde en als groot bijvak capita uit de hoge energie fysika.

Gedurende de zes daarop volgende jaren heb ik in het Fysisch Laboratorium van de Universiteit van Nijmegen onder leiding van Prof.dr. R.T. Van de Walle en in samenwerking met enkele andere Europese instituten gewerkt aan de bepaling van vormfactoren bij diverse vervalswijzen van het K^+ meson.

Sedert 1972 ben ik als docent natuurkunde en wiskunde verbonden aan het Chr. Atheneum te Arnhem.

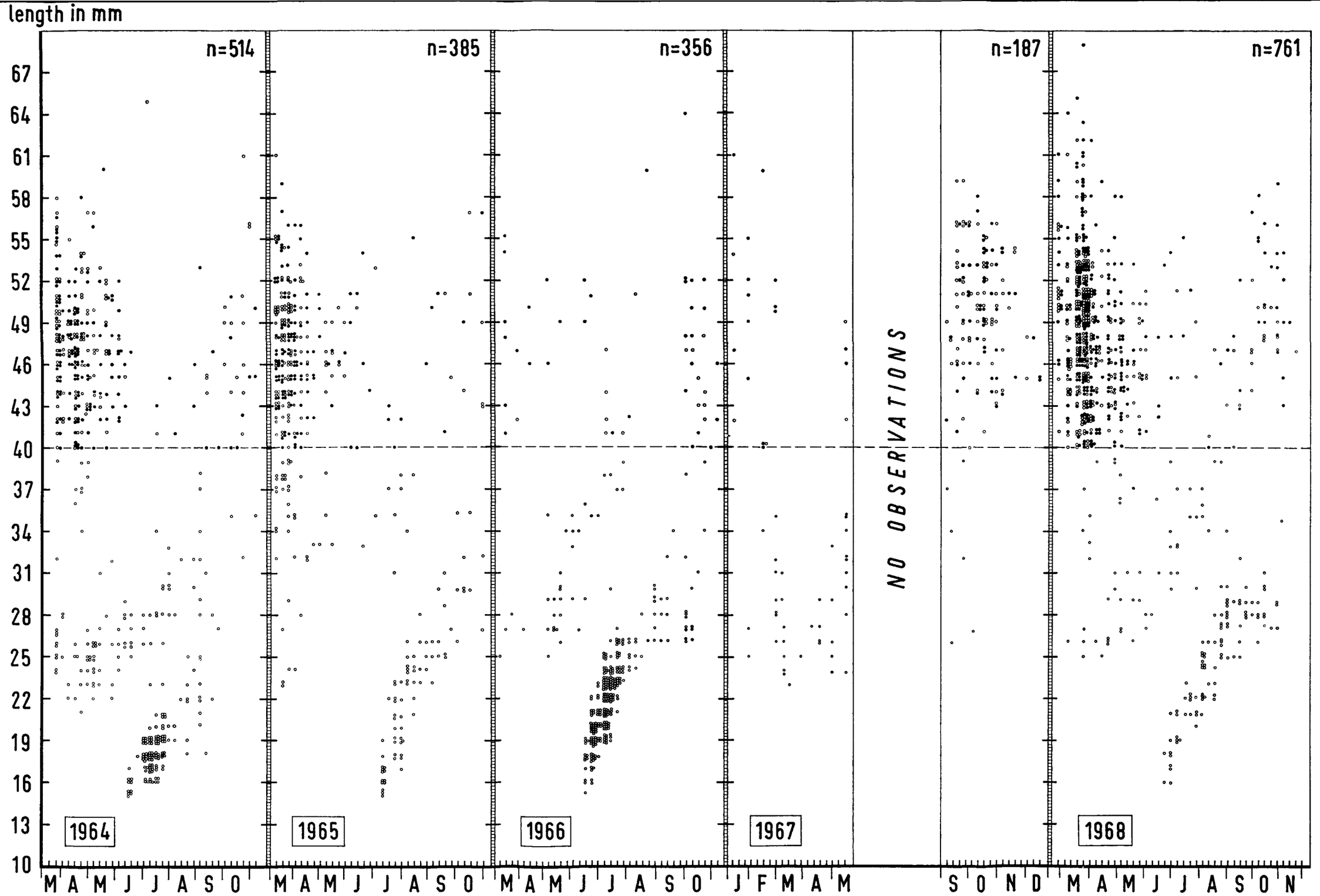

Fig. 2. Synopsis of captured frogs. Each dot represents one frog; above interrupted line an open circle indicates a male, a black dot a female.

STELLINGEN

I

De door Beier *et al.* gegeven theoretische verdeling van K^+_{e4} en K^-_{e4} verschijnselen in de effectieve dilepton massa is onjuist.

E.W. Beier *et al.*, Phys. Rev. Letters **29**, 511 (1972)

II

De berekende distributies van K^+_{e4} verschijnselen in de diverse variabelen, gegeven door Ely *et al.*, zijn niet voldoende nauwkeurig.

R.P. Ely *et al.*, Phys. Rev. **180**, 1319 (1969)

III

De door Johnstad *et al.* verrichte spin-pariteit analyse van de N*(1688) resonantie op basis van $\Delta\pi$-verval, berust op een onvoldoende bewezen uitgangspunt.

H. Johnstad *et al.*, Nucl. Phys. **B42**, 558 (1972)

IV

Het feit, dat Scott een geringere invloed van de door hem toegepaste oriëntatie-middeling op de waarschijnlijkheden voor rotatie-overgangen vindt dan hij verwachtte, is eenvoudig te verklaren.

P.B. Scott, Journal of Chem. Phys. **58**, 644 (1973)

V

De criteria, volgens welke in veel computercentra programmeurs gerecruteerd worden, is de voornaamste reden voor de huidige software crisis.

Datamation, May 1972

VI

Het verdient aanbeveling om bij het voorbereidend wetenschappelijk onderwijs in de natuurkunde reeds vroegtijdig een basis te leggen voor de relativiteitstheorie.

Interimrapport Commissie Modernisering Leerplan Natuurkunde (1969)

VII

Aan afgestudeerden van universiteiten en technische hogescholen behoren gelijkwaardige eisen te worden gesteld ten aanzien van onderwijsbekwaamheid en -bevoegdheid.

VIII

Het verdient aanbeveling om VHF en UHF zenders van circulair polariserende antennes te voorzien.

A. Hock, UKW Berichte **12**, 181 (1972)

IX

Het opnieuw invoeren van de zomertijd, bij voorkeur in geheel West-Europa, dient te worden gepropageerd.

X

Het uitgeven van een rijbewijs en een wapenvergunning zijn vergelijkbare risico's.

C.D. Esveld
Nijmegen, 4 oktober 1973